RELEASE DATE FEB 2 4 1948

Copy No. - UNAVAILABLE

CONFIDENTIAL

RM No. SA8B04

CLASSIFICATION CANCELLED

NACA RM No. SA8B04

Source of Acquisition
CASI Acquired

PERMANENT FILE COPY

NACA

CLASSIFICATION CANCELLED

RESEARCH MEMORANDUM

for the

Air Materiel Command, U. S. Air Force

INVESTIGATION OF THE FLYING MOCK-UP OF THE CONSOLIDATED VULTEE XP-92 AIRPLANE IN THE AMES 40- by 80-FOOT WIND TUNNEL.- FORCE AND MOMENT CHARACTERISTICS

By Bradford H. Wick and David Graham

Ames Aeronautical Laboratory,
Moffett Field, Calif.

[redacted]

CLASSIFICATION CANCELLED

Authority NACA RESEARCH ABSTRACTS and Reclassification Notice No. 104

Date 7/20/56 By

UNAVAILABLE

NATIONAL ADVISORY COMMITTEE FOR AERONAUTICS

WASHINGTON

FEB 13 1948

CONFIDENTIAL

CLASSIFICATION CANCELLED

110

NATIONAL ADVISORY COMMITTEE FOR AERONAUTICS

RESEARCH MEMORANDUM

for the

Air Materiel Command, U. S. Air Force

INVESTIGATION OF THE FLYING MOCK-UP OF THE CONSOLIDATED VULTEE XP-92 AIRPLANE IN THE AMES 40- by 80-FOOT WIND TUNNEL.- FORCE AND MOMENT CHARACTERISTICS

By Bradford H. Wick and David Graham

SUMMARY

This report contains the results of the investigation of the aerodynamic characteristics of the flying mock-up of the Consolidated Vultee XP-92 airplane as conducted in the Ames 40- by 80-foot wind tunnel. Data are presented for test conditions which would give information as to the limits of stability and controllability, and also, the effect of Reynolds number. No analysis of the data has been made.

INTRODUCTION

At the request of the Air Materiel Command, U. S. Air Force, the aerodynamic characteristics of the flying mock-up of the Consolidated Vultee XP-92 airplane have been investigated in the Ames 40- by 80-foot wind tunnel. The XP-92 is a pursuit-type airplane designed for flight at moderate supersonic speeds. The major features of the airplane are (1) a triangular plan-form wing equipped with full-span constant-chord trailing-edge flaps for both longitudinal and lateral control, (2) a fin-rudder arrangement similar to the wing-flap arrangement to provide directional stability and control, and (3) a cylindrically shaped fuselage resulting from the requirements for the combination ram-jet and rocket power plant.

The flying mock-up was built to investigate the subsonic flight characteristics of the present XP-92 configuration and thus provide information for arriving at a final design configuration. The mock-up is not, however, an exact model of the present XP-92 configuration. The difference arises from the difference in power plants. The mock-up is to be powered by a turbojet unit for its subsonic flights and therefore has a more slender appearing fuselage as a result of the smaller inlet and outlet openings required for the turbojet unit. Other than the differences in power plant and fuselage, the mock-up and the present airplane design are essentially the same.

Considerable information on the aerodynamic characteristics of this triangular wing configuration have already been obtained at small scale. However, because of the unusual nature of the configuration and the consequent uncertainty as to the effects of Reynolds number on the results, it was deemed advisable to conduct full-scale wind-tunnel tests of the mock-up before initiating the flight tests. Since the most important information required for the flight tests are the limits of stability and controllability, the test conditions (i.e., angles of attack, sideslip angles, control positions, etc.) for the present wind-tunnel investigation were selected mainly from this standpoint.

No analysis of the data have been made in order to make the data available as soon as possible.

SYMBOLS AND COEFFICIENTS

The standard NACA coefficients and symbols used within this report are defined below and in figure 1:

A aspect ratio (b^2/S)

A_e duct exit area, square feet

A_i duct inlet area, square feet

α free-stream angle of attack (with reference to wing chord plane), degrees

α_T increment of angle of attack due to wind-tunnel-wall interference, degrees

b wing span, feet

β angle of sideslip (with reference to vertical plane of symmetry), degrees

c wing chord, measured parallel to airplane center line, feet

$\bar{c}$ wing mean aerodynamic chord, measured parallel to airplane center line, feet

$\bar{c}_v$ vertical-tail mean aerodynamic chord, measured parallel to airplane center line, feet

C wind-tunnel-test section area, normal to air stream, square feet

C_L lift coefficient $\left(\frac{\text{lift}}{qS}\right)$

C_D drag coefficient $\left(\frac{\text{drag}}{qS}\right)$

C_{D_i} internal drag coefficient $\left(\frac{\text{internal drag}}{qS}\right)$

C_{D_S} increment of drag coefficient due to support-strut interference

C_{D_T} increment of drag coefficient due to wind-tunnel-wall interference

C_m pitching-moment coefficient $\left(\frac{\text{pitching moment}}{qS\bar{c}}\right)$

C_{m_S} increment of pitching-moment coefficient due to support-strut interference

C_l rolling-moment coefficient $\left(\frac{\text{rolling moment}}{qSb}\right)$

C_n yawing-moment coefficient $\left(\frac{\text{yawing moment}}{qSb}\right)$

C_Y side-force coefficient $\left(\frac{\text{side force}}{qS}\right)$

δ_e elevator deflection (measured with reference to wing chord plane in a plane perpendicular to the hinge line), degrees

δ_a aileron deflection (measured with reference to wing chord plane in a plane perpendicular to the hinge line), degrees

δ_r rudder deflection (measured with reference to tail chord plane in a plane perpendicular to the hinge line), degrees

δ_w wind-tunnel-wall-interference correction factor

H free-stream total head, pounds per square foot

H_e average total head as indicated by duct exit rake, pounds per square foot

p_e average static head as indicated by duct exit rake, pounds per square foot

ν kinematic viscosity, square feet per second

q dynamic pressure, pounds per square foot

R Reynolds number $\left(\frac{Vc}{\nu}\right)$

S wing area, square feet

S_v exposed vertical-tail area, square feet

V free-stream velocity, feet per second

V_i duct inlet velocity, feet per second

DESCRIPTION OF AIRPLANE AND APPARATUS

The investigation of the flying mock-up of the Consolidated Vultee XP-92 airplane was conducted in the Ames 40- by 80-foot wind tunnel. A three-view drawing of the mock-up is shown in figure 2, and photographs of the mock-up mounted in the tunnel are shown in figure 3. Dimensional data for the mock-up are given in table I.

The turbojet unit that is to power the mock-up was removed for these wind-tunnel tests, and the tail pipe and outlet-rake arrangement shown in figure 4 were installed. This open duct condition was used for most of the tests. A closed duct condition was obtained by plugging the outlet of the tail pipe.

The purpose of the tail pipe was to provide a smoother flow of air at the outlet than otherwise would have been obtained, and thus improve the accuracy of the outlet-rake readings. The rake itself was an integrating type, with twenty total head tubes and four static-pressure tubes. The total head tubes were connected to the individual tubes of a water-in-glass manometer; whereas the static-pressure tubes were connected together and then connected to a single manometer tube.

The main landing-gear configuration was modified in a number of ways. The first modification consisted of the removal of the landing-gear doors which fitted the contour of the fuselage. The next modification consisted of the removal of all the landing-gear doors which were attached to the landing-gear proper, leaving in place the doors that were attached to the wing (fig. 3(e)). This change was followed by the addition of fairings to the horizontal members of the landing-gear configuration with the doors still removed (fig. 3(f)).

Sharp leading edges were simulated on the wing by the addition of dural caps, dimensions of which are given in figure 5.

The flaps and rudder were operated remotely by means of a hydraulic system that was connected into the airplane hydraulic system for actuating each of the control surfaces. This actuating system for each control surface consisted basically of a double-acting piston arrangement that had one side of the piston mechanically linked to the control surface. The necessary pressure differential across the piston was supplied during the wind-tunnel tests by hydraulic pressure lines brought into the airplane at the rear support strut (fig. 3 (d)). Pressure gages were attached to each of hydraulic lines to measure the pressure differentials required to maintain the desired control positions under the air loads imposed.

Remote indication of the control-surface positions was provided by calibrated autosyn transmitters and receivers.

TESTS, RESULTS, AND DISCUSSIONS

The types of tests conducted and the range of test conditions (angles of attack, sideslip angles, etc.) are fully shown in table II. This table should also serve as an index for figures 6 to 29 in which the basic data (with the exception of the control-system cylinder pressures) are presented. In both the table and figures the notation $\pm10^\circ$ for aileron deflection, refers to 10° down-deflection of the right flap and 10° up-deflection of the left flap in combination with the specified elevator deflection for each flap. Unless otherwise noted on the figures, the sideslip angle was 0.13°.

The maximum control-system cylinder pressures measured during the tests are presented in the following table. Only the maximum value for each control surface is given, since the pressures generally showed no systematic variation with any of the test variables (angle of attack, control deflection, etc.) due to the large amount of friction in the control system relative to the air loads on the control surfaces. (The control surface hinge moments at the air speeds used for the tests were of the order of 5 percent of those expected at high speed.)

Control surface	Pressure differential across piston (lb per sq in.)
Right flap	133
Left flap	167
Rudder	57

In reducing the data to coefficient form, the dimensions of the complete triangular plan form of the wing were used. These same dimensions were also used for the sharp-leading-edge data. All of the coefficients have been referred to the stability axes, and the moment coefficients had as their center the point on the fuselage center line and chord plane of the wing corresponding to the longitudinal location of the quarter-chord station of the mean aerodynamic chord.

It should be noted that except for figures 28 and 29, the values of drag coefficient presented in the report are for the total drag of the airplane (external plus internal). Figures 28 and 29 present typical values of internal drag coefficient, and inlet-velocity ratio which were computed by the following equations:

$$C_{D_i} = 2\,\frac{V_i A_i}{VS}\left(1 - \sqrt{1 - \frac{(H-H_e)}{q}}\right)$$

$$V_i/V = \sqrt{\frac{H_e-p_e}{q}\,\frac{A_e}{A_i}}$$

No values of internal drag coefficient and inlet-velocity ratio are presented for the controls deflected tests, since a few representative calculations for these tests showed no difference from the controls neutral results.

The angles of attack and the drag coefficients have been corrected for stream-angle inclination and for wind-tunnel-wall effects, the latter corrections being those for a wing of the same span but with rectangular plan form. The wall corrections, based on theory of reference 1 for a wind tunnel with oval cross section, are as follows:

$$\alpha_T = \delta_w\,\frac{S}{C} \times C_L \times 57.3$$

$$C_{D_T} = \delta_w\,\frac{S}{C}\,C_L^{\,2}$$

where

$$\delta_w = 0.110$$

$$C = 2856 \text{ sq ft}$$

The data were also corrected for support-strut interference by applying support tares derived from tests of a rectangular wing (aspect ratio of 6) at zero sideslip. The support tares (shown in table III as a function of lift coefficient) were subtracted algebraically from the gross coefficients. As will be noted from the table, only the drag- and pitching-moment coefficients were so corrected, as they were the only coefficients found to be affected by the support struts during the tests of the rectangular wing.

When considering the drag data, it should be kept in mind that the drag coefficients are with reference to the longitudinal stability axis rather than the wind axis. Thus, so referencing, the drag coefficients gave a minimum drag that decreased with increasing sideslip until it was nearly zero at the higher angles (figs. 6 and 7). The drag that must be overcome in propelling the airplane is, of course, in the longitudinal wind axis direction. The minimum drag in this direction would increase with increasing sideslip angle, as in the case for more conventional airplanes. It is believed that the minimum drag in stability axis direction was nearly zero at the higher sideslip angles because the resultant force on the vertical tail was tilted forward with respect to the longitudinal stability axis. Thus there was a component of the force on the vertical tail tending to offset the drag of the airplane. This component was due to the leading-edge thrust[1] on the vertical tail. If there had been no leading-edge thrust (as in the case of a sharp leading edge), the resultant force would have been normal to the longitudinal stability axis and thus without effect on the drag in this direction.

Another feature of the test results to which attention should be called is the increasingly erratic variations of rolling-moment coefficient with lift coefficient as the elevators were deflected more negatively. The erratic nature of the variation became more pronounced with both aileron deflection and increasing sideslip angle. (See figs. 8, 9, and 10.) In the case where the elevator deflection was -20° and the sideslip angle was -20.2° (fig. 8), the erratic variation was traced to an unsteady flow condition. The test points shown on the figures are the average of five separate balance

[1]See Durand's Aerodynamic Theory, division E II 10 and division J 11 1 for discussions of leading-edge thrust.

readings which were obtained at approximately 5-second intervals. In order to illustrate the unsteadiness of the flow, there are shown on figure 8, at a C_L of 0.63, the lowest and the highest as well as the average of the five balance readings. Because of the inertia of the balance system, these points do not necessarily represent the actual fluctuation of the airplane rolling moment. The airplane rolling moment may have fluctuated more or less than the rolling moment recorded by the balances and the average rolling moment may also have differed from that indicated by the balances. A similar comparison of balance readings is shown in figure 10 for the aileron deflection in combination with the -20° elevator deflection. The erratic variation in this case started at low lift coefficients and does not appear to have been due to unsteadiness of flow. This conclusion is borne out by the rolling-moment data presented in figure 16 for the cases where there were rudder deflections in addition to the aileron and elevator deflections. For these cases, the variation of rolling moment with lift is very similar to that with the rudder undeflected; whereas with unsteady flow, one would hardly have expected any such consistency in the variation.

Ames Aeronautical Laboratory,
National Advisory Committee for Aeronautics,
Moffett Field, Calif.

REFERENCE

1. Tani, Itiro and Sanuki, Matao: The Wall Interference of a Wind Tunnel of Elliptic Cross Section. NACA TM No. 1075, Nov. 1944.

TABLE I.- GEOMETRIC DATA OF THE FLYING MOCK-UP OF THE XP-92 AIRPLANE

Wing Dimensions	
Type	Triangular, leading-edge sweepback of 60°, apex angle of 60°
Airfoil section (measured parallel to airplane center line)	NACA 65_1-006.5
Aspect ratio	2.309
Area, S (total)	425 sq ft
Area exposed outside of fuselage	296 sq ft
Span, b	31.33 ft
Wing chord at center line of airplane	27.13 ft
Wing chord at wing-fuselage intersection	22.40 ft
Tip chord	0
Mean aerodynamic chord, $\bar{c}$	18.09 ft
$\frac{\bar{c}}{4}$ location in percent fuselage length from nose of fuselage	53.6 percent
Trailing-edge angle	7°40'
Geometric twist	0°
Dihedral	0°
Angle of incidence (with respect to airplane center line)	0°
Trailing-Edge Flaps	
Area (total both flaps aft of hinge line)	76.60 sq ft
Area (total with horn balance)	78.02 sq ft
Chord (aft of hinge line - constant except for tip)	3.05 ft

TABLE I.– CONTINUED. XF-92 AIRPLANE

Span exposed (wing span minus fuselage width at wing trailing edge)	27.30 ft
Total wing area affected by movable control surface	296.0 sq ft
Aerodynamic balance	None – nose radius
Tail length $\left(\frac{\bar{c}}{4} \text{ to } \frac{\text{elevon chord}}{2}\right)$	0.665 $\bar{c}$
Tail length $\left(\frac{\bar{c}}{4} \text{ to elevon hinge line}\right)$	0.581 $\bar{c}$
Travel	-33° to $+30^\circ$
Vertical Tail (with theoretical sharp tip)	
Type . . Triangular, leading-edge sweepback of 60°, apex angle 30°	
Airfoil section (measured parallel to airplane center line)	NACA 65_1-006.5
Aspect ratio	1.227
Area, S_V (total exposed above fuselage)	76.10 sq ft
Span exposed above fuselage at trailing edge	9.66 ft
Root chord at deck line	16.17 ft
Tip chord	0
Mean aerodynamic chord, $\bar{c}_V$ (exposed tail)	10.78 ft
Tail length $\left(\frac{\bar{c}}{4} \text{ to } \frac{\bar{c}_V}{4}\right)$	5.48 ft
Rudder (with theoretical sharp tip)	
Area (aft of hinge line)	15.50 sq ft
Chord aft of hinge line (constant except for tip)	1.71 ft
Span	9.66 ft

TABLE I.- CONCLUDED. XP-92 AIRPLANE.

Travel	$\pm 25^{\circ}$
Balance	None – nose radius
Fuselage	
Length over all	41.33 ft
Maximum diameter	5.50 ft
Inlet area of duct	2.07 sq ft
Exit area of duct	2.14 sq ft
Frontal area (maximum)	23.7 sq ft
Fineness ratio $\left(\frac{\text{over-all length}}{\text{maximum diameter}}\right)$	7.52
Canopy	
Maximum height above fuselage line	17.50 in.
Maximum width	27.20 in.
Length	109.31 in.

TABLE II.- SUMMARY OF CONFIGURATIONS TESTED, XP-92 AIRPLANE

Figure	Configuration	Angle of sideslip, β, deg	Control deflection, deg δ_e	δ_a	δ_r	Reynolds No.	Data presented
			Aerodynamic Characteristics at Various Angles of Sideslip				
6	Basic[a]	0.13	0	0	0	[b]16.4×10^6	C_L vs α, C_D, C_m, C_l, C_n, C_Y
		−1.90					
		−5.00					
7	Do.	−10.06	0	0	0	[b]16.4×10^6	C_L vs α, C_D, C_m, C_l, C_n, C_Y
		−15.20					
		−20.20					
			Longitudinal Control Effectiveness				
8	Basic	0.13	−10, −20	0	0	16.4×10^6	C_L vs α, C_D, C_m, C_l, C_n, C_Y
		−10.06	−10, −20				
		−20.20	−10, −20				
			Longitudinal and Lateral Control Effectiveness				
9	Basic	0.13	0, −10, −20	[c]±10	0	16.4×10^6	C_L vs α, C_D, C_m, C_l, C_n, C_Y
10	Do.	−10.06	0, −10, −20	±10	0	16.4×10^6	C_L vs α, C_D, C_m, C_l, C_n, C_Y
11	Do.	−20.20	0, −10	±10	0	16.4×10^6	C_L vs α, C_D, C_m, C_l, C_n, C_Y
			Longitudinal and Directional Control Effectiveness				
12	Basic	0.13	−10	0	−10, −20	16.4×10^6	C_L vs α, C_D, C_m, C_l, C_n, C_Y
13	Do.	−10.06	−10	0	−10, +10, −20, +20	[d]13.3×10^6 and 16.4×10^6	C_L vs α, C_D, C_m, C_l, C_n, C_Y
14	Do.	−20.20	−10	0	−20, +20	13.3×10^6 and 16.4×10	C_L vs α, C_D, C_m, C_l, C_n, C_Y
			Longitudinal, Lateral and Directional Control Effectiveness				
15	Basic	0.13	−10	±10	−10, +10, −20	16.4×10^6	C_L vs α, C_D, C_m, C_l, C_n, C_Y
16	Do.	−10.06	−10	±10	−10, +10	[b]13.3×10^6 and 16.4×10^6	C_L vs α, C_D, C_m, C_l, C_n, C_Y
			−20	↓	−20, +20		
17	Do.	−20.20	−10	±10	−10, +10	16.4×10^6	C_L vs α, C_D, C_m, C_l, C_n, C_Y
			Effect of Reynolds Number on Longitudinal Characteristics				
18	Basic	0.13	0	0	0	10.6×10^6 to 35.4×10^6	C_L vs α, C_D, C_m
			Effect of Internal Flow Through the Ducted Fuselage on Longitudinal Characteristics				
19	Basic	0.13	0	0	0	16.4×10^6	C_L vs α, C_D, C_m
	Basic, with duct closed						

[a]The basic configuration consisted of the airplane as shown in figure 3(a–d) with open duct.
[b]Flagged symbols indicate data obtained at a Reynolds number of 14.9×10^6.
[c]Right aileron deflection is positive, left aileron deflection negative.
[d]Reynolds number for all runs with +20° rudder deflection was 13.3×10^6.

TABLE II.- CONTINUED. XP-92 AIRPLANE

Figure	Configuration	Angle of sideslip, β, deg	Control deflection, deg			Reynolds No.	Data presented
			δ_e	δ_a	δ_r		
Effect of Landing Gear and Modifications Thereof on Stability and Control							
20	Basic	0.13	0	0	0	16.4×10^6	C_L vs α, C_D, C_m, C_l, C_n, C_Y
	Basic, with gear extended					↓	
	Basic	−20.20					
	Basic, with gear extended					10.6×10^6	
21	Basic, with gear extended	0.13	−10	0	0	16.4×10^6	C_L vs α, C_D, C_m, C_l, C_n, C_Y
				±10	↓		
		−10.06	↓	↓	−10		
22	Basic	0.13	0	0	0	16.4×10^6	C_L vs α, C_D, C_m
	Basic, without gear doors						
	Basic, with gear extended						
	Basic, with gear extended, without doors, with fairings						
Effect of Sharp Leading Edges on Longitudinal Characteristics							
23	Basic	0.13	0	0	0	16.4×10^6	C_L vs α, C_D, C_m
	Basic with sharp leading edges installed						
Effect of Reynolds Number on Drag Coefficient							
24	Basic	0.13	0	0	0	10.6×10^6 to 36.4×10^6	C_D vs R for three values of C_L
Effect of Landing Gear and Modifications Thereof on Drag							
25	Basic	0.13	0	0	0	10.6×10^6 to 36.4×10^6	C_D vs R
	Basic, without gear doors						
	Basic, with gear extended						
26	Basic	0.13	0	0	0	16.4×10^6	C_L vs R
	Basic, without gear doors						
	Basic, with gear extended						
	Basic, with gear extended, without fuselage doors						
	Basic, with gear extended, without gear doors						
	Basic, with gear extended, without gear doors, with fairings						

TABLE II.- CONCLUDED. XP-92 AIRPLANE

Figure	Configuration	Angle of sideslip, β, deg	Control deflection, deg			Reynolds No.	Data Presented
			δ_e	δ_a	δ_r		
Effect of Sharp Leading Edges on the Variation of Drag Coefficient With Reynolds Number							
27	Basic	0.13	0	0	0	16.4×10^6	C_L vs α, C_D, C_m
	Basic, with sharp leading edges installed						
Internal Drag and Inlet Velocity Ratio of the Ducted Fuselage							
28	Basic	0.13	0	0	0	16.4×10^6	C_{D_i}, V_i/V vs α
		−5.00					
		−10.06					
		−15.20					
		−20.20					
29	Basic	0.13	0	0	0	10.6×10^6 to 36.4×10^6	C_{D_i}, V_i/V vs α

NACA RM No. SA8B04

TABLE III.- CORRECTIONS FOR SUPPORT-STRUT INTERFERENCE, XP-92 AIRPLANE

C_L	C_{D_s}	C_{m_s}
-0.2	0.0032	-0.0020
0	.0022	-.0020
.2	.0014	-.0028
.4	.0006	-.0028
.6	-.0001	-.0032
.8	-.0007	-.0036
1.0	-.0012	-.0040
1.2	-.0014	-.0040

FIGURE LEGENDS

Figure 1.- Sign convention for the standard NACA coefficients. All forces, moments, angles, and control-surface deflections are shown as positive.

Figure 2.- Three-view drawing of the flying mock-up of the XP-92 airplane.

Figure 3.- The flying mock-up of the XP-92 airplane as installed in the Ames 40- by 80-foot wind tunnel. (a) Plan view.

Figure 3.- Continued. (b) Three-quarter front view from below the wing.

Figure 3.- Continued. (c) Three-quarter front view from above the wing.

Figure 3.- Continued. (d) Three-quarter rear view from below the wing.

Figure 3.- Continued. (e) Three-quarter front view with gear retracted and landing-gear doors removed.

Figure 3.- Concluded. (f) Three-quarter front view with gear extended, landing-gear doors removed, and fairings added.

Figure 4.- Detail of tailpipe.

Figure 5.- Detail of sharp leading-edge configuration.

Figure 6.- Aerodynamic characteristics at various angles of sideslip with controls neutral.

Figure 6.- Continued.

Figure 6.- Continued.

Figure 6.- Continued.

Figure 6.- Continued.

Figure 6.- Concluded.

Figure 7.- Aerodynamic characteristics at various angles of sideslip with controls neutral.

Figure 7.- Continued.

Figure 7.- Continued.

Figure 7.- Continued.

Figure 7.- Continued.

Figure 7.- Concluded.

Figure 8.- Longitudinal control effectiveness with undeflected rudder.

Figure 8.- Continued.

Figure 8.- Continued.

Figure 8.- Continued.

Figure 8.- Continued.

Figure 8.- Concluded.

Figure 9.- Longitudinal and lateral control effectiveness with undeflected rudder, $\beta = 0.13^{\circ}$.

Figure 9.- Continued.

Figure 9.- Continued.

Figure 9.- Continued.

Figure 9.- Continued.

Figure 9.- Concluded.

Figure 10.- Longitudinal and lateral control effectiveness with undeflected rudder, $\beta = -10.06^{\circ}$.

Figure 10.- Continued.

Figure 10.- Continued.

Figure 10.- Continued.

Figure 10.- Continued.

Figure 10.- Concluded.

Figure 11.- Longitudinal and lateral control effectiveness with undeflected rudder, $\beta = -20.20^{\circ}$.

Figure 11.- Continued.

Figure 11.– Continued.

Figure 11.– Continued.

Figure 11.– Continued.

Figure 11.– Concluded.

Figure 12.– Longitudinal and directional control effectiveness, $\beta = 0.13^\circ$.

Figure 12.– Continued.

Figure 12.– Continued.

Figure 12.– Continued.

Figure 12.– Continued.

Figure 12.– Concluded.

Figure 13.– Longitudinal and directional control effectiveness, $\beta = -10.06^\circ$.

Figure 13.– Continued.

Figure 13.– Continued.

Figure 13.– Continued.

Figure 13.– Continued.

Figure 13.– Concluded.

Figure 14.– Longitudinal and directional control effectiveness, $\beta = -20.20^\circ$.

Figure 14.– Continued.

Figure 14.– Continued.

Figure 14.– Continued.

Figure 14.– Continued.

Figure 14.– Concluded.

Figure 15.– Longitudinal, lateral and directional control effectiveness, $\beta = 0.13^\circ$.

Figure 15.– Continued.

Figure 15.- Continued.

Figure 15.- Continued.

Figure 15.- Continued.

Figure 15.- Concluded.

Figure 16.- Longitudinal, lateral and directional control effectiveness, $\beta = -10.06^\circ$.

Figure 16.- Continued.

Figure 16.- Continued.

Figure 16.- Continued.

Figure 16.- Continued.

Figure 16.- Concluded.

Figure 17.- Longitudinal, lateral and directional control effectiveness, $\beta = -20.20^\circ$.

Figure 17.- Continued.

Figure 17.- Continued.

Figure 17.- Continued.

Figure 17.- Continued.

Figure 17.- Concluded.

Figure 18.- Effect of Reynolds number on longitudinal characteristics with controls neutral.

Figure 18.- Continued.

Figure 18.- Concluded.

Figure 19.- Effect of internal flow through the ducted fuselage on longitudinal characteristics with controls neutral.

Figure 19.- Continued.

Figure 19.- Concluded.

Figure 20.- Effects of extended landing gear on stability.

Figure 20.- Continued.

Figure 20.– Continued.

Figure 20.– Continued.

Figure 20.– Continued.

Figure 20.– Concluded.

Figure 21.– Effects of extended landing gear on controls.

Figure 21.– Continued.

Figure 21.– Continued.

Figure 21.– Continued.

Figure 21.– Continued.

Figure 21.– Concluded.

Figure 22.– Effects of various landing-gear configurations on longitudinal characteristics with controls neutral.

Figure 22.– Continued.

Figure 22.– Concluded.

Figure 23.– Effect of sharp leading edges on longitudinal characteristics with controls neutral.

Figure 23.– Continued.

Figure 23.– Concluded.

Figure 24.– Effect of Reynolds number on drag coefficient at constant lift coefficient.

Figure 25.– Effect of various landing-gear configurations on the variation of drag coefficient with Reynolds number, $C_L = 0$.

Figure 26.– Effect of various landing-gear configurations on drag coefficient variation with lift coefficient.

Figure 27.– Effect of sharp leading edges on the variation of drag coefficient with Reynolds number, $C_L = 0$.

Figure 28.– Internal drag coefficient and inlet velocity ratio of the ducted fuselage at various angles of sideslip.

Figure 29.– Internal drag coefficient and inlet velocity ratio of the ducted fuselage at various Reynolds numbers, $\beta = 0.13^{\circ}$.

NACA SA8B04

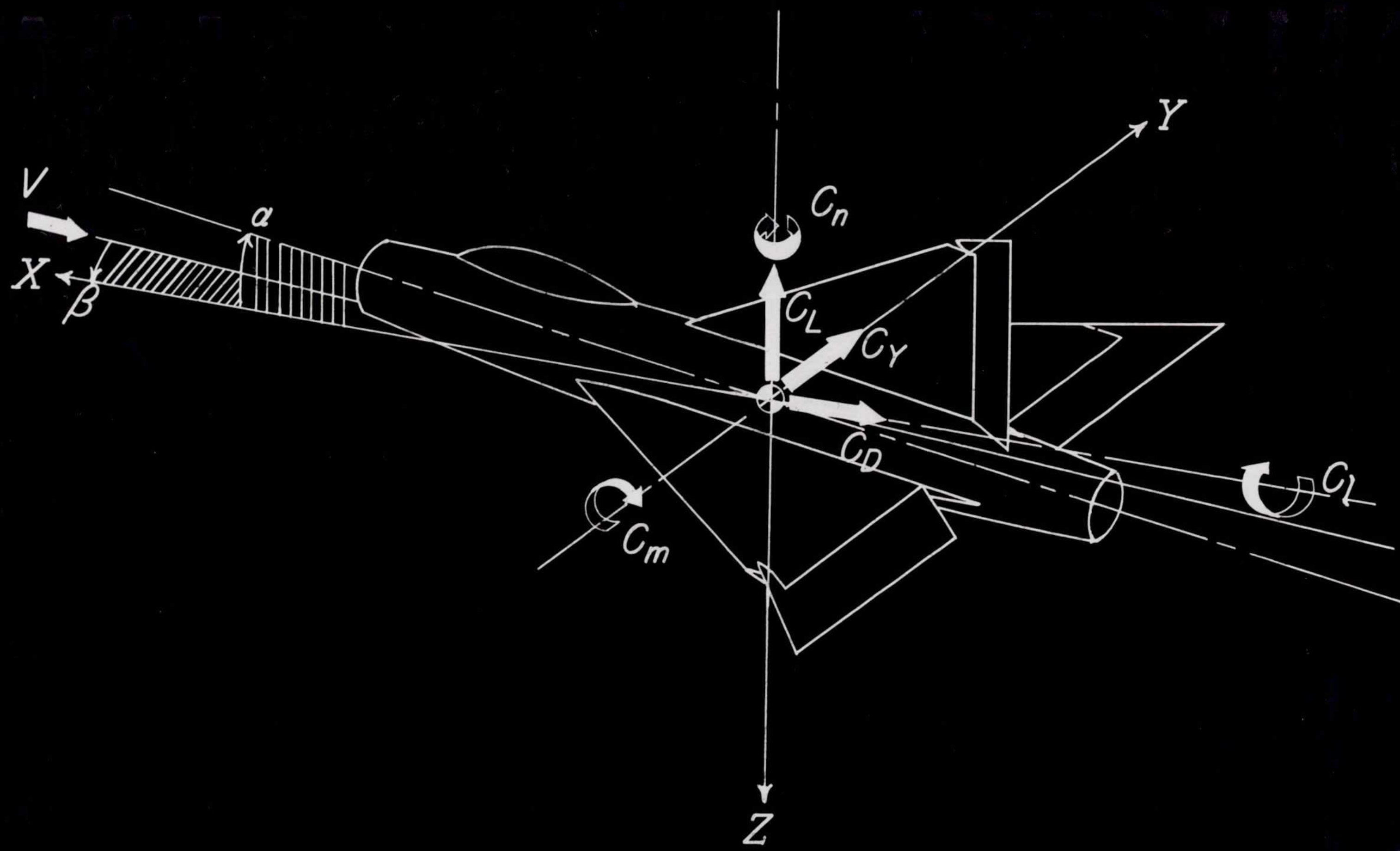

Figure 1.- Sign convention for the standard NACA coefficients. All forces, moments, angles, and control-surface deflections are shown as positive.

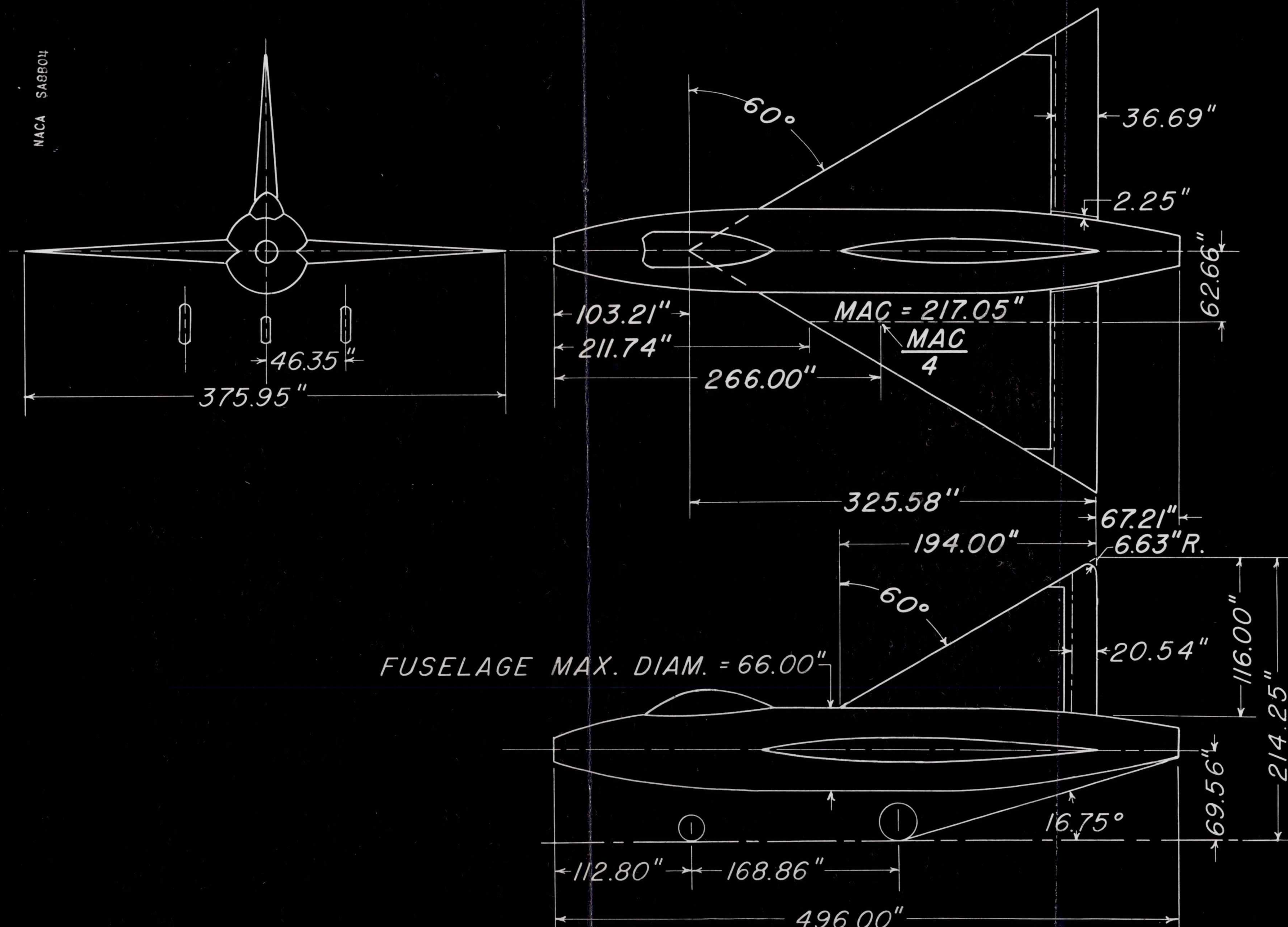

Figure 2.- Three view drawing of the flying mock-up of the XP-92 airplane.

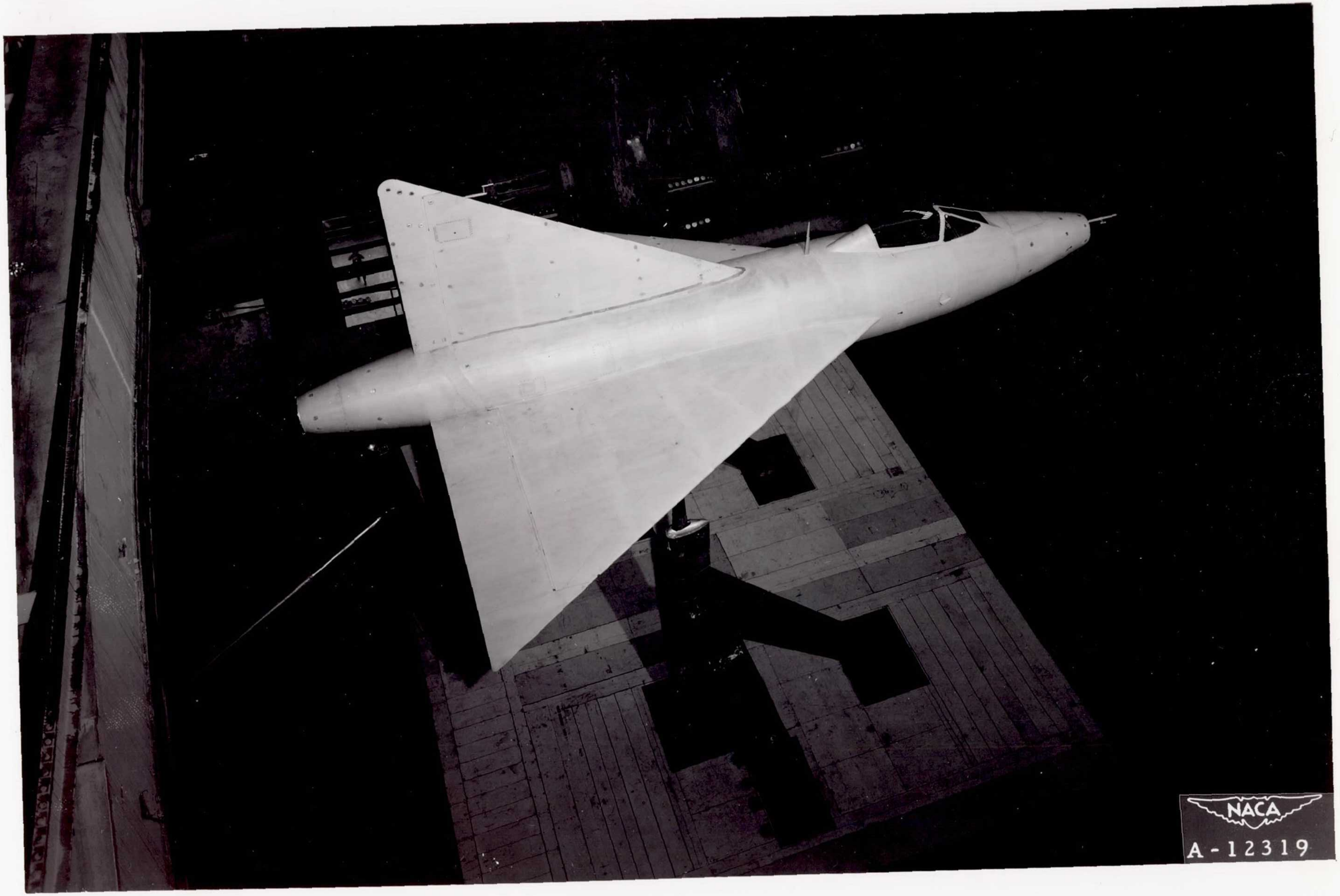

(a) Plan view

Figure 3.- The flying mock-up of the XP-92 airplane as installed in the Ames 40- by 80-foot wind tunnel.

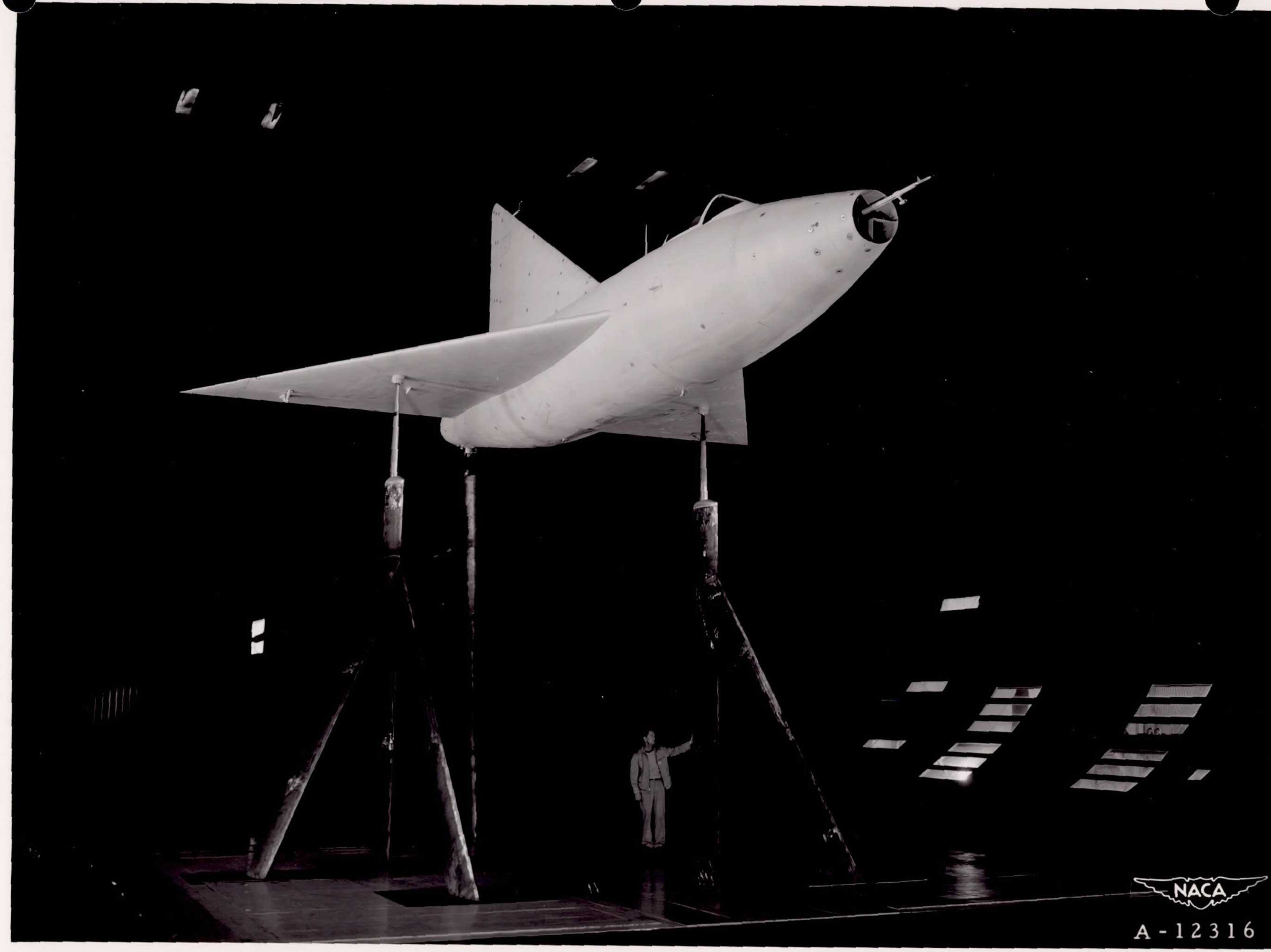

(b) Three-quarter front view from below the wing.

Figure 3.- Continued.

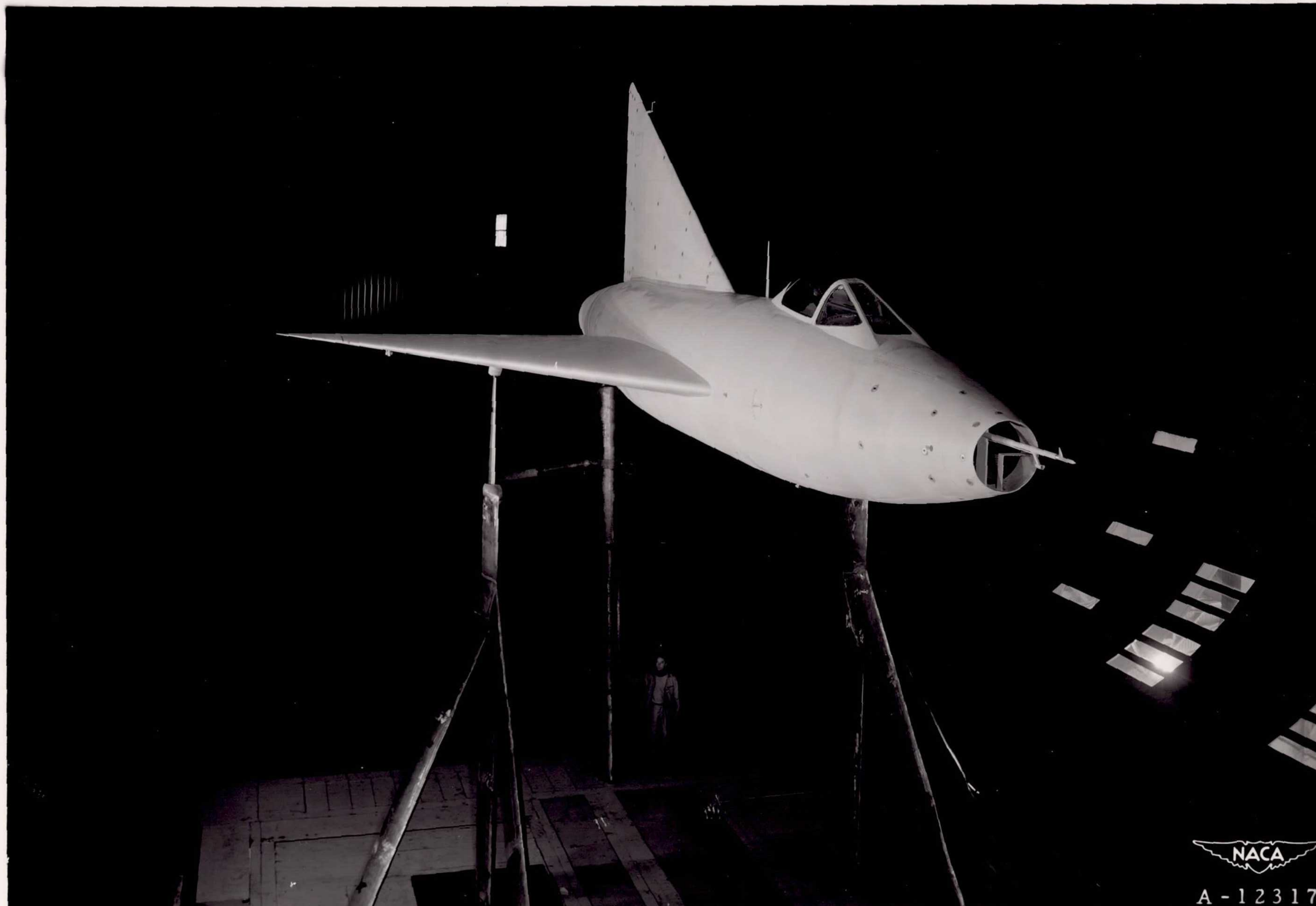

(c) Three-quarter front view from above the wing.

Figure 3.-Continued.

(d) Three-quarter rear view from below the wing.

Figure 3.-Continued.

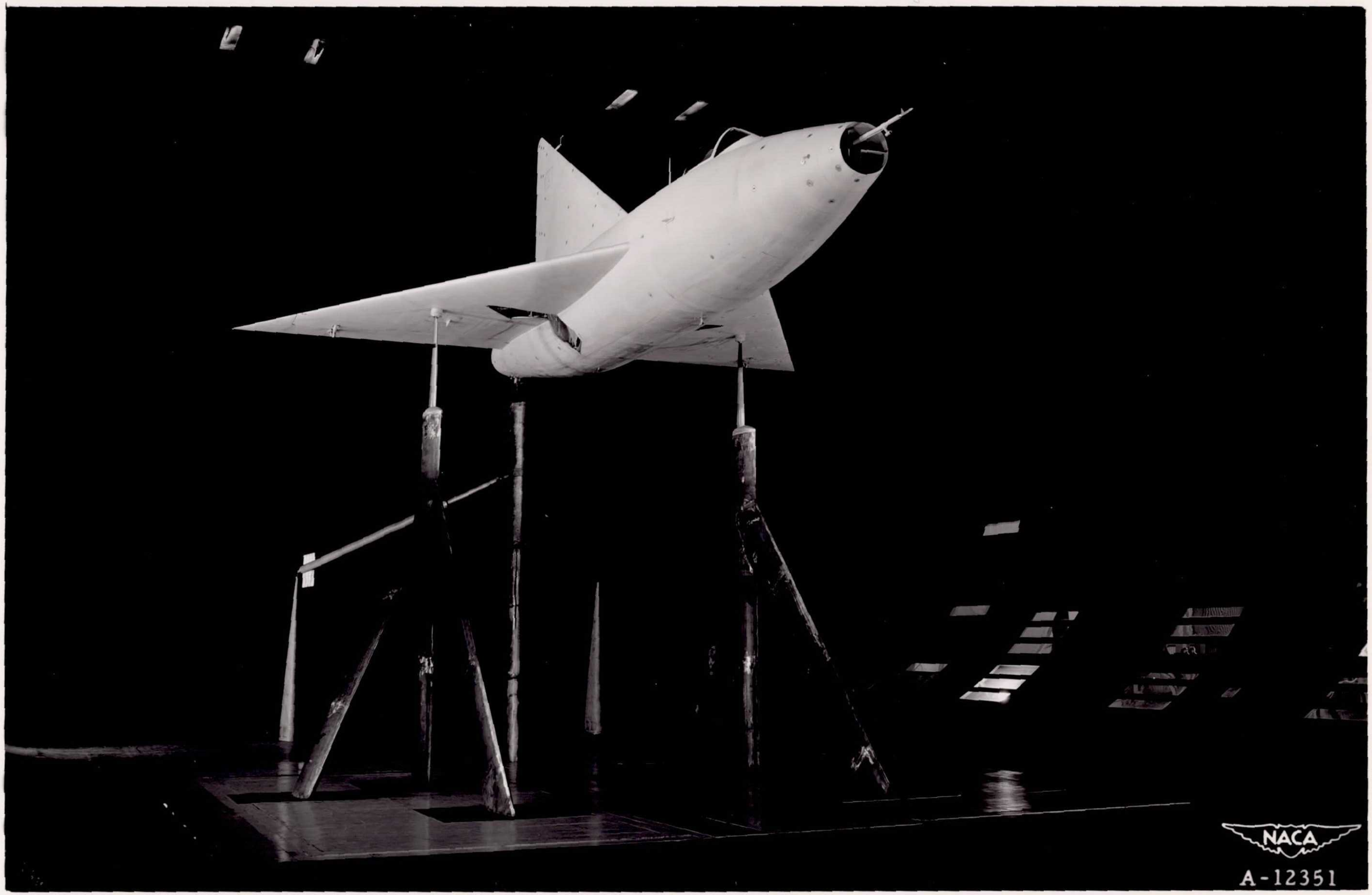

(e) Three-quarter front view with gear retracted and landing-gear doors removed.

Figure 3.-Continued.

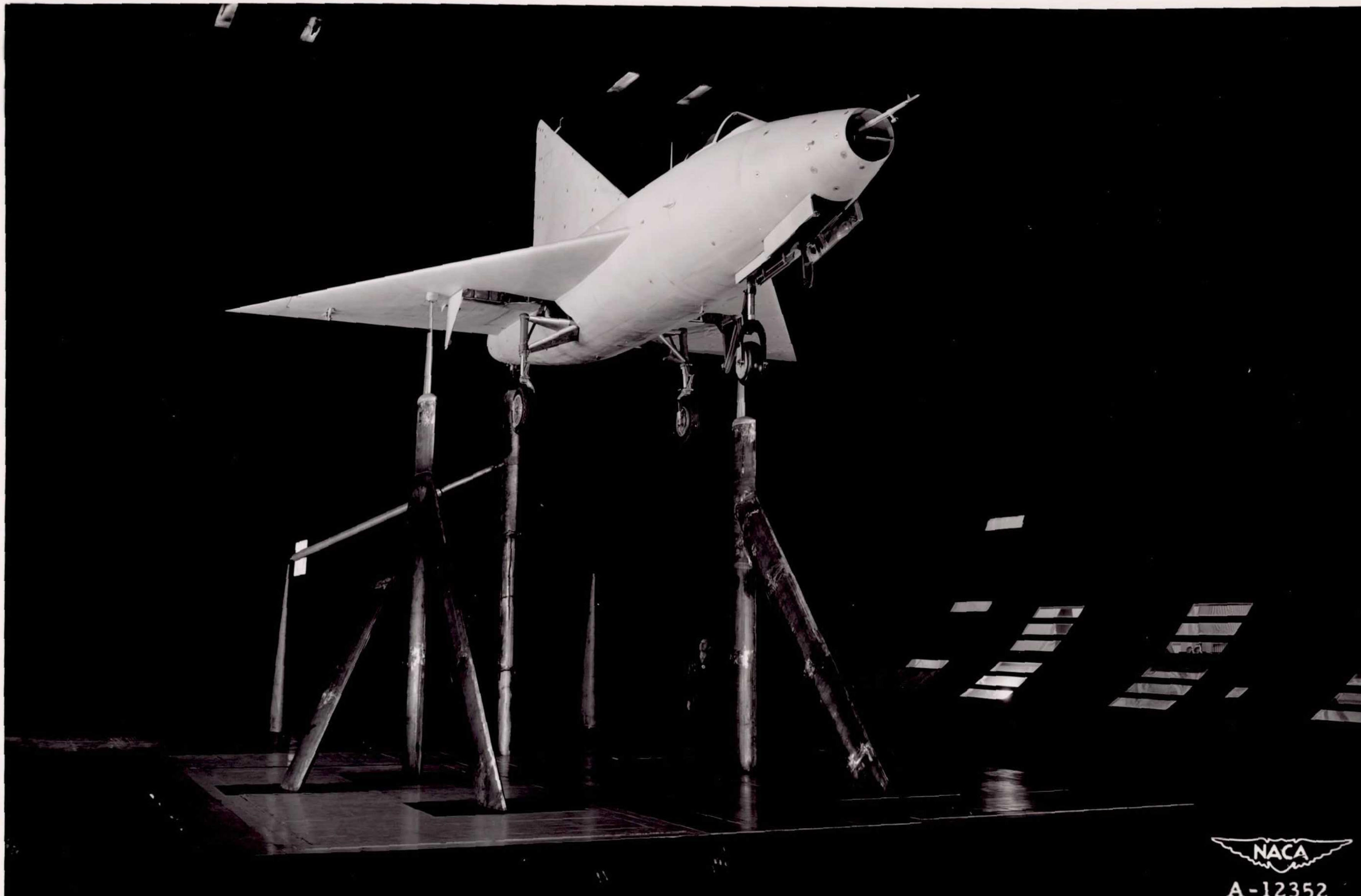

(f) Three-quarter front view with gear extended, landing-gear doors removed, and fairings added.

Figure 3.-Concluded.

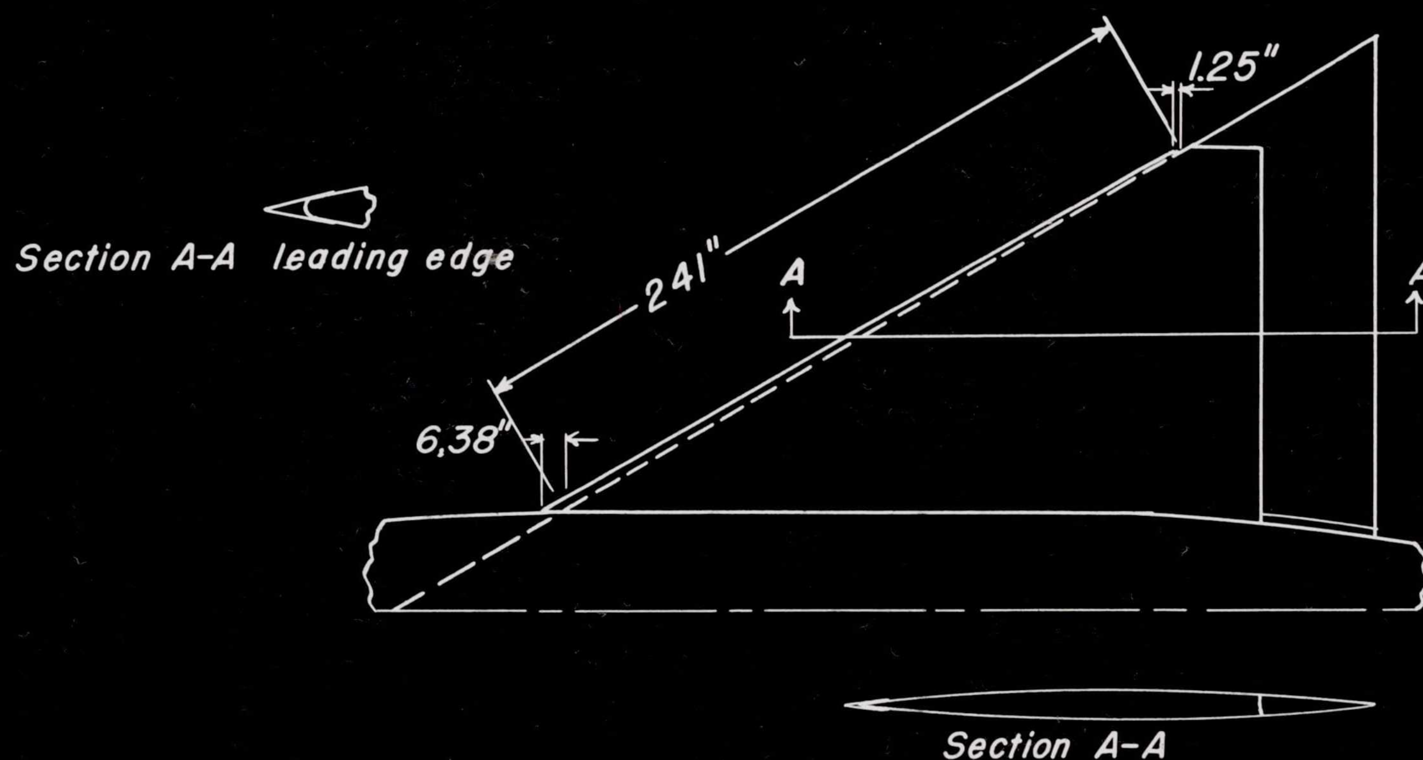

Figure 5.- Detail of sharp leading edge configuration.

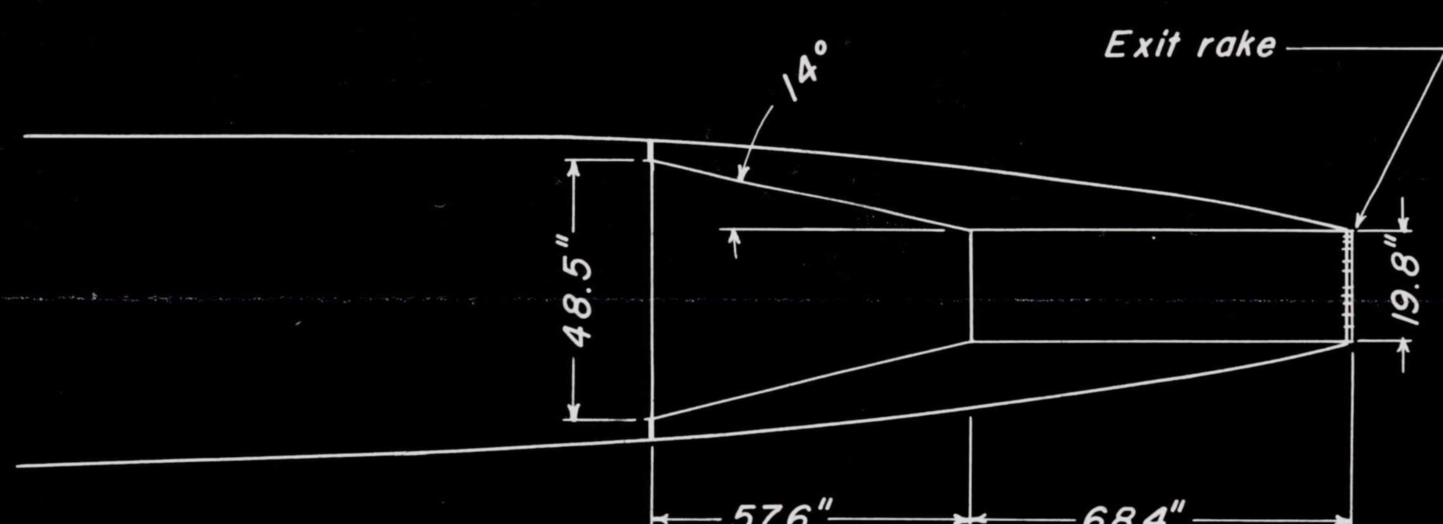

Figure 4.- Detail of tailpipe

NACA 8A804

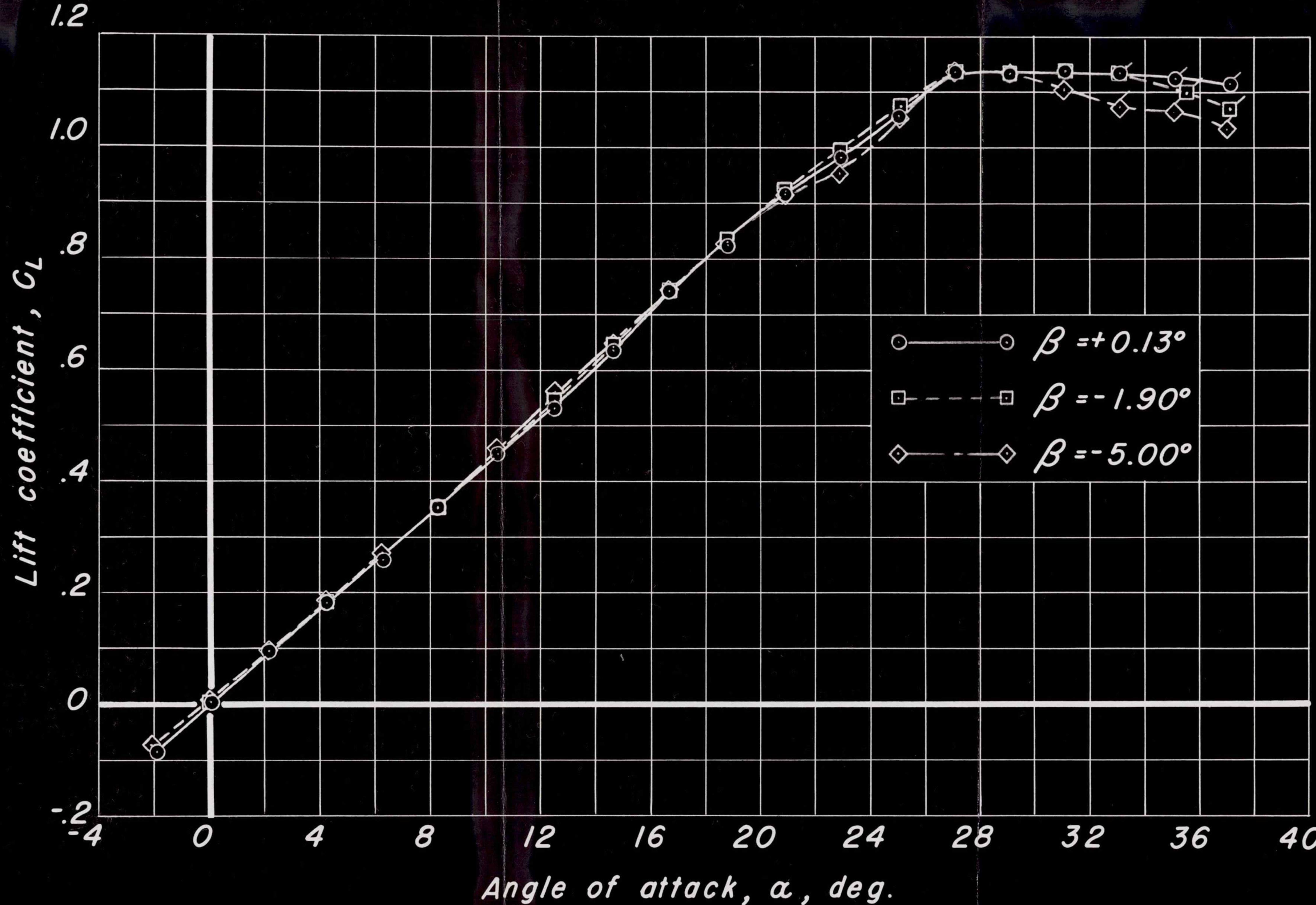

Figure 6. – Aerodynamic characteristics at various angles of sideslip with controls neutral.

NACA 8A8B04

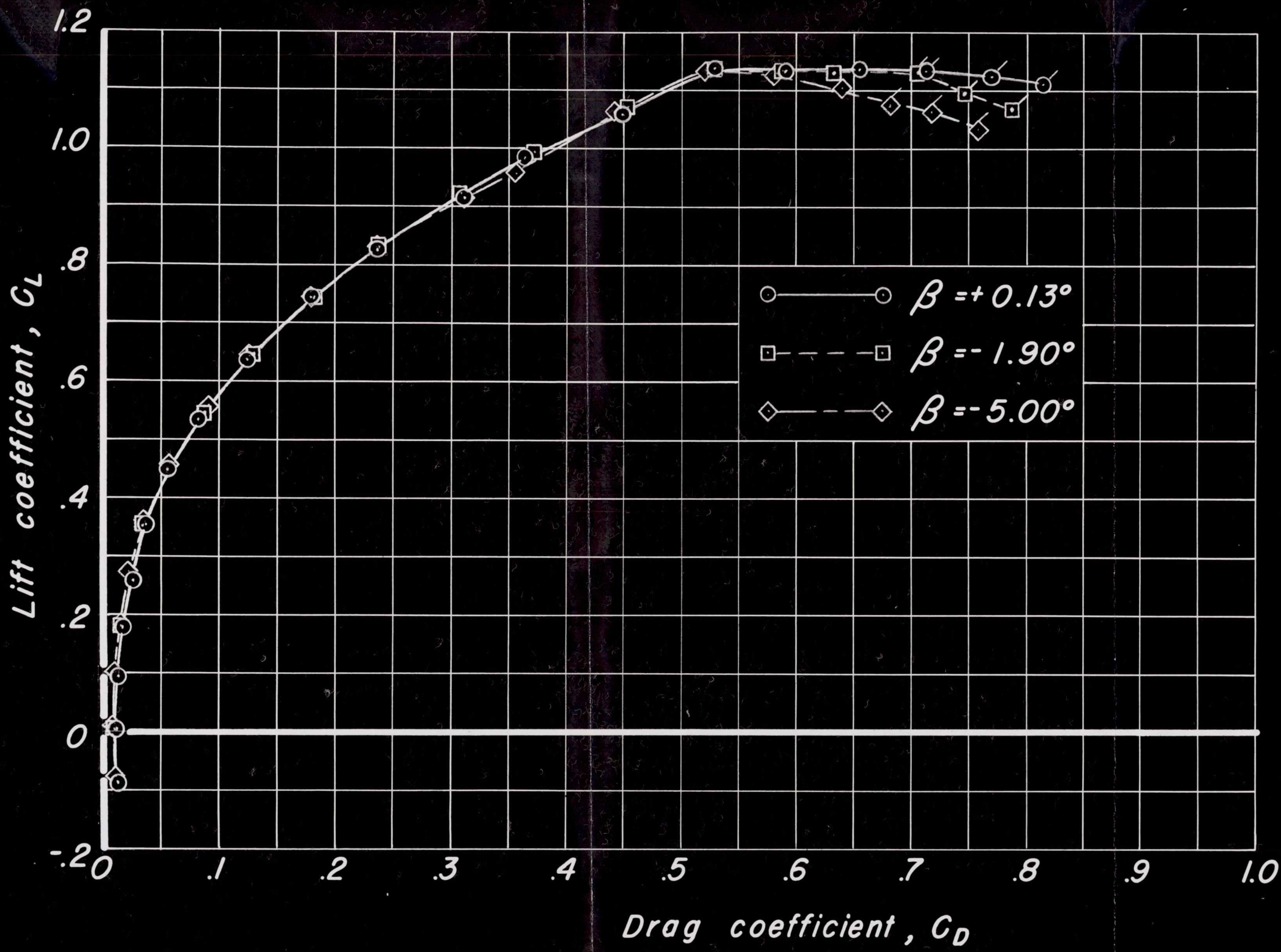

Figure 6. - Continued.

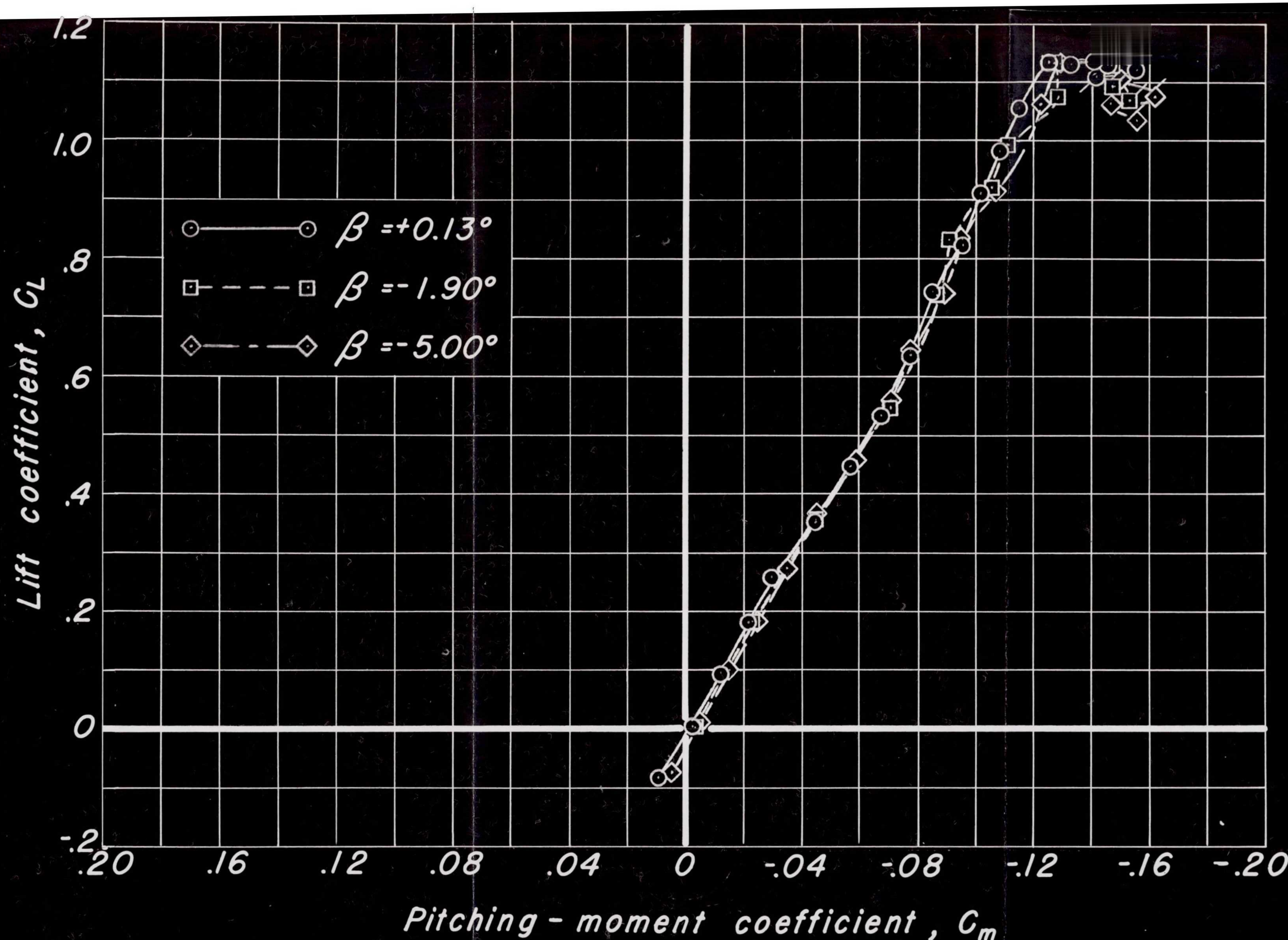

Figure 6. — Continued.

NACA 8A8B04

NACA 8A8B04

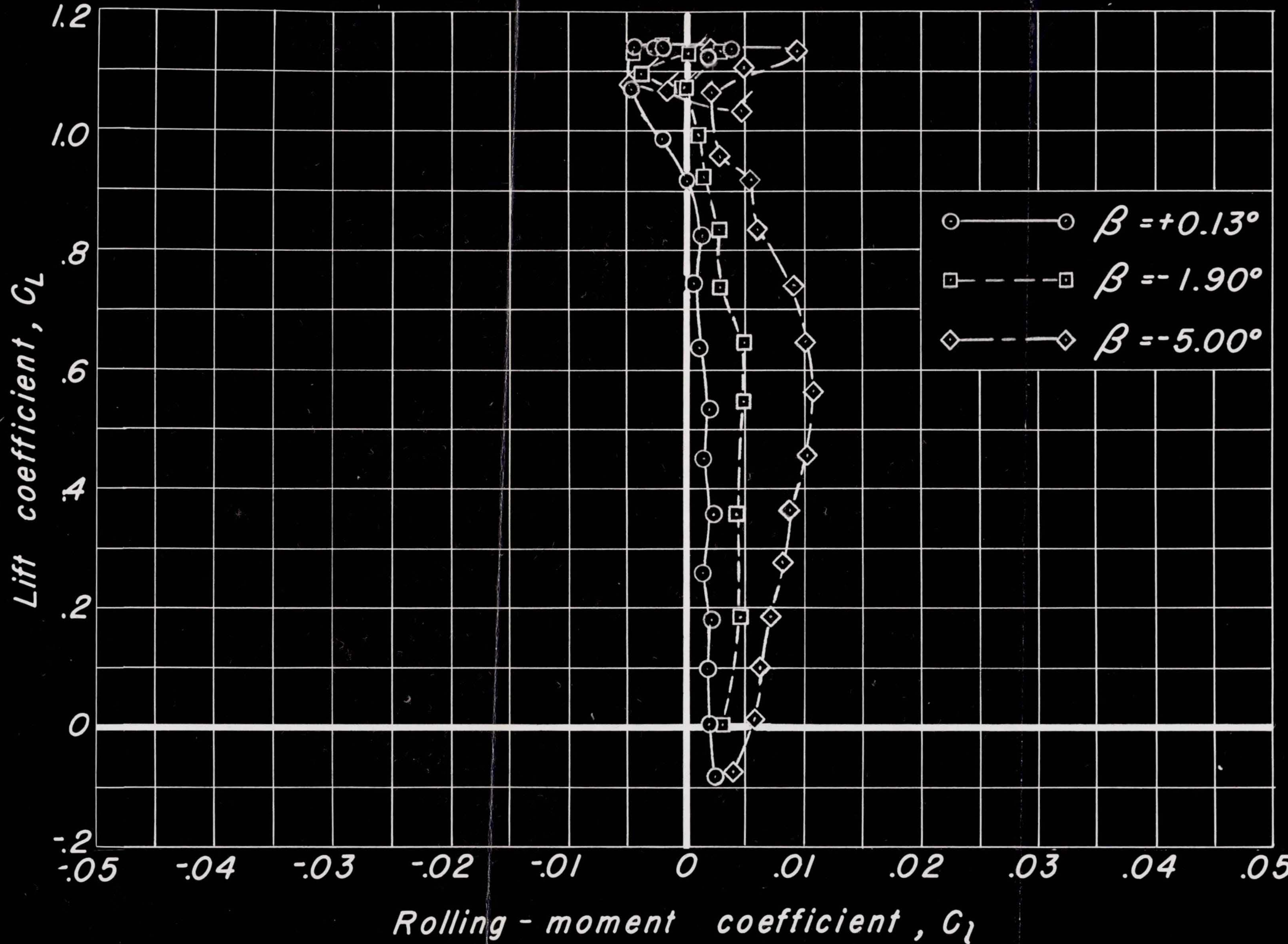

Figure 6. — Continued.

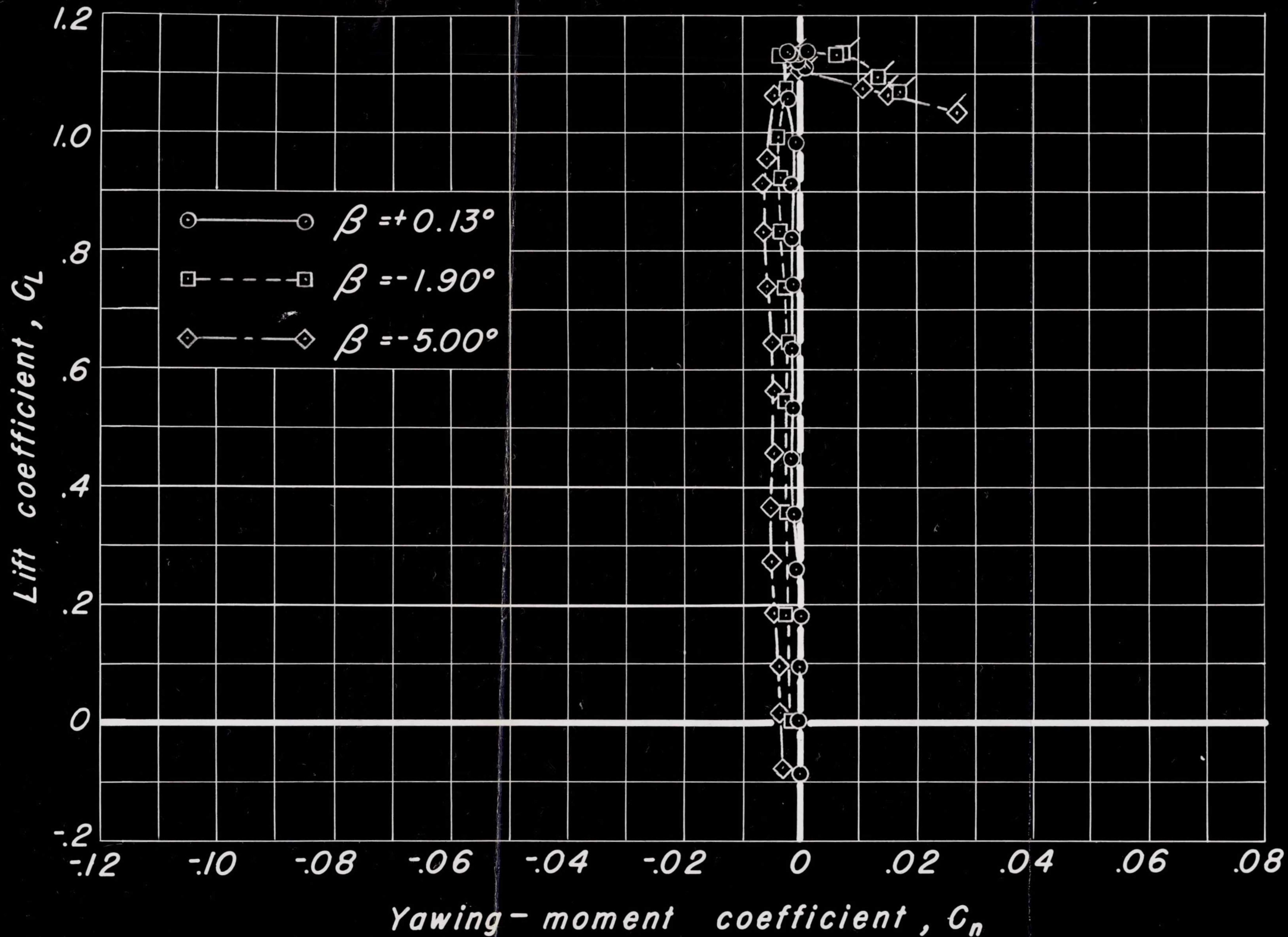

Figure 6. – Continued.

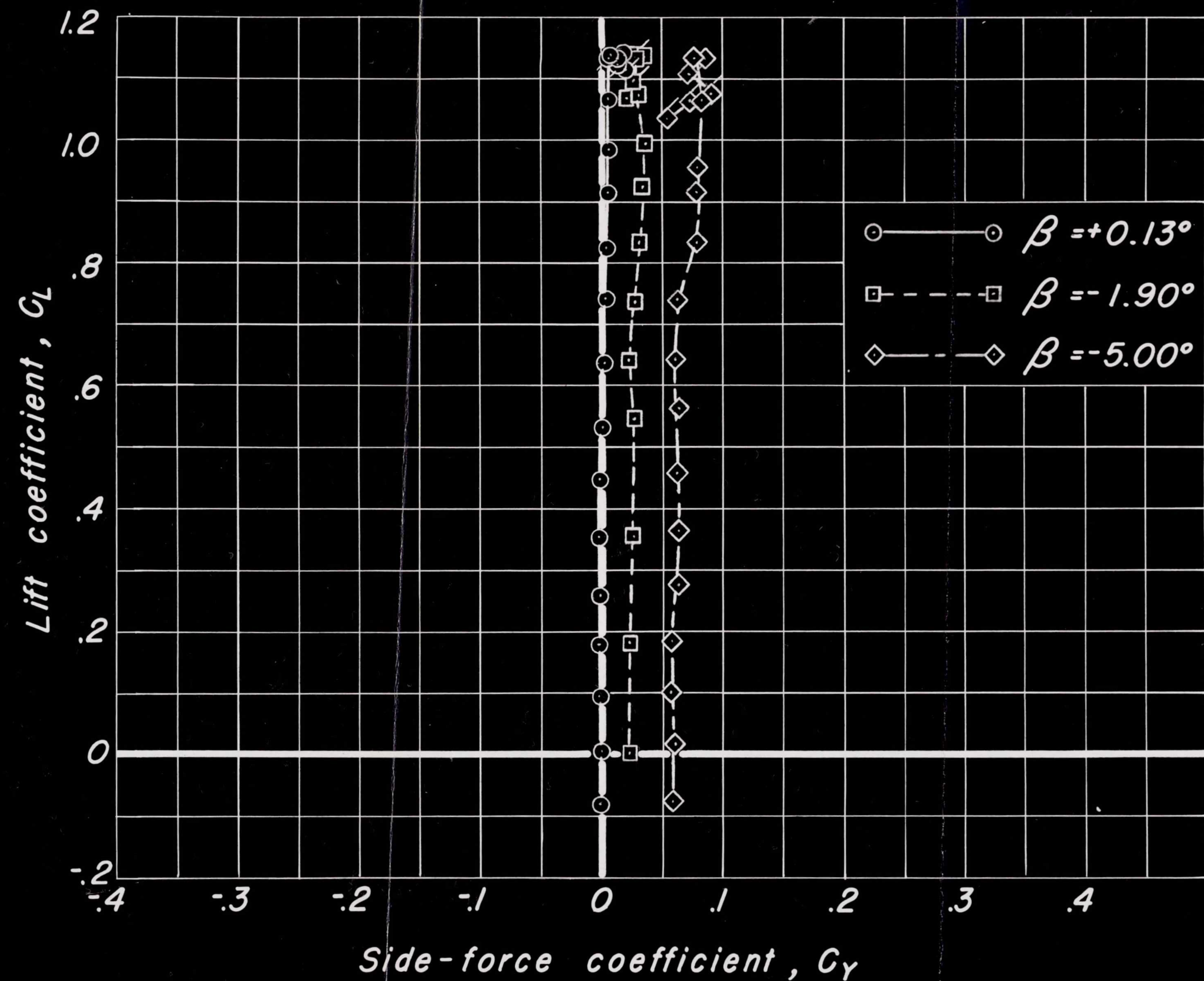

Figure 6. - Concluded.

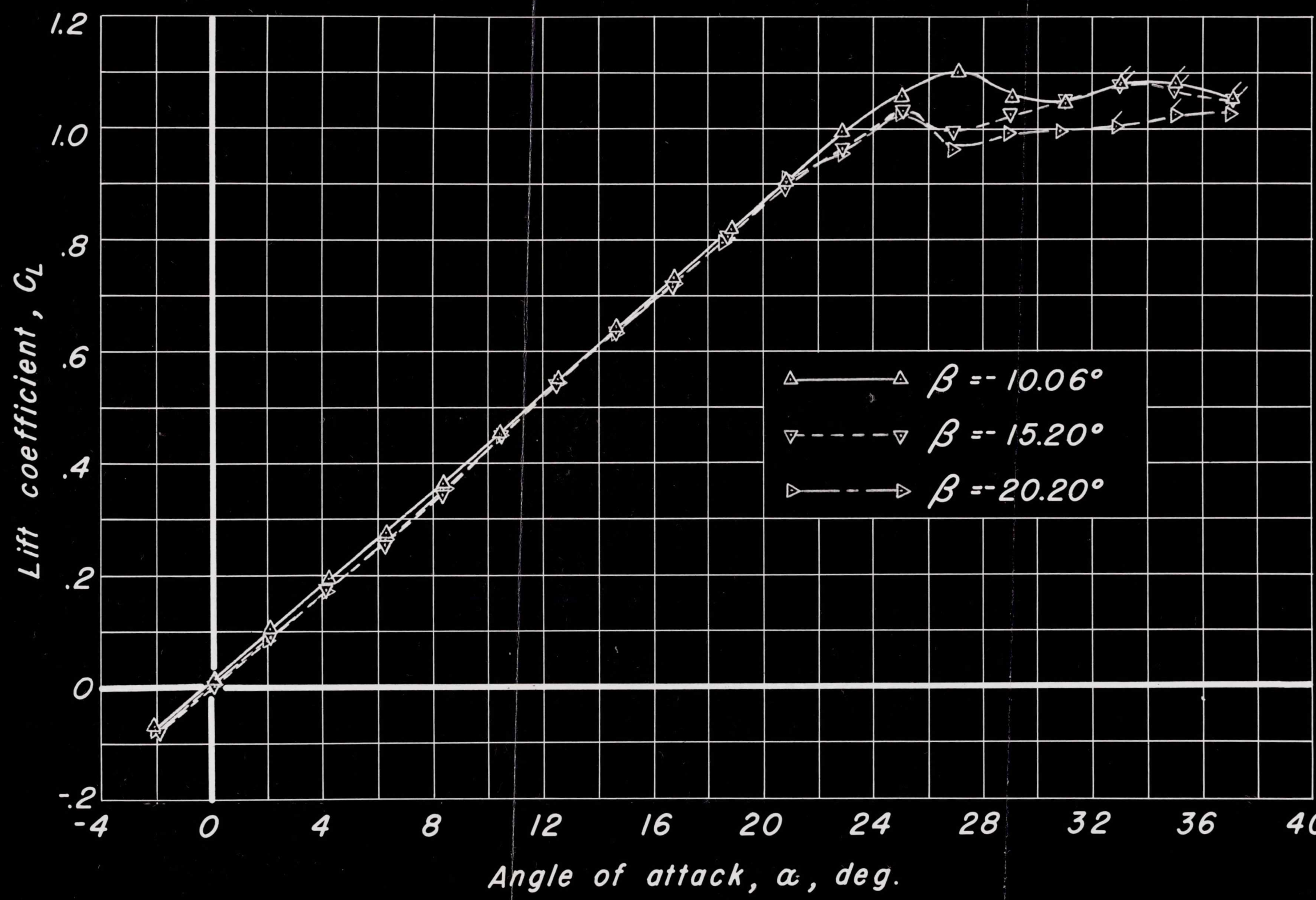

Figure 7. – Aerodynamic characteristics at various angles of sideslip with controls neutral.

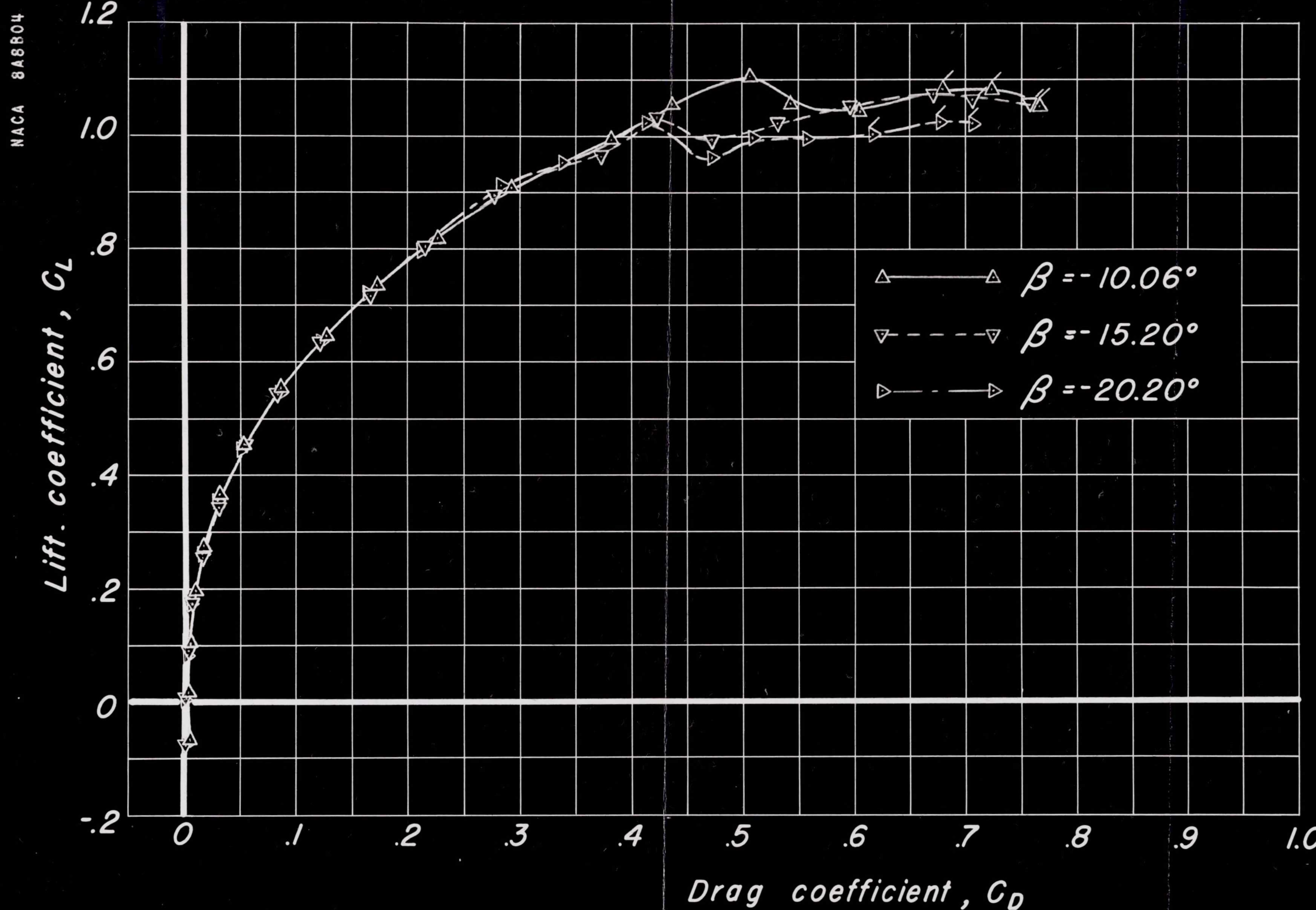

Figure 7. – Continued.

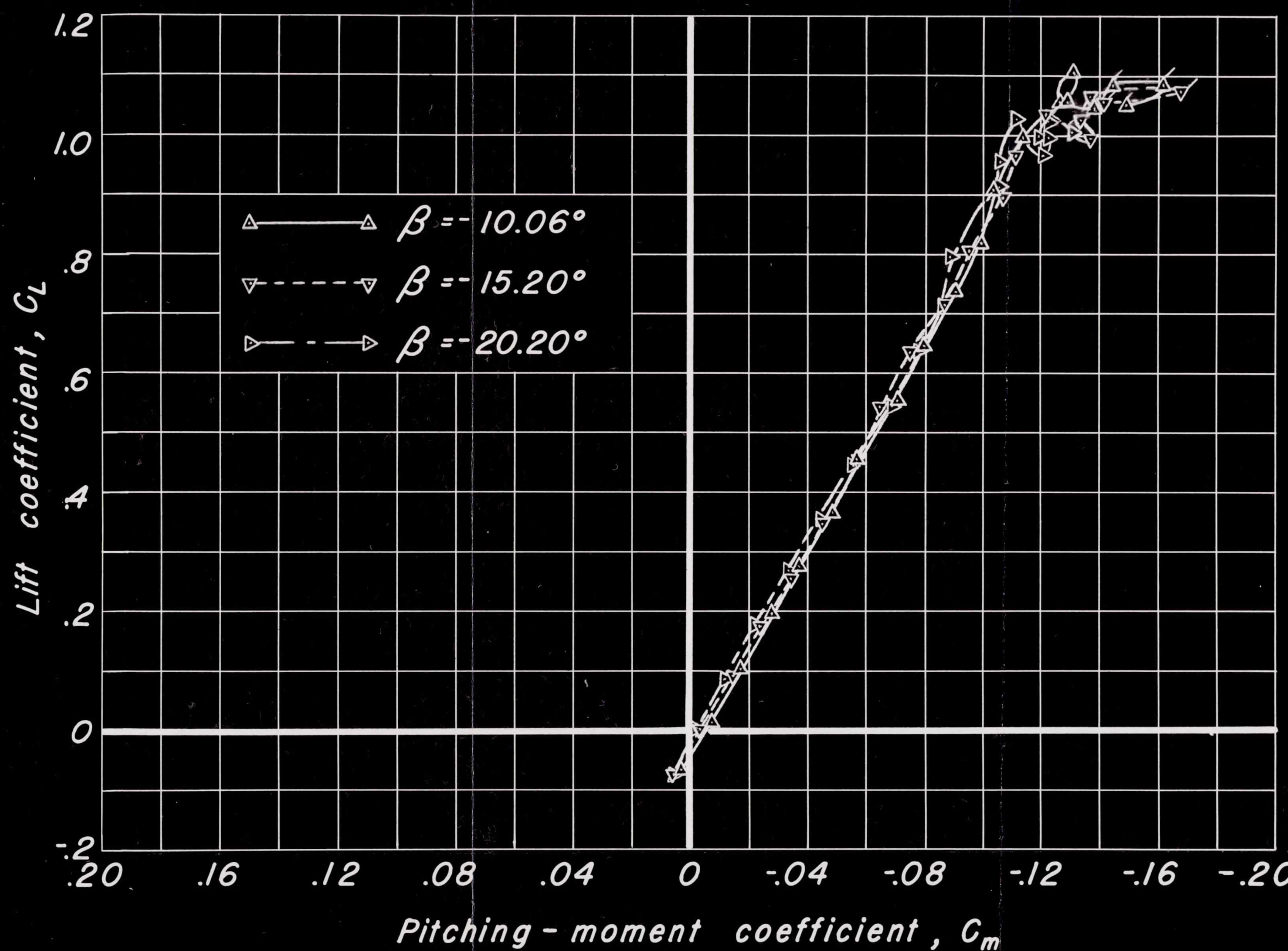

Figure 7. - Continued.

NACA RM A8B04

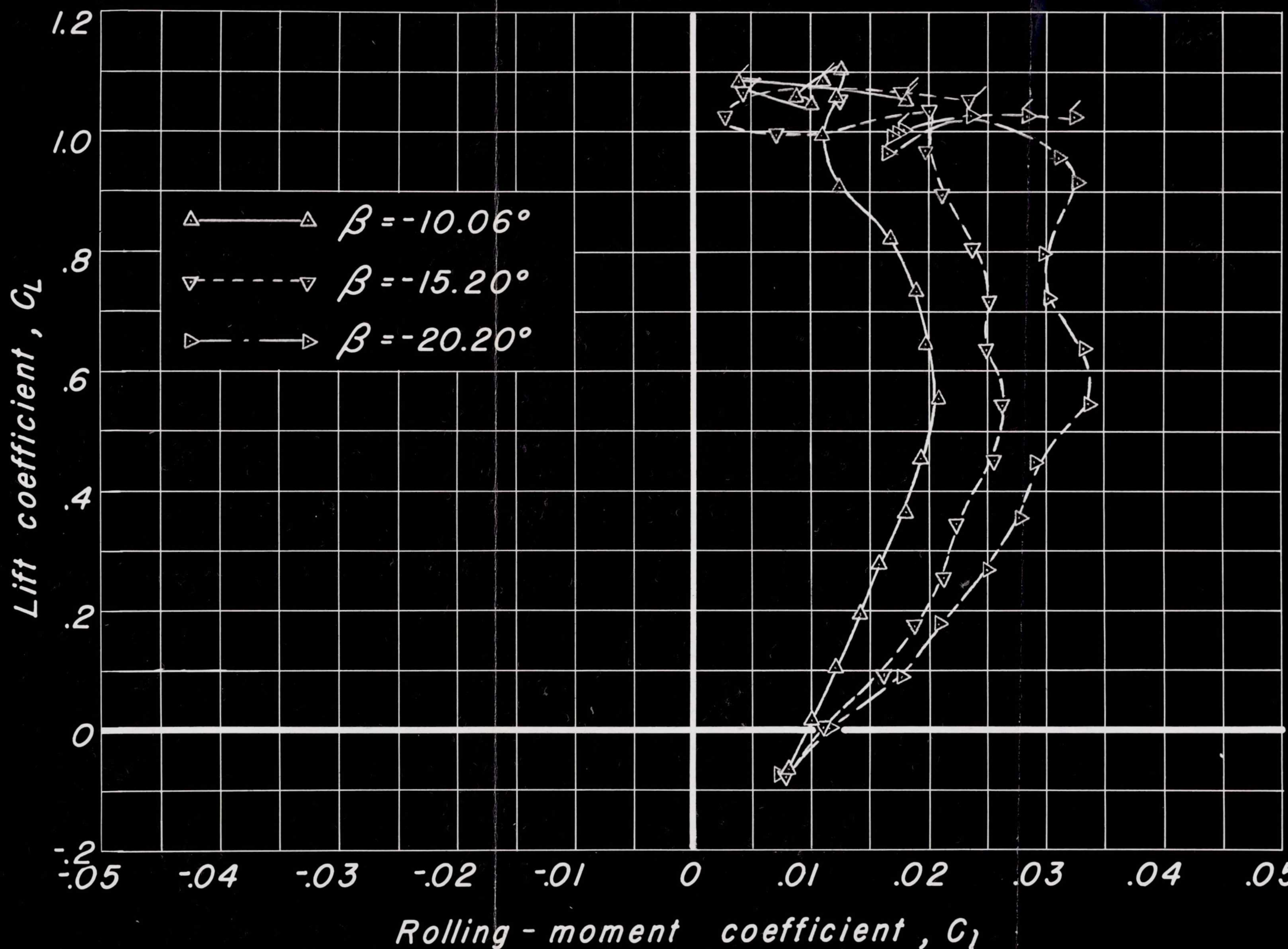

Figure 7. – Continued.

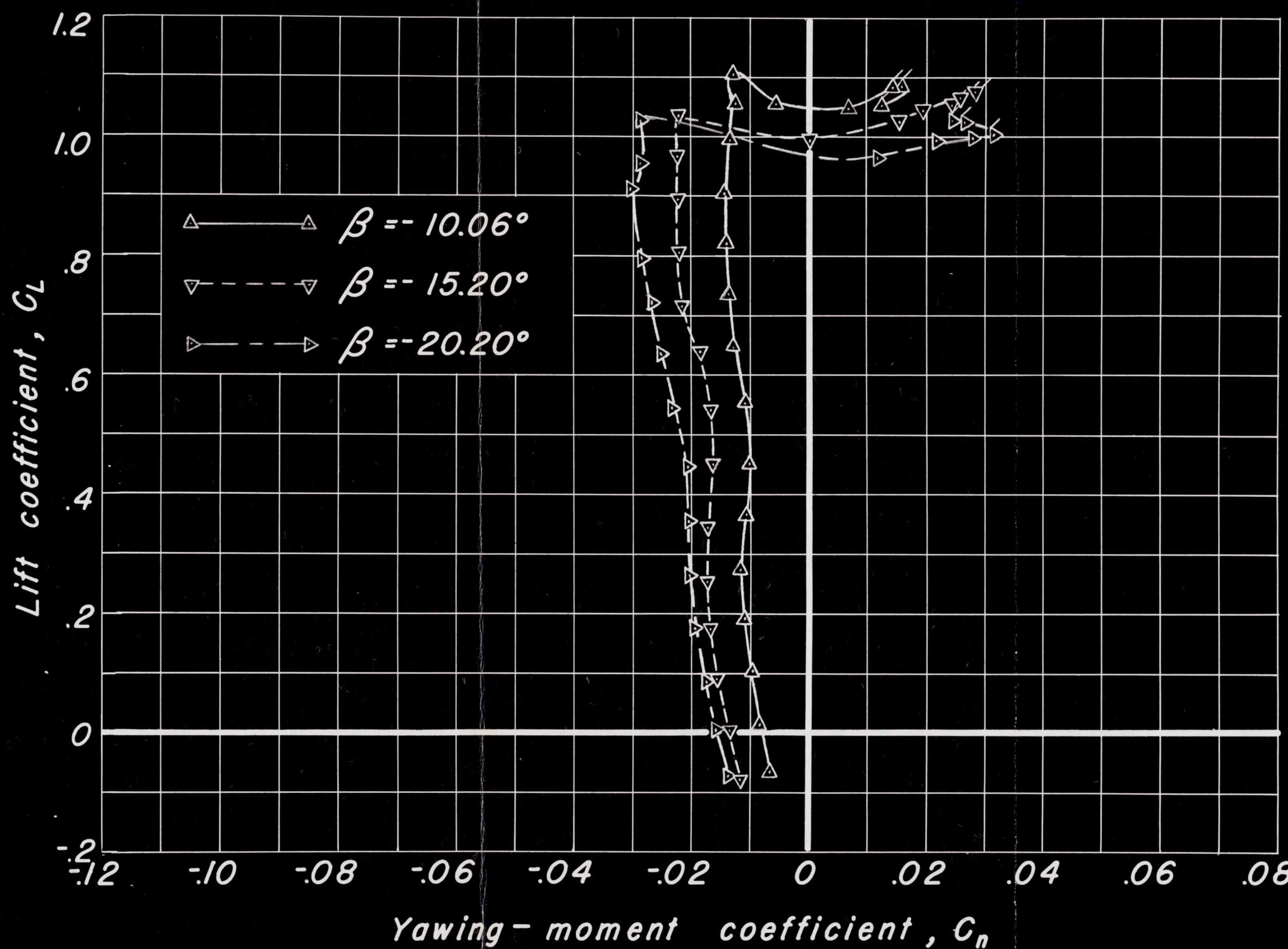

Figure 7. - Continued.

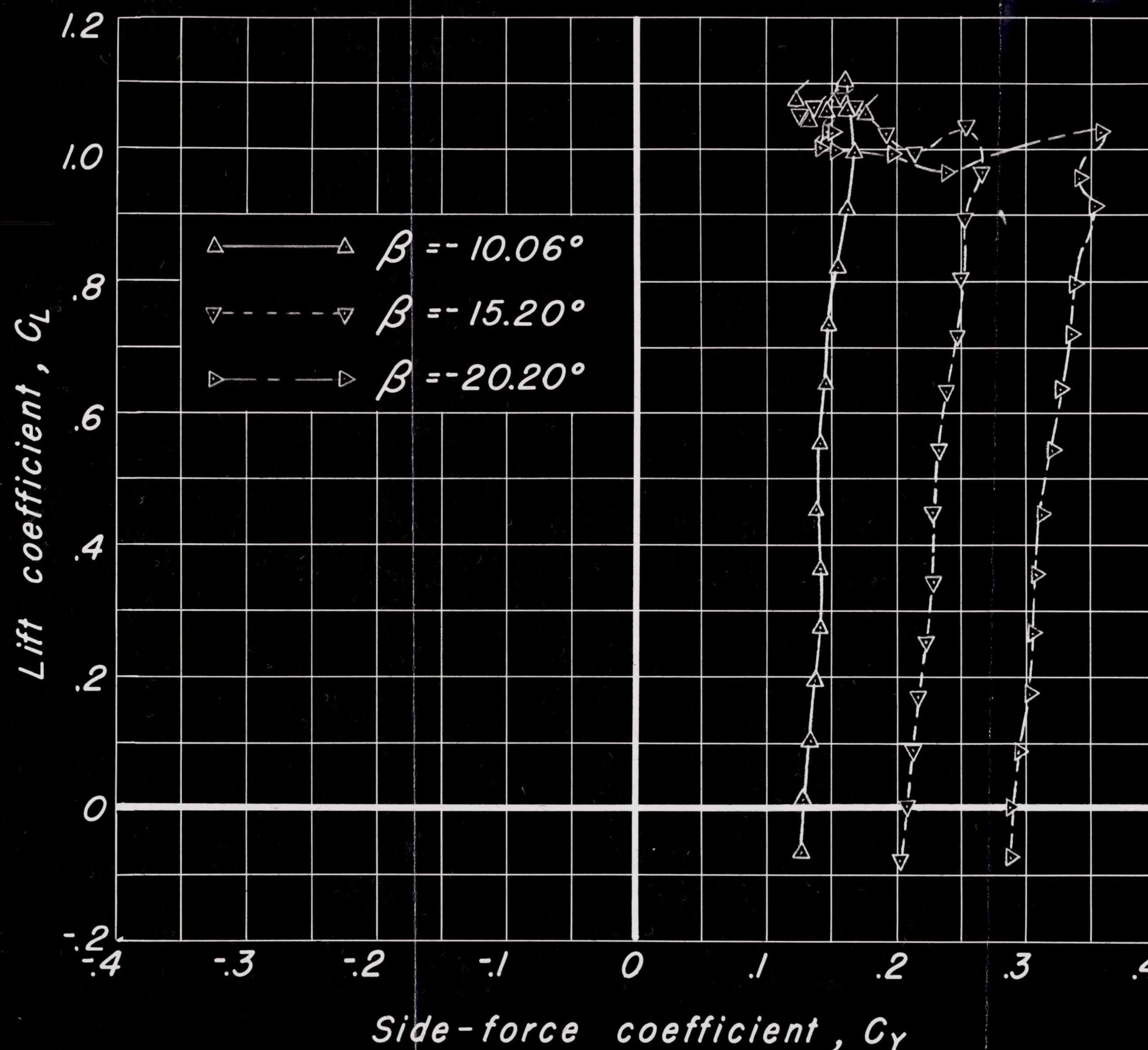

Figure 7. - Concluded.

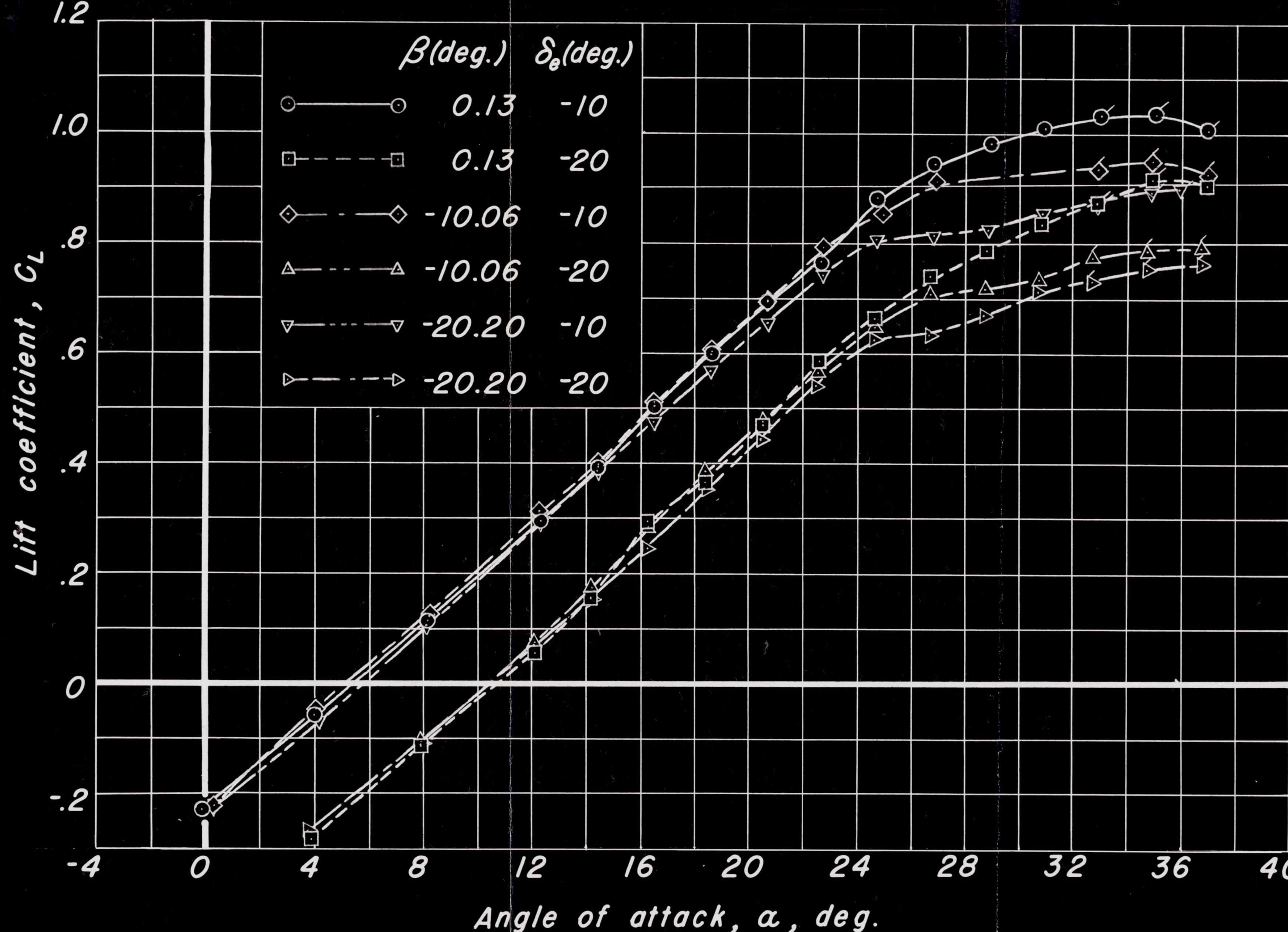

Figure 8. – Longitudinal control effectiveness with undeflected rudder.

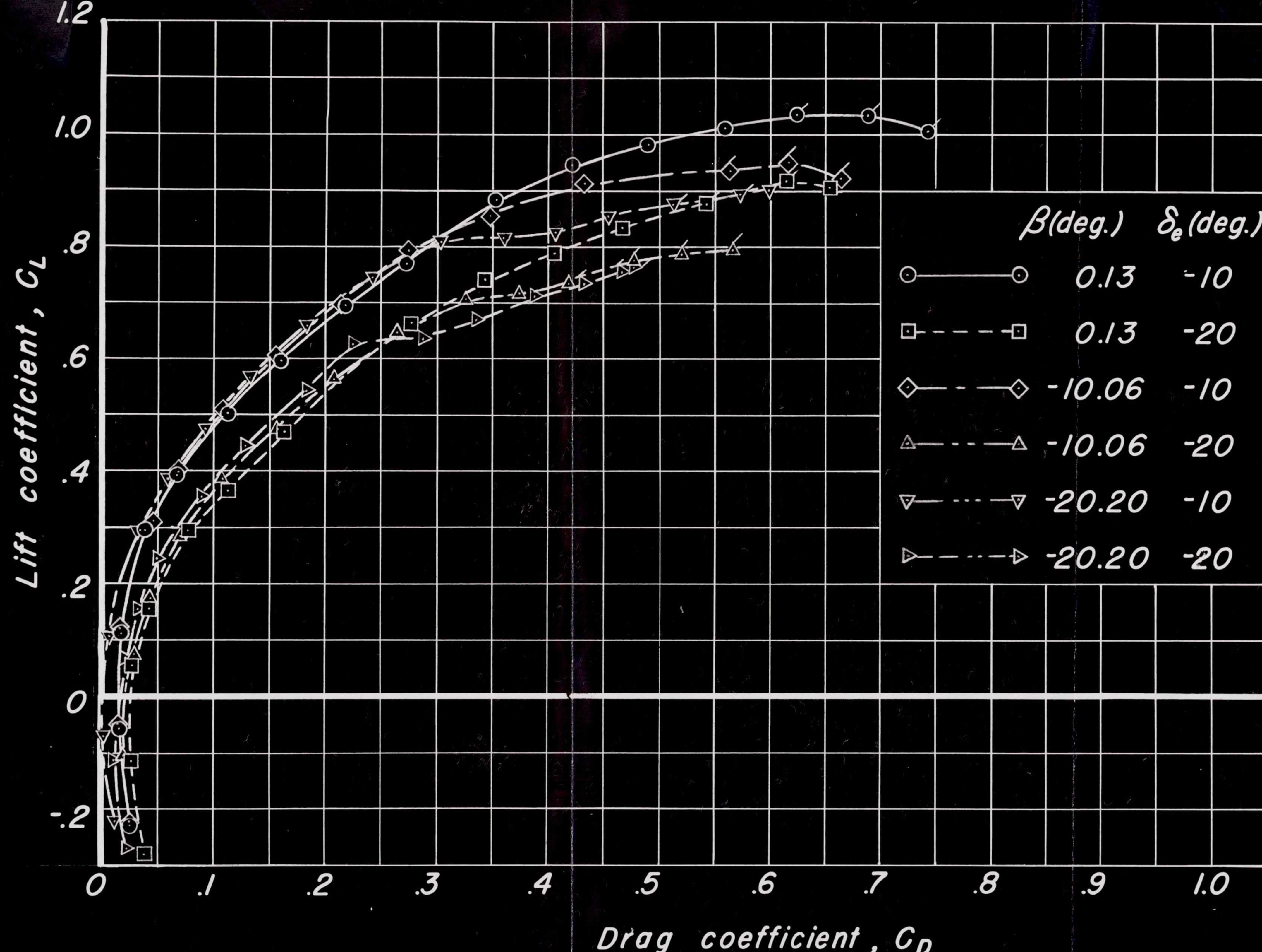

Figure 8. —Continued.

NACA RM A8B04

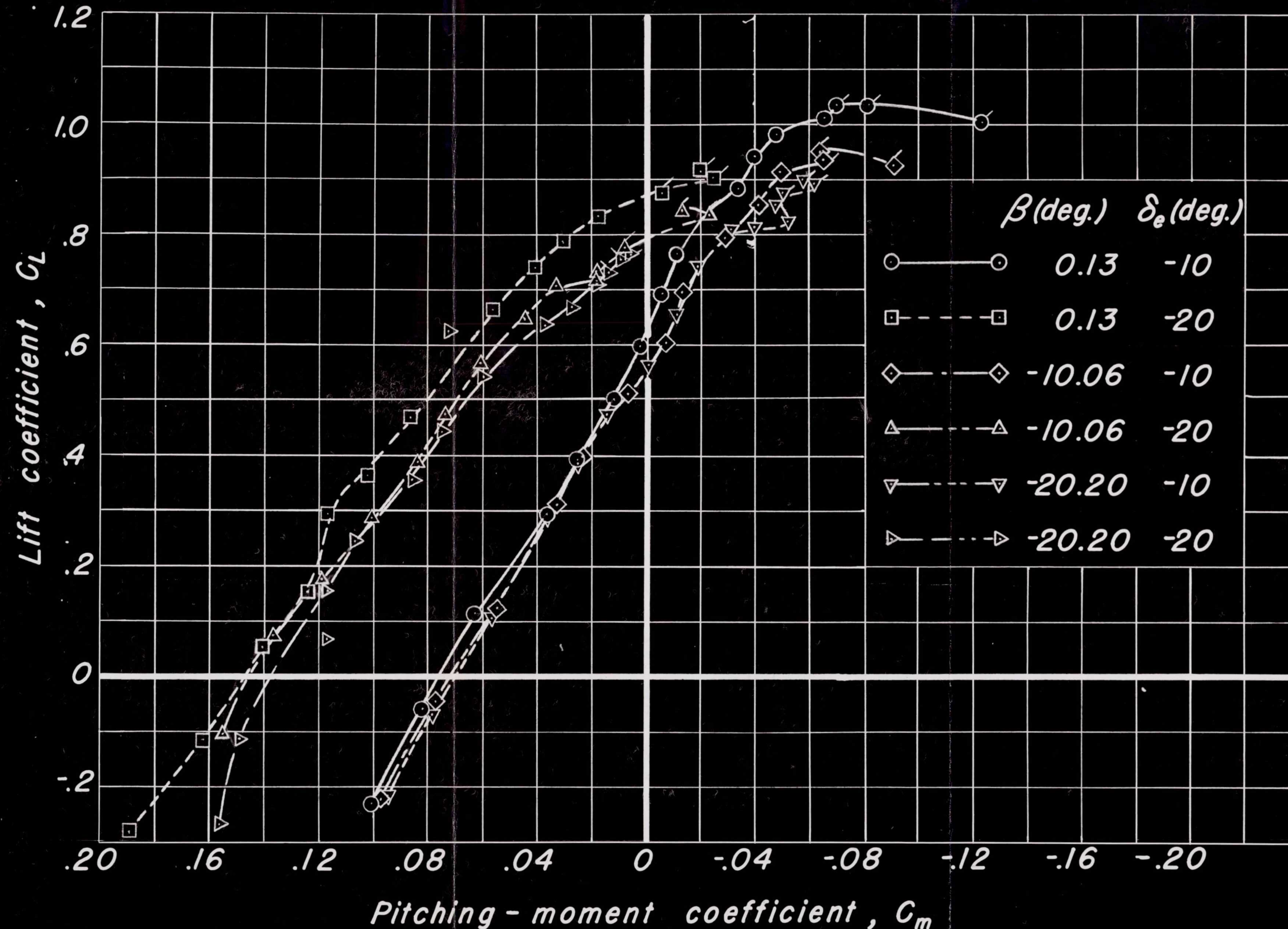

Figure 8. - Continued.

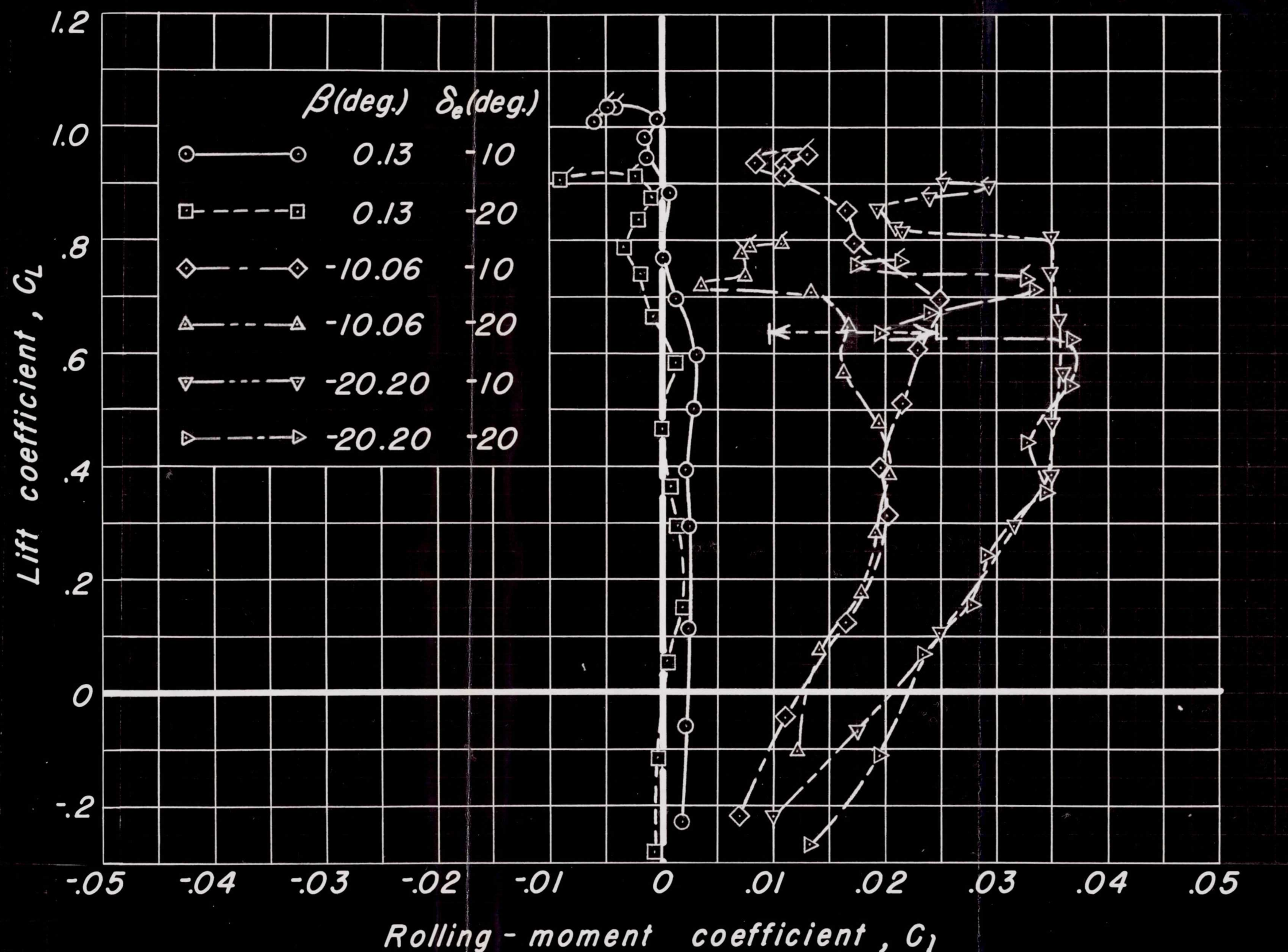

Figure 8. - Continued.

NACA RM SA8B04

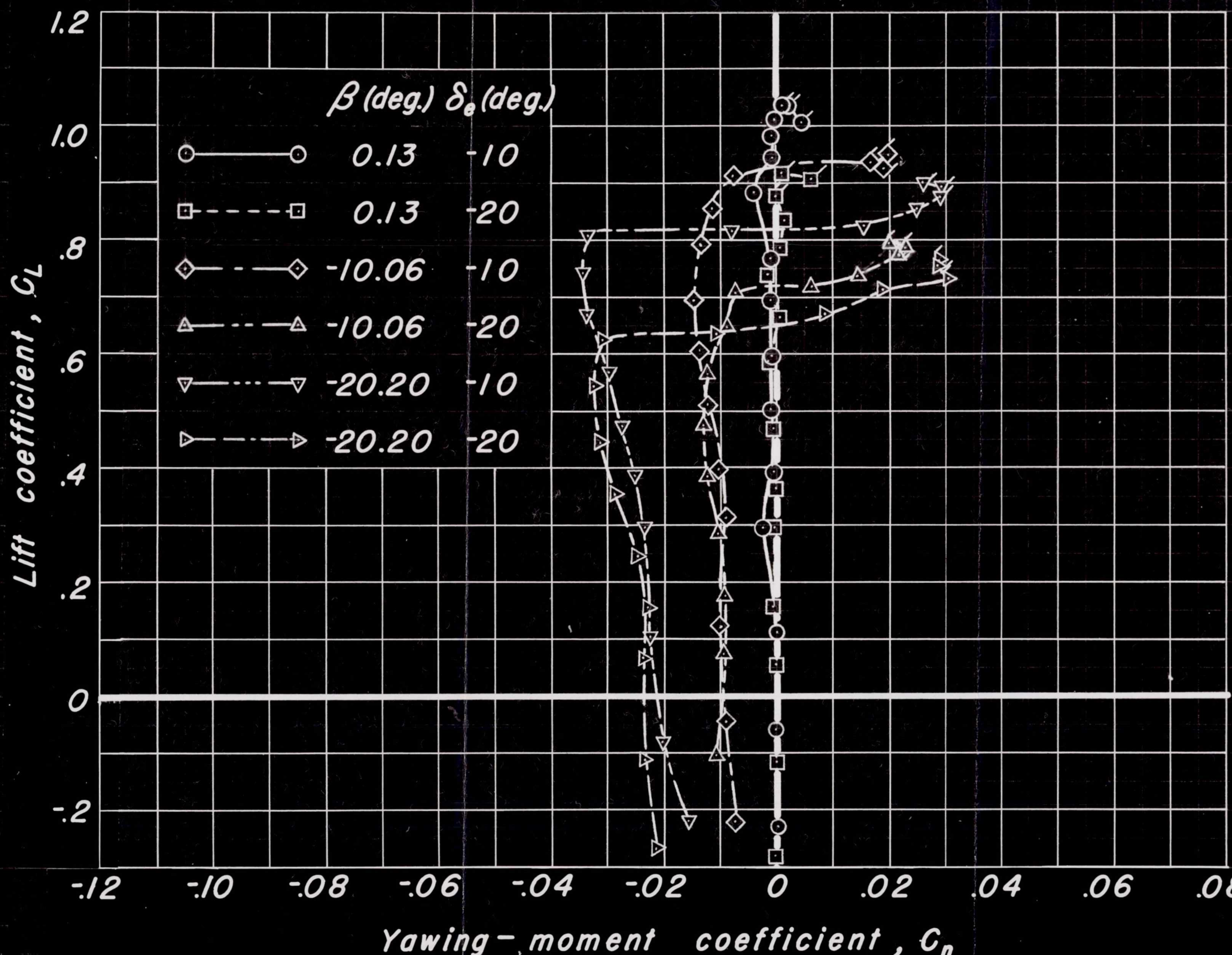

Figure 8. — Continued.

Figure 8. —Concluded.

NACA 8A8B04

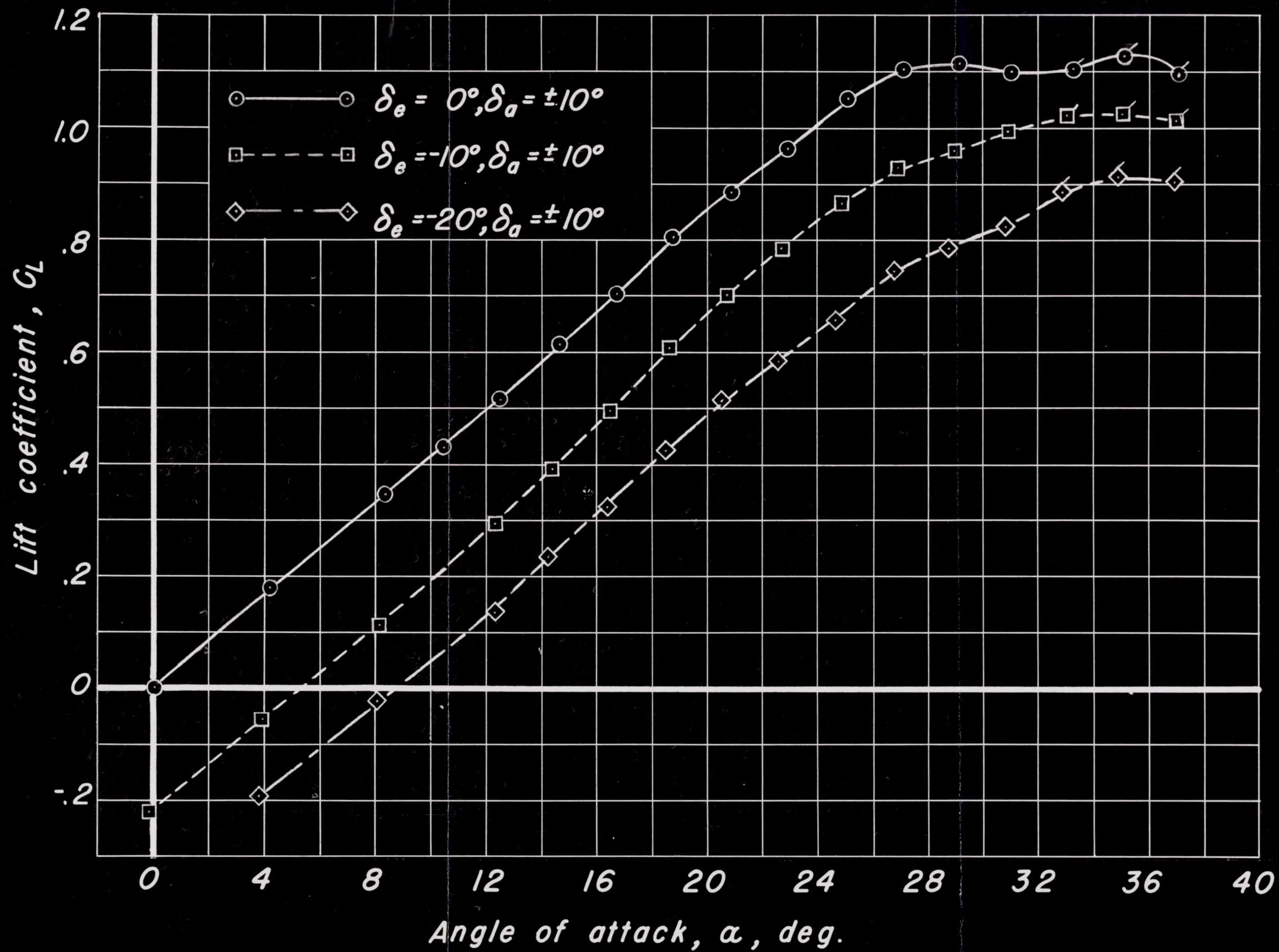

Figure 9. - Longitudinal and lateral control effectiveness with undeflected rudder, $\beta = 0.13°$.

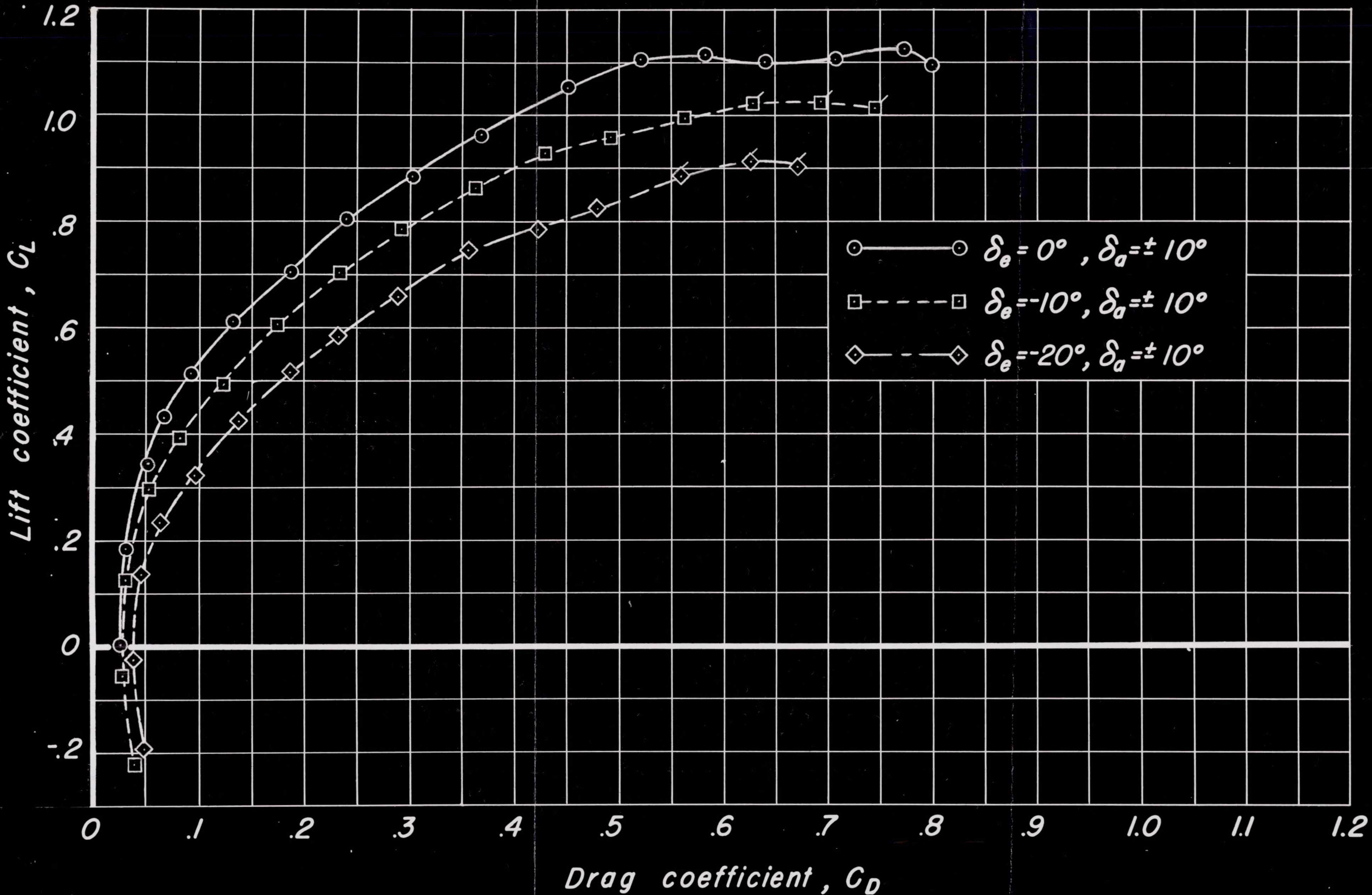

Figure 9. - Continued.

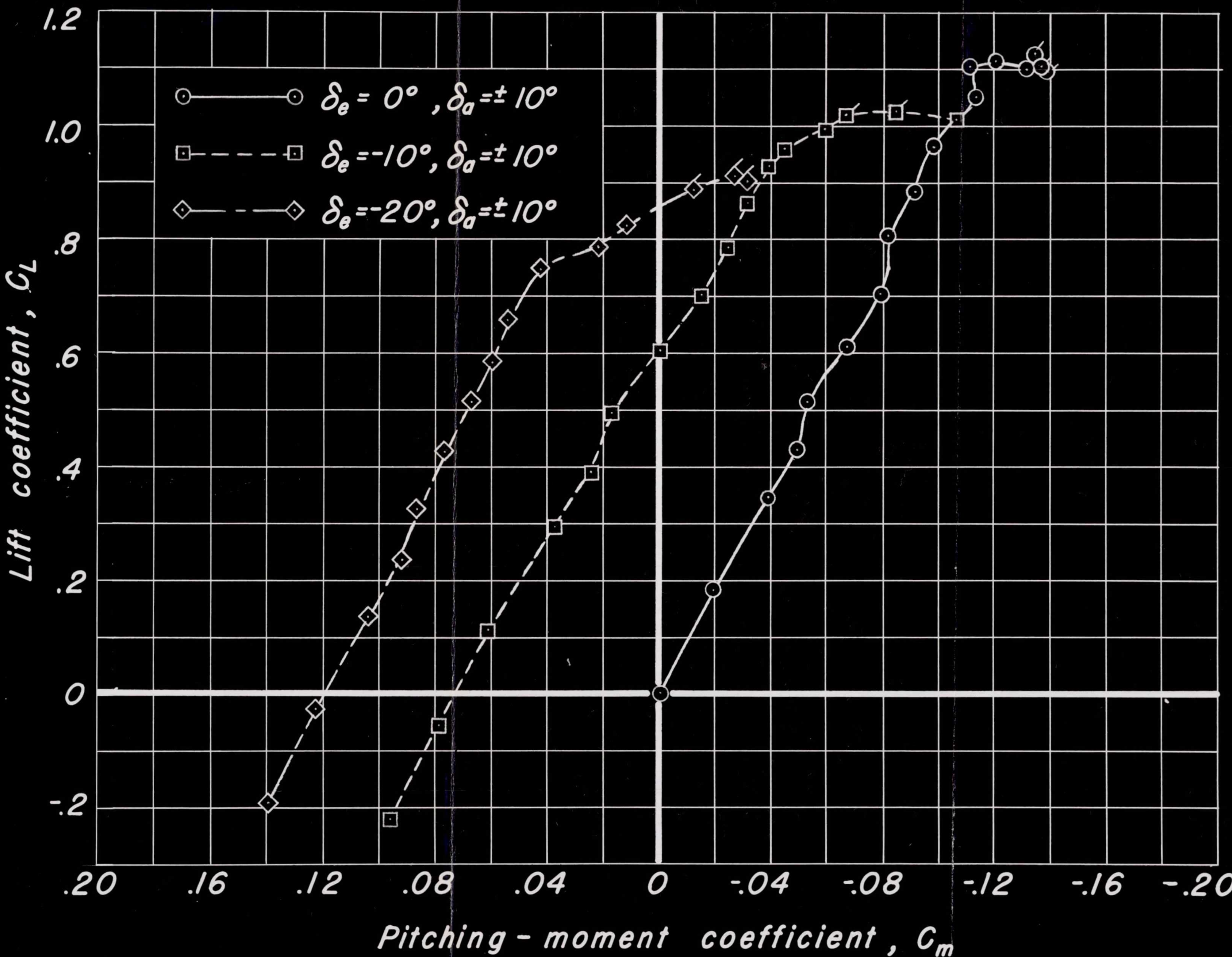

Figure 9. - Continued.

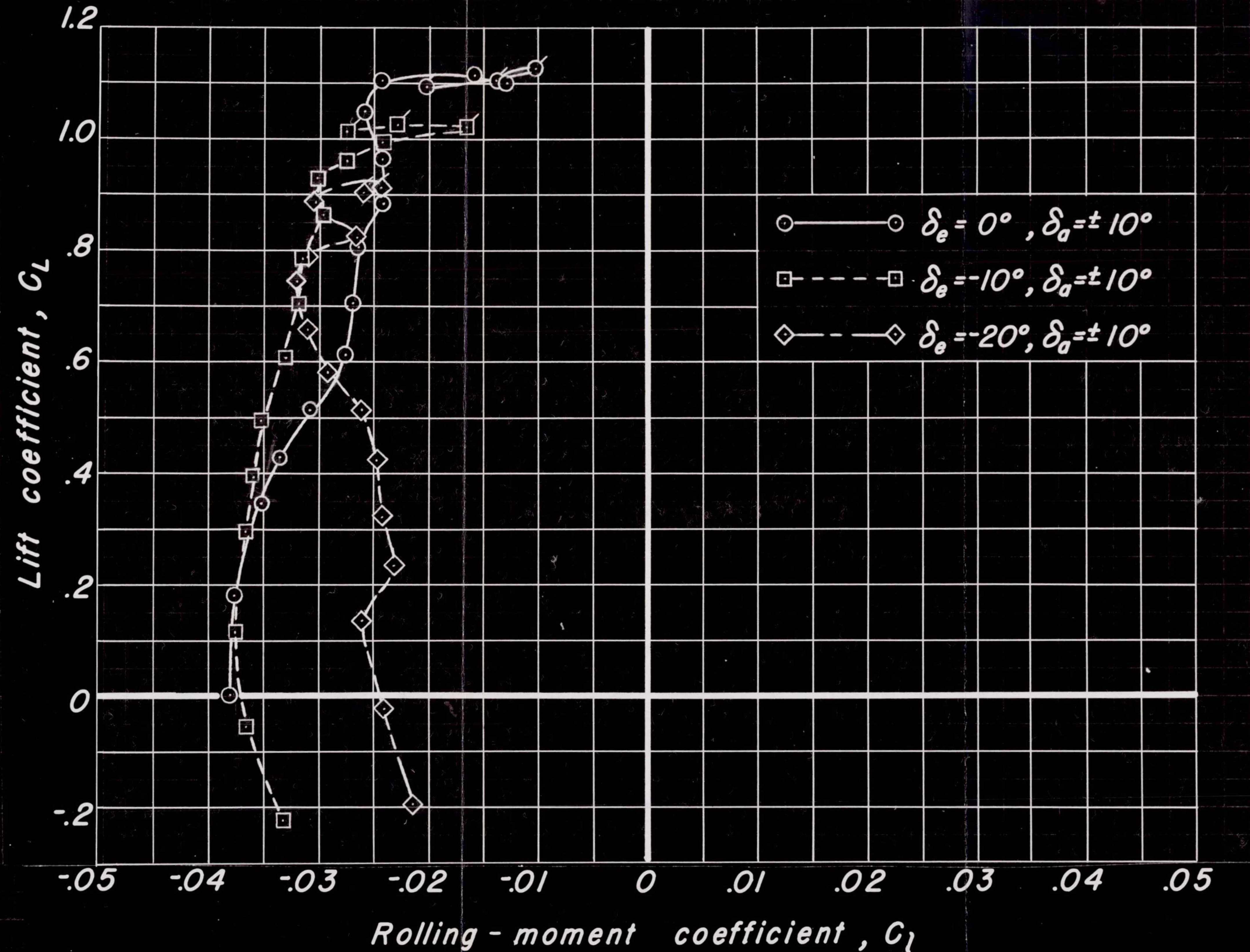

Figure 9. -Continued.

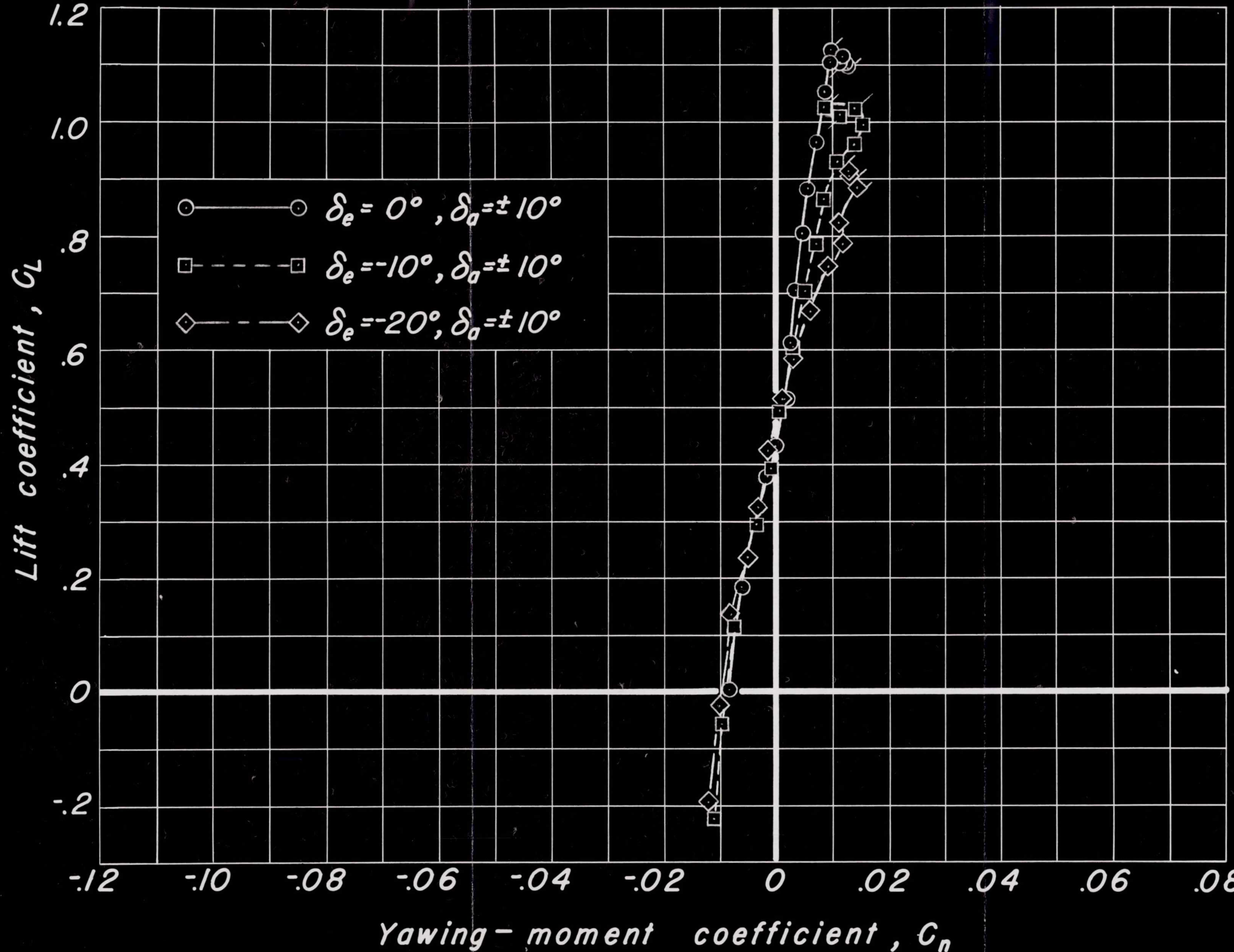

Figure 9. - Continued.

NACA RM A8B04

Figure 9. - Concluded.

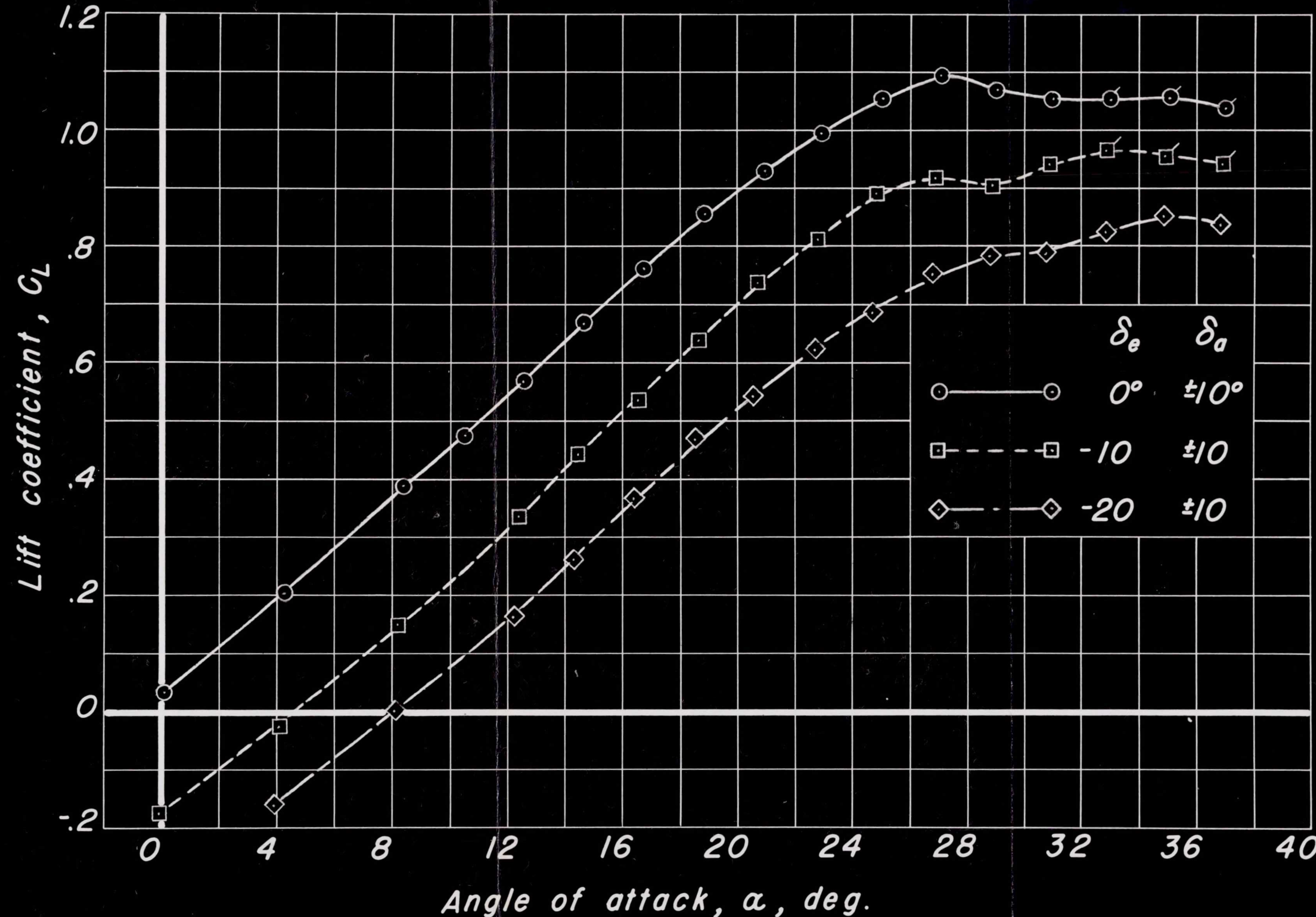

Figure 10.—Longitudinal and lateral control effectiveness with undeflected rudder, $\beta = -10.06°$.

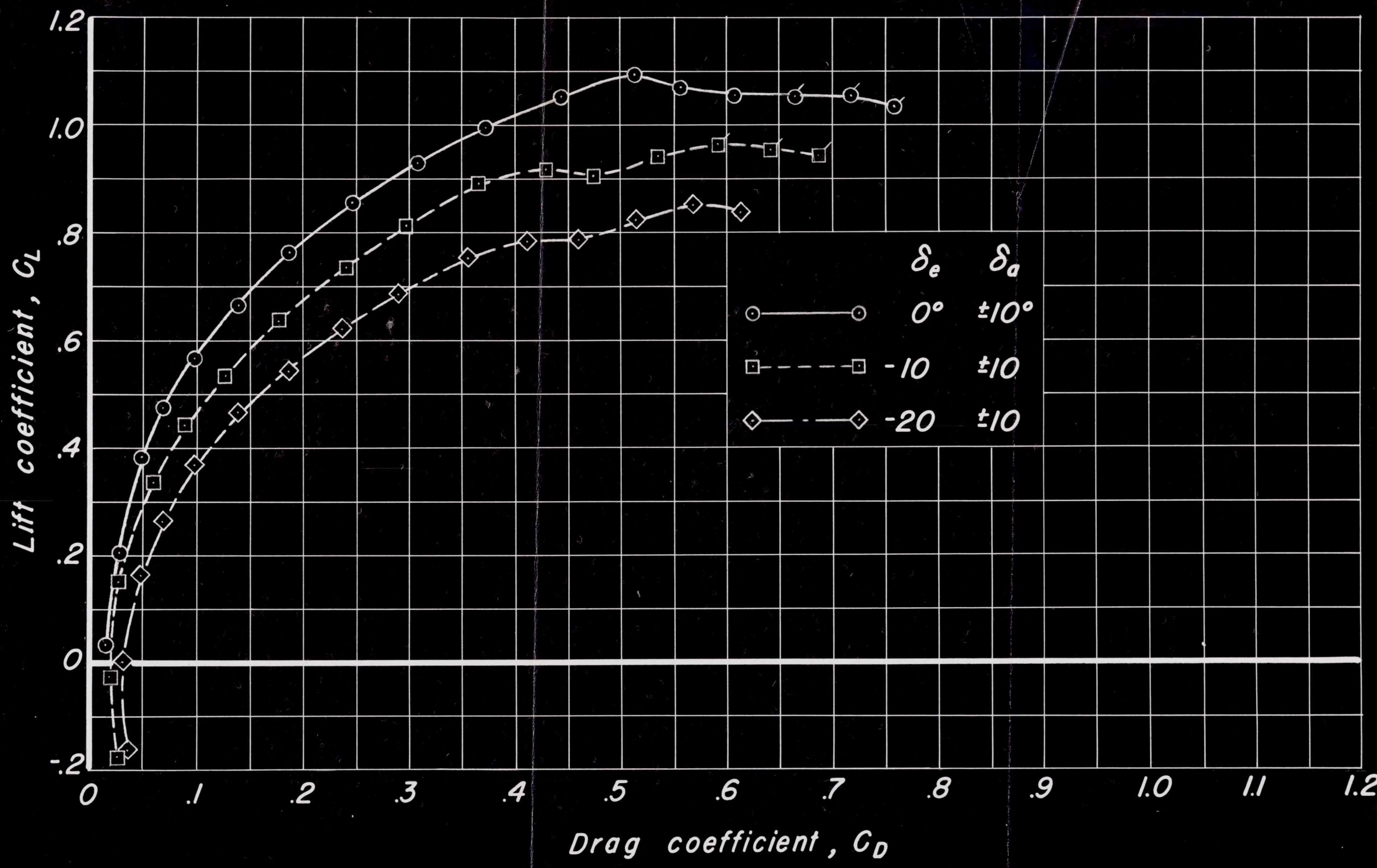

Figure 10.— Continued.

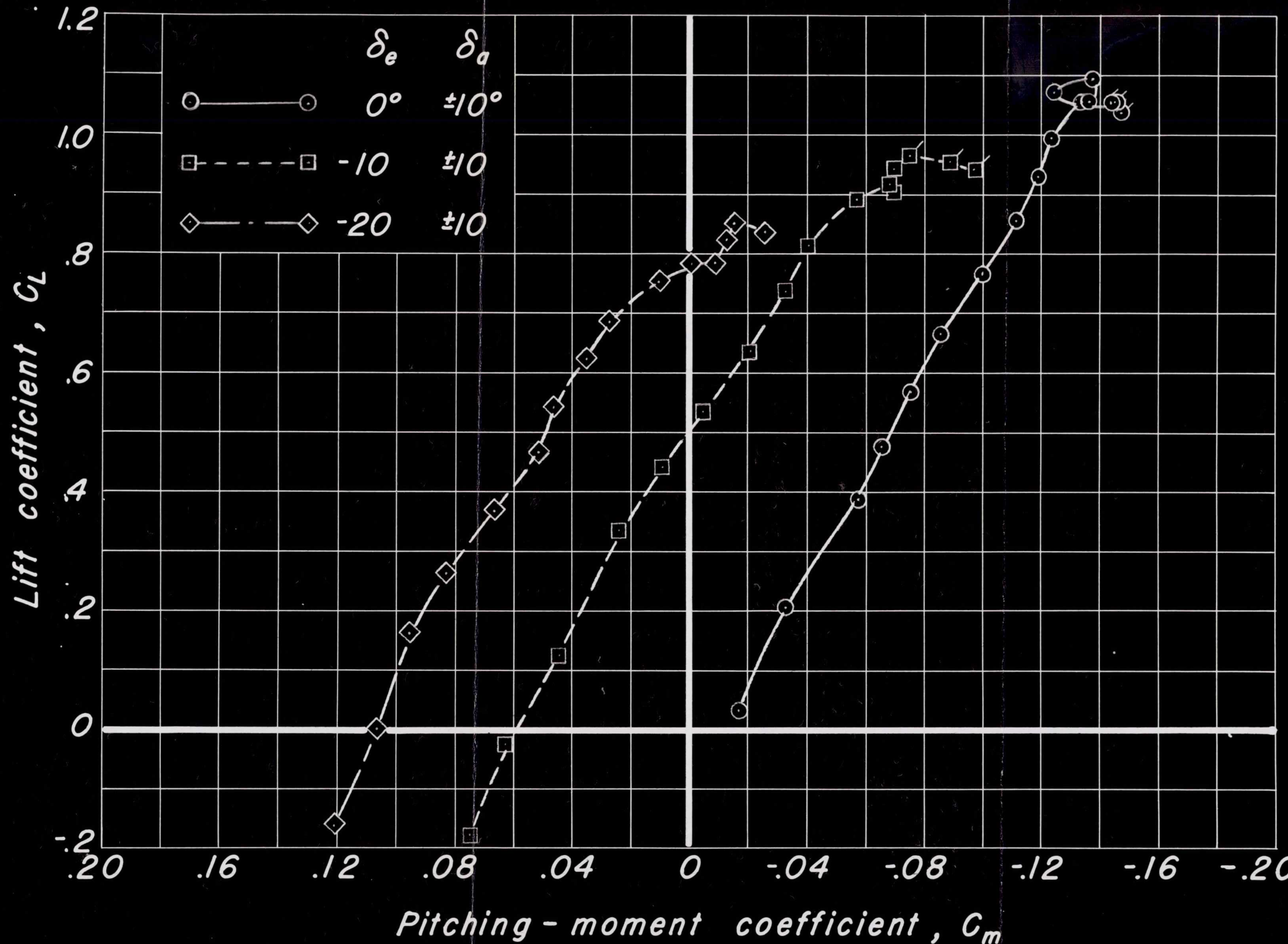

Figure 10.— Continued.

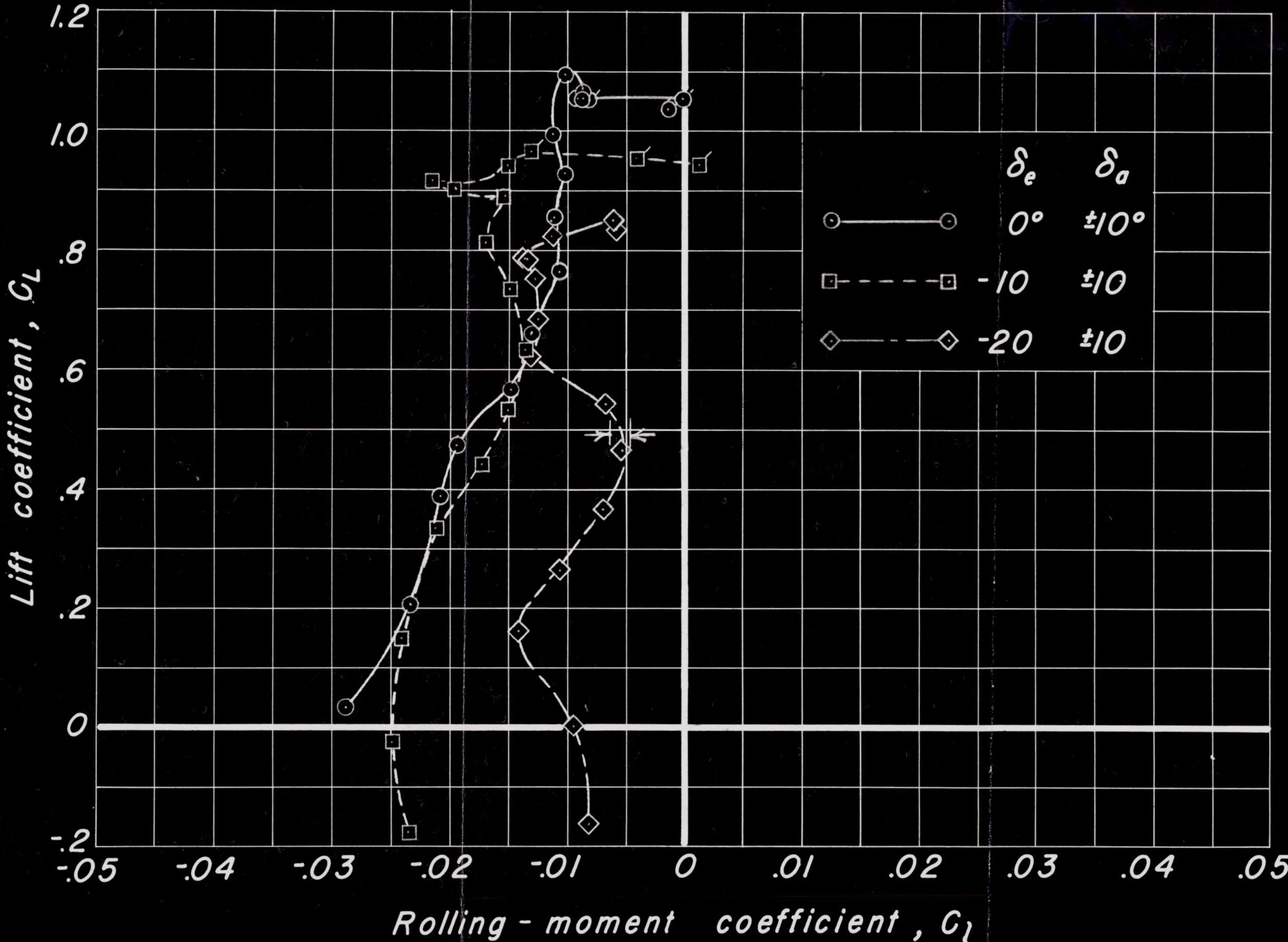

Figure 10.—Continued.

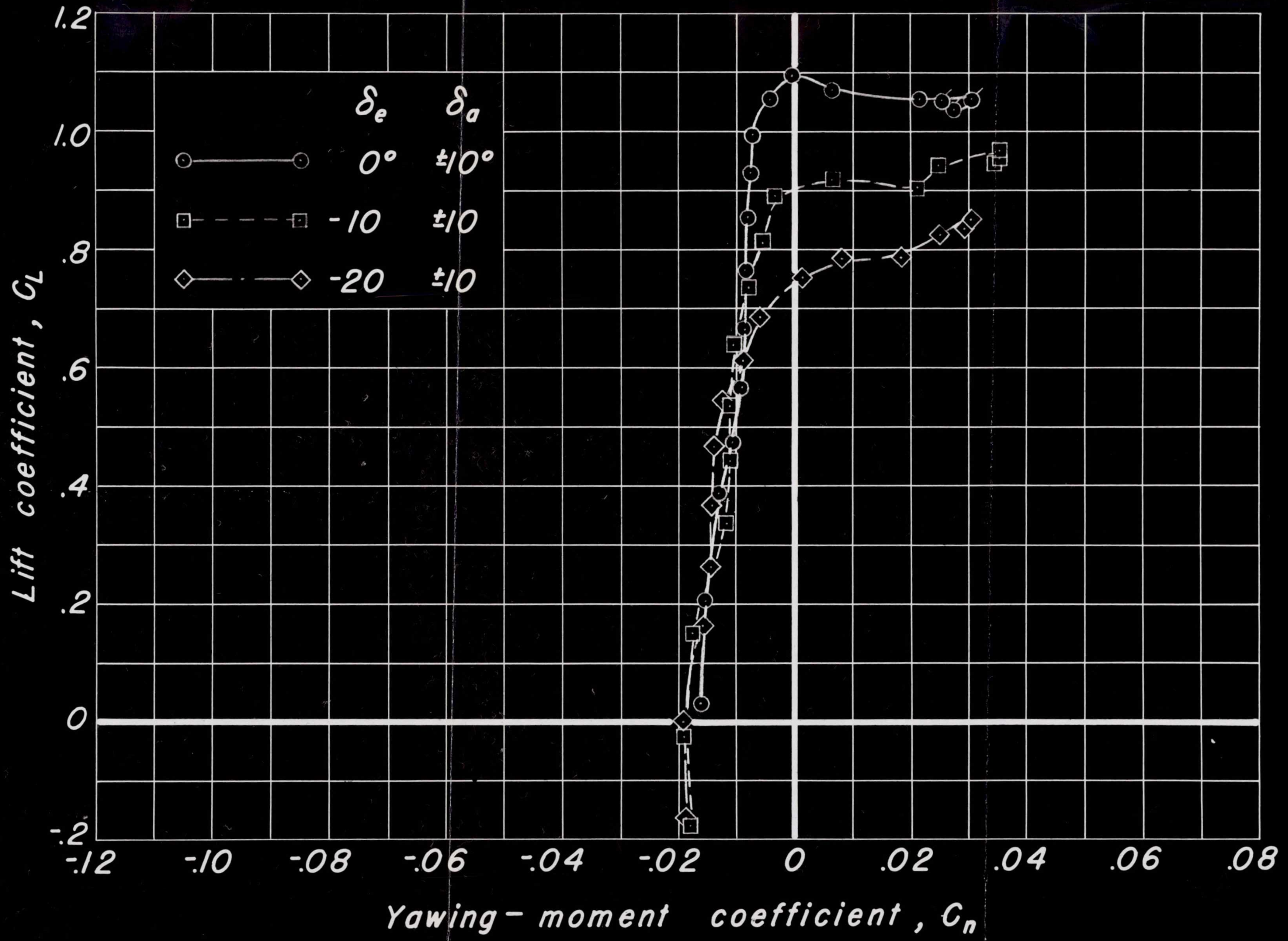

Figure 10.– Continued.

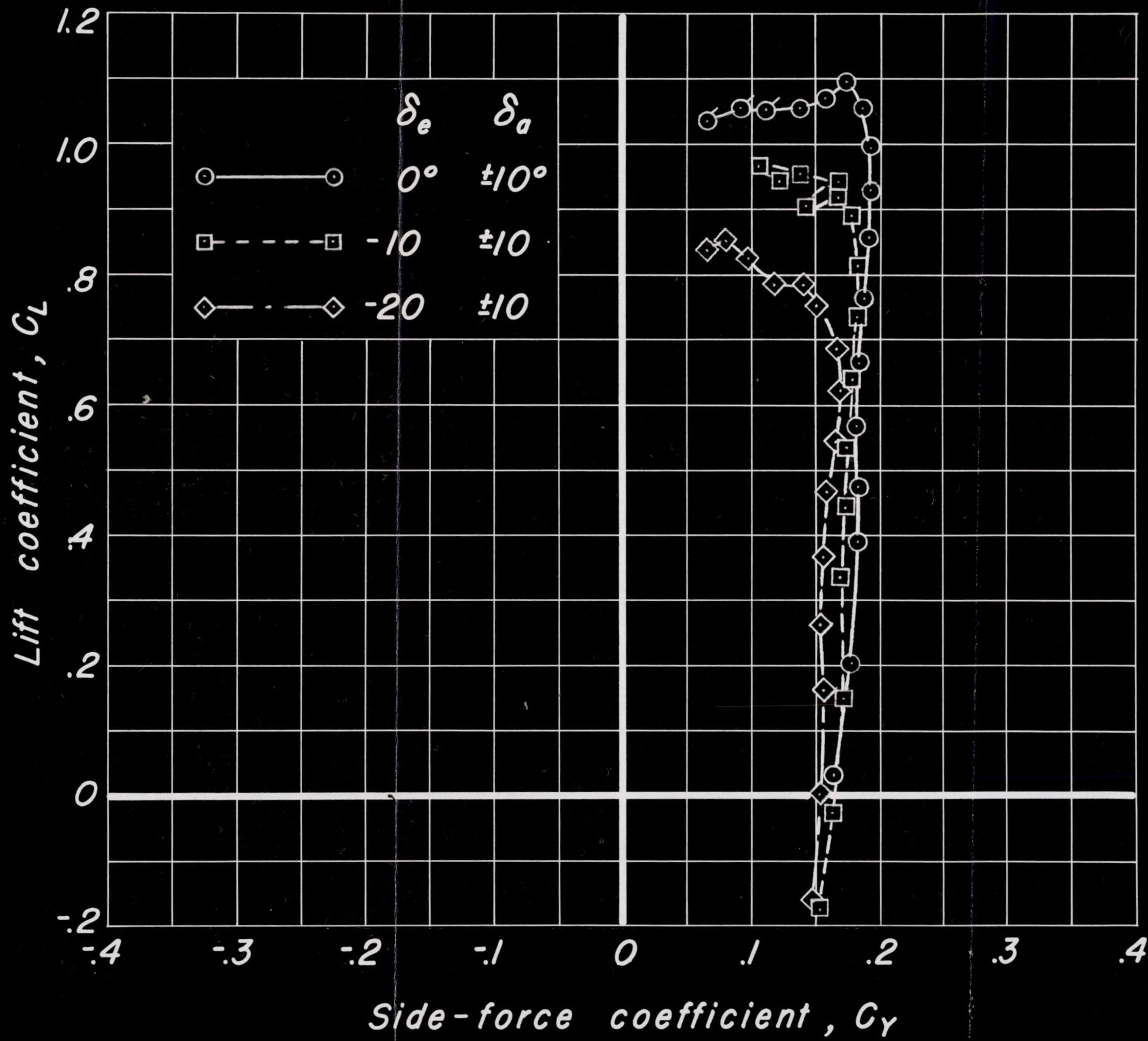

Figure 10.– Concluded.

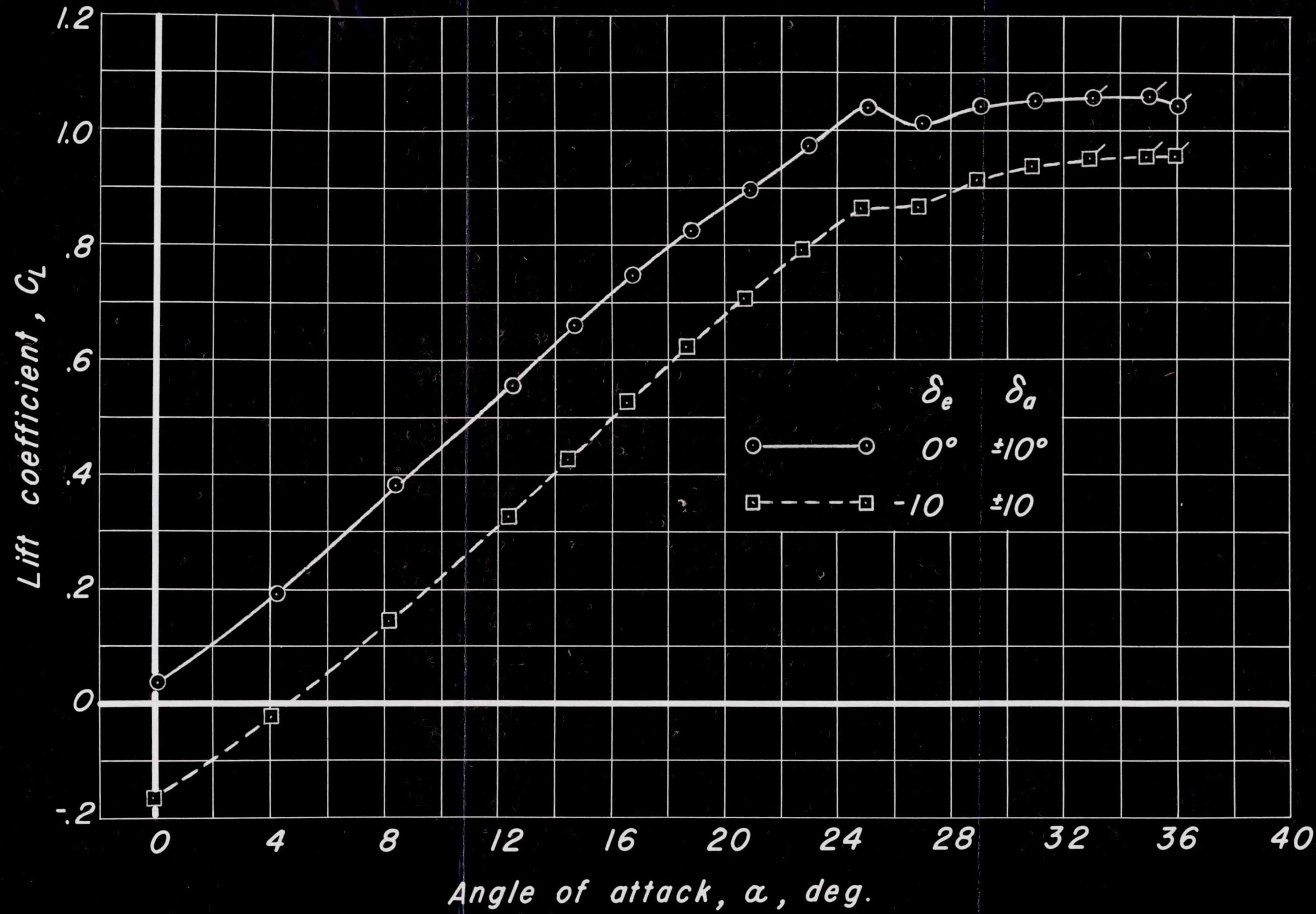

Figure 11. – Longitudinal and lateral control effectiveness with undeflected rudder, $\beta = -20.20°$.

NACA 8A8B04

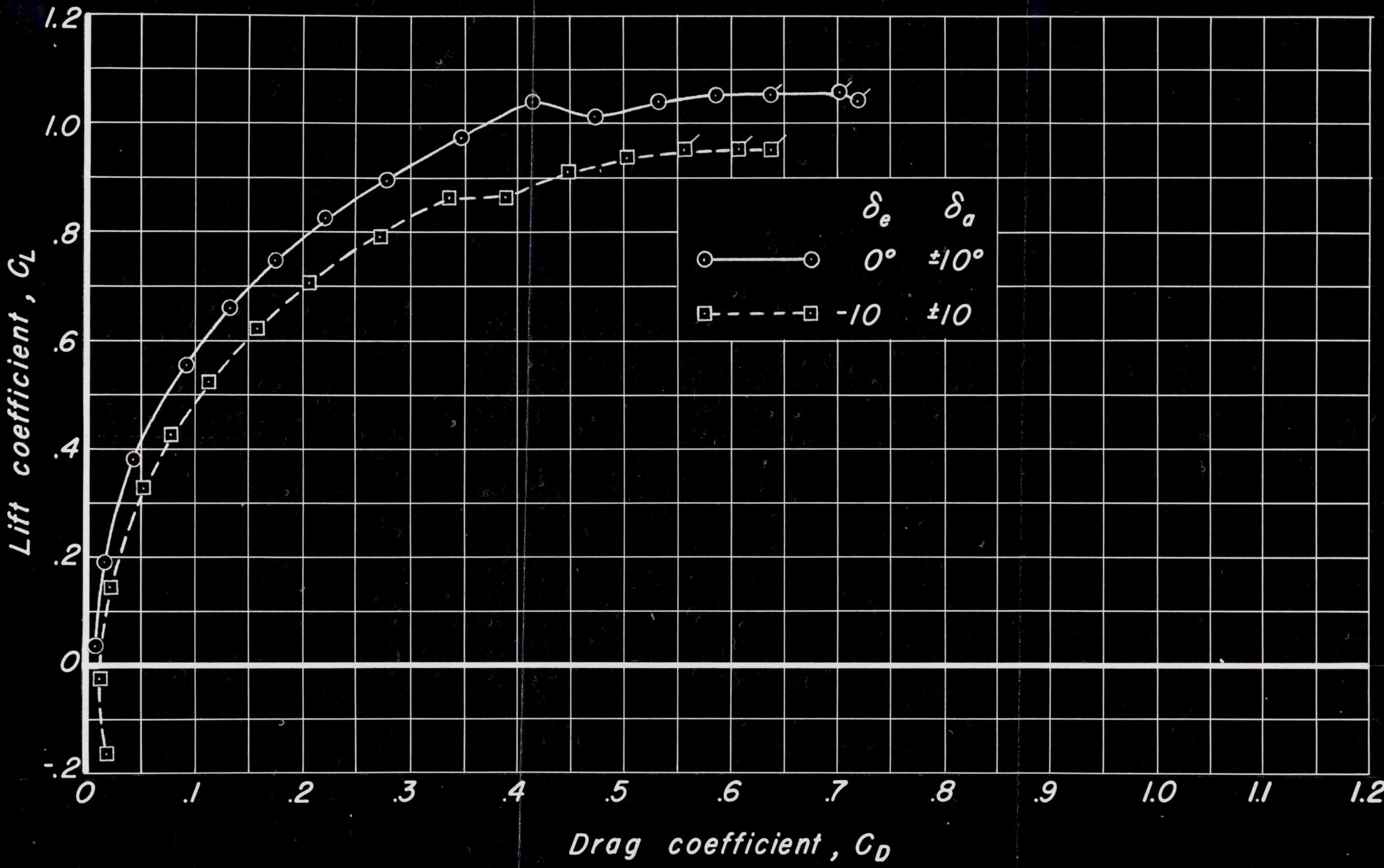

Figure 11. – Continued.

NACA 8A8B04

Figure 11. – Continued.

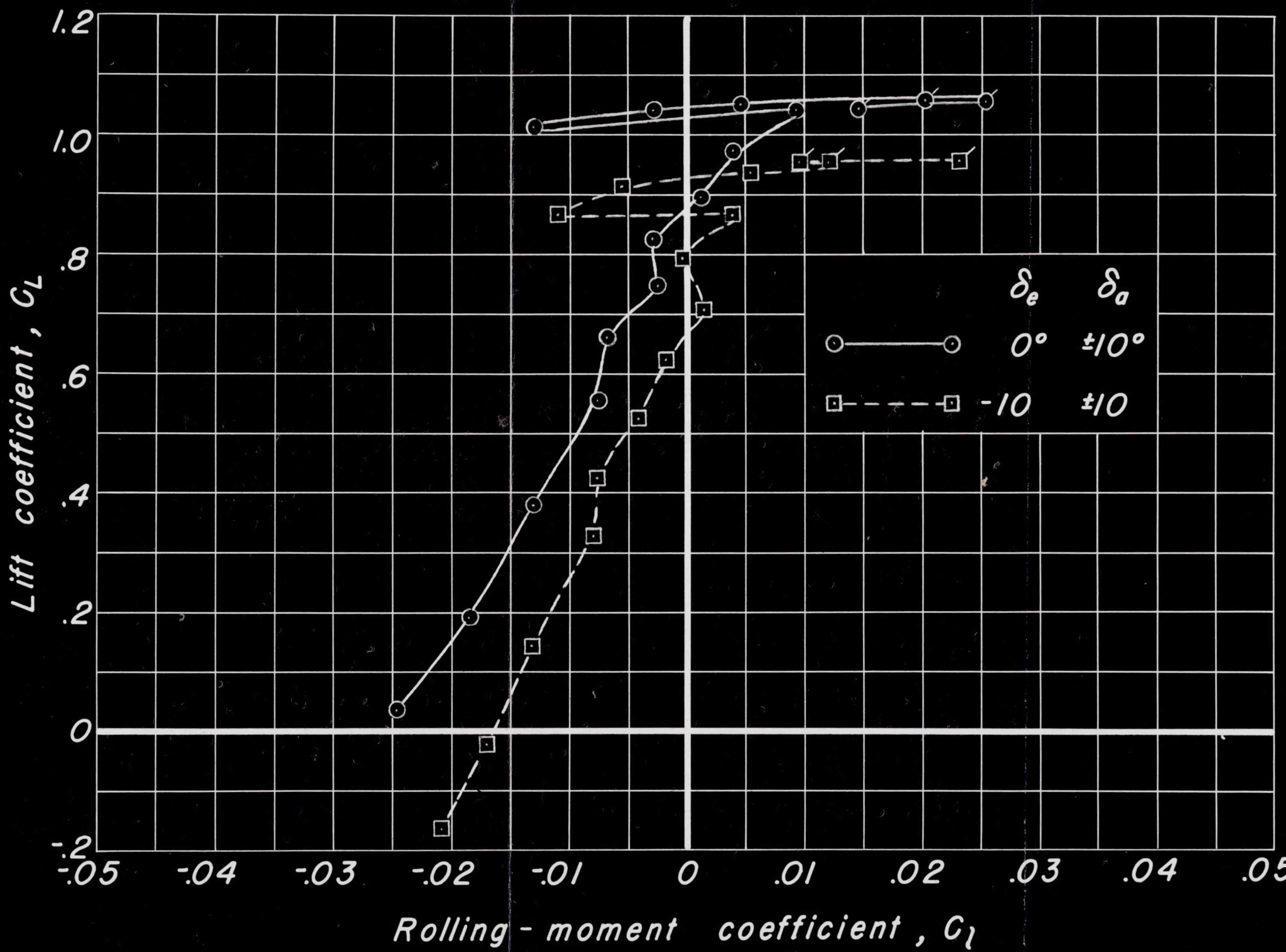

Figure 11. - Continued.

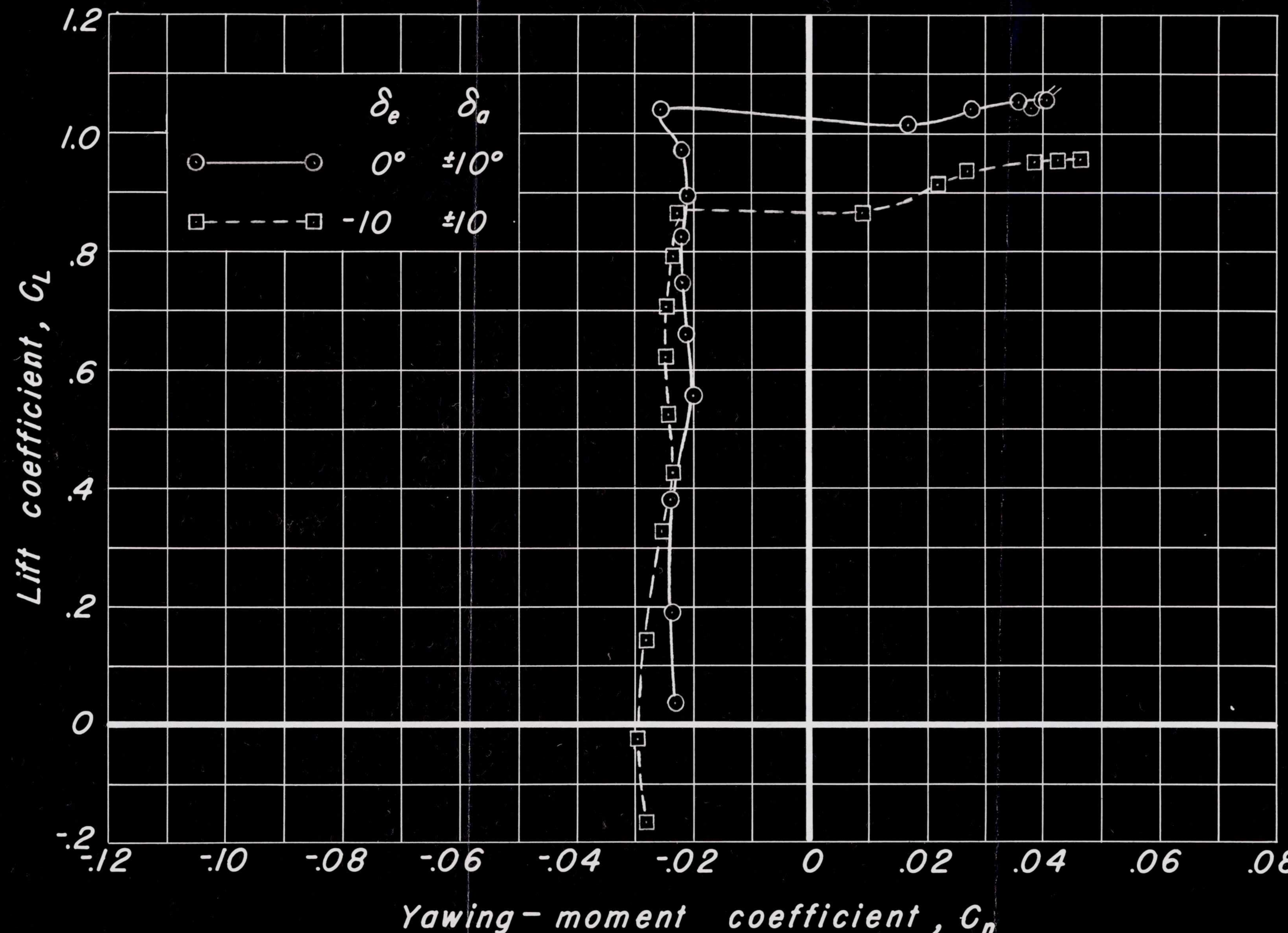

Figure 11. – Continued.

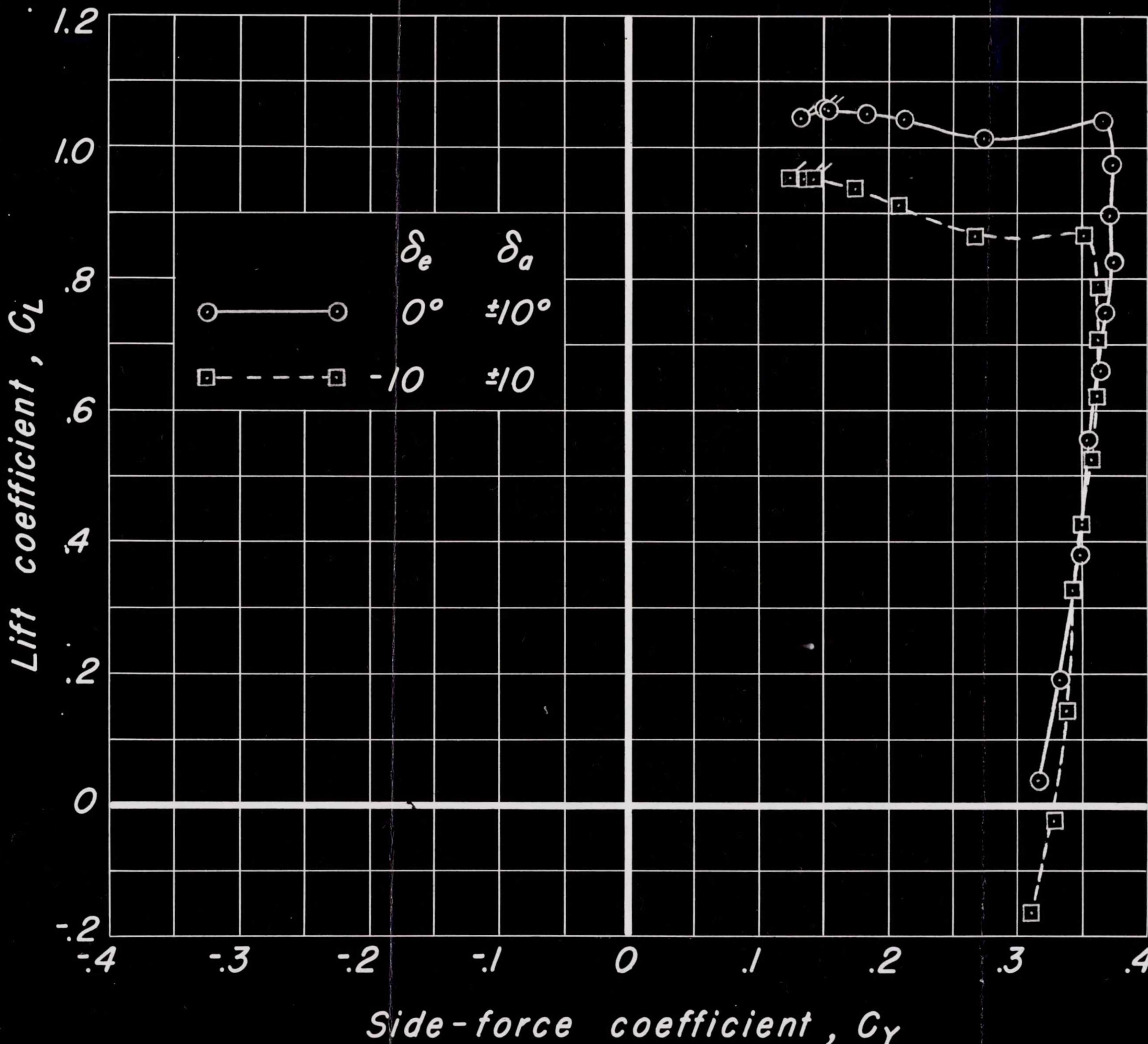

Figure 11. - Concluded.

NACA 8A8B04

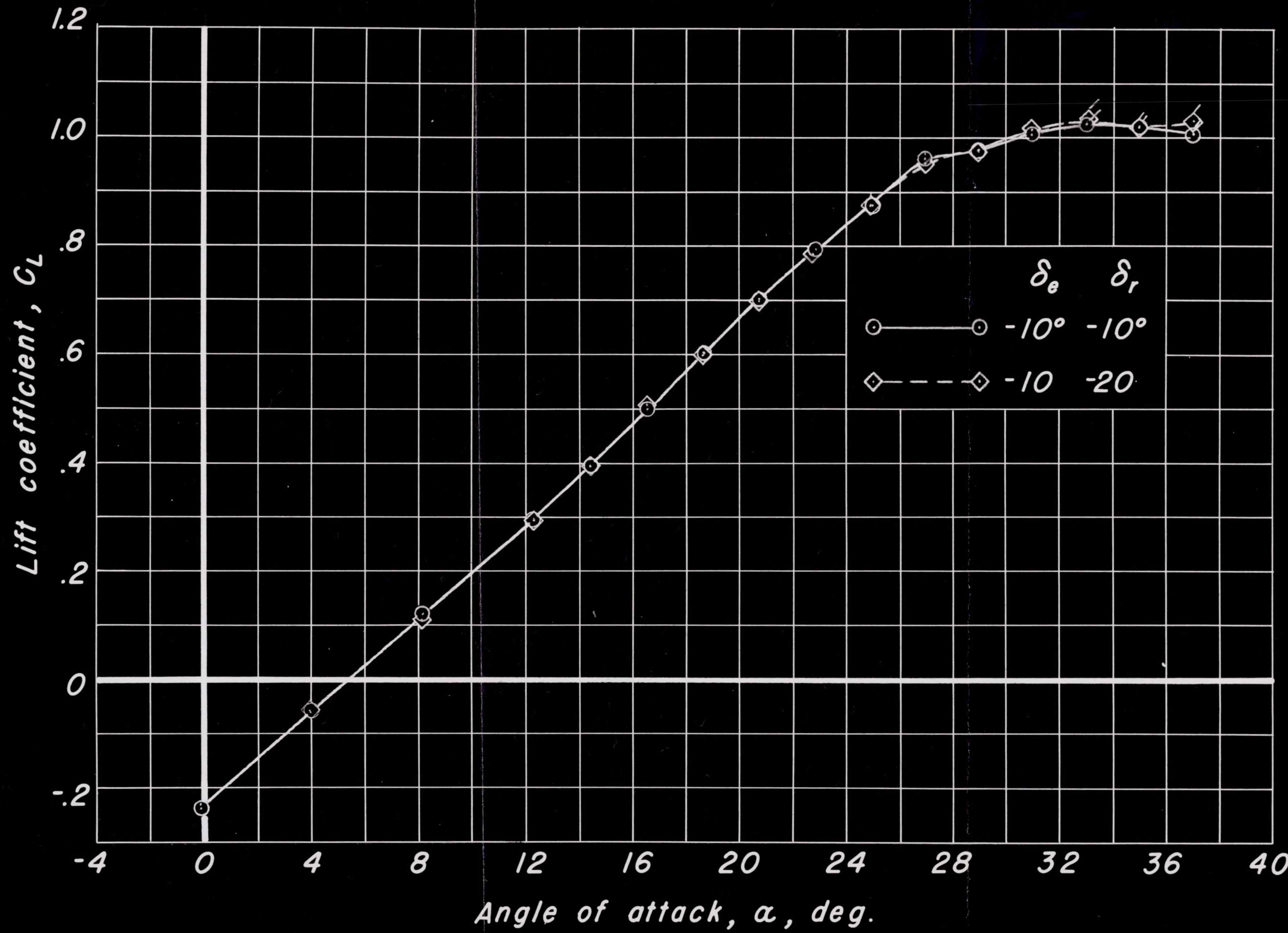

Figure 12.—Longitudinal and directional control effectiveness, $\beta = 0.13°$.

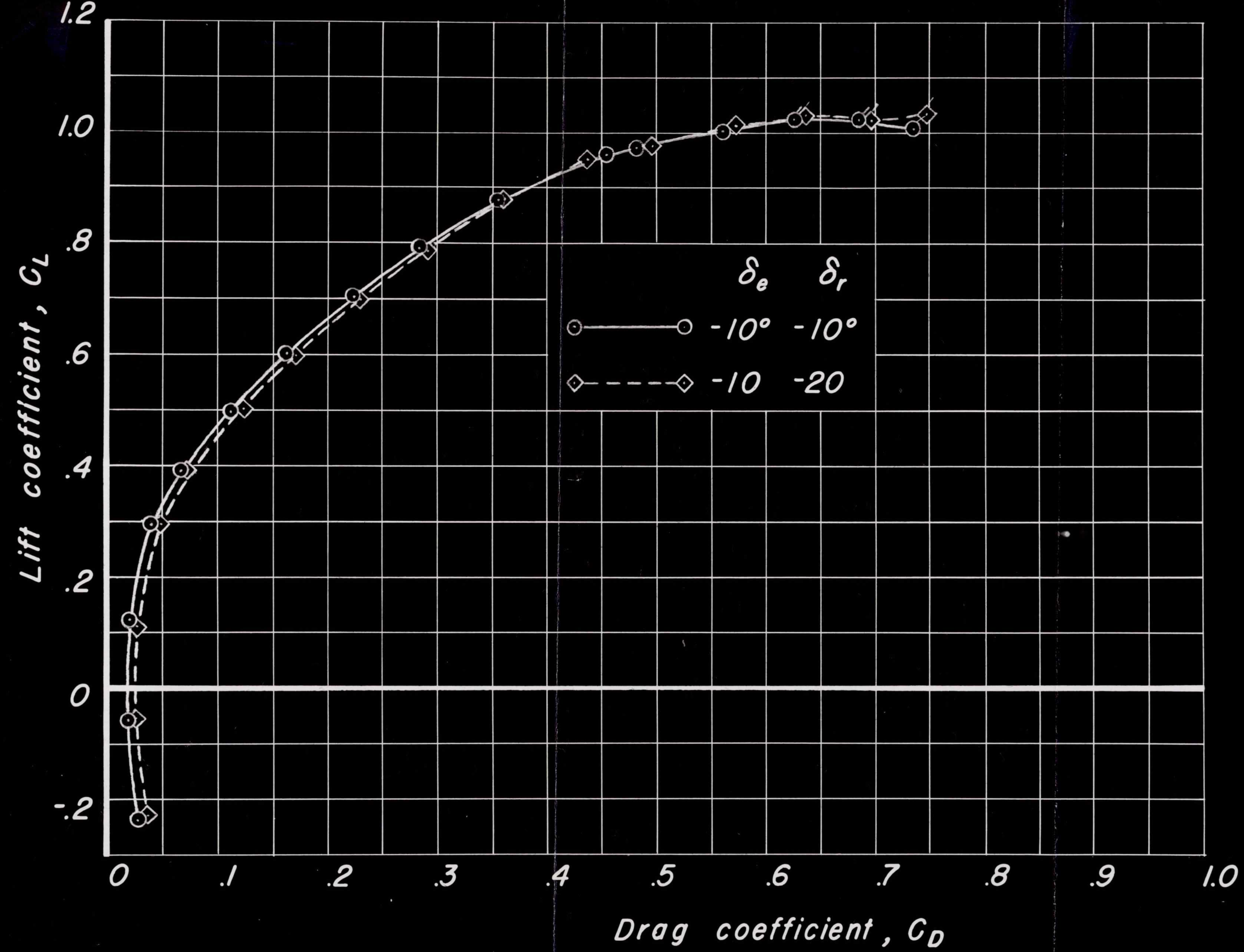

Figure 12.—Continued.

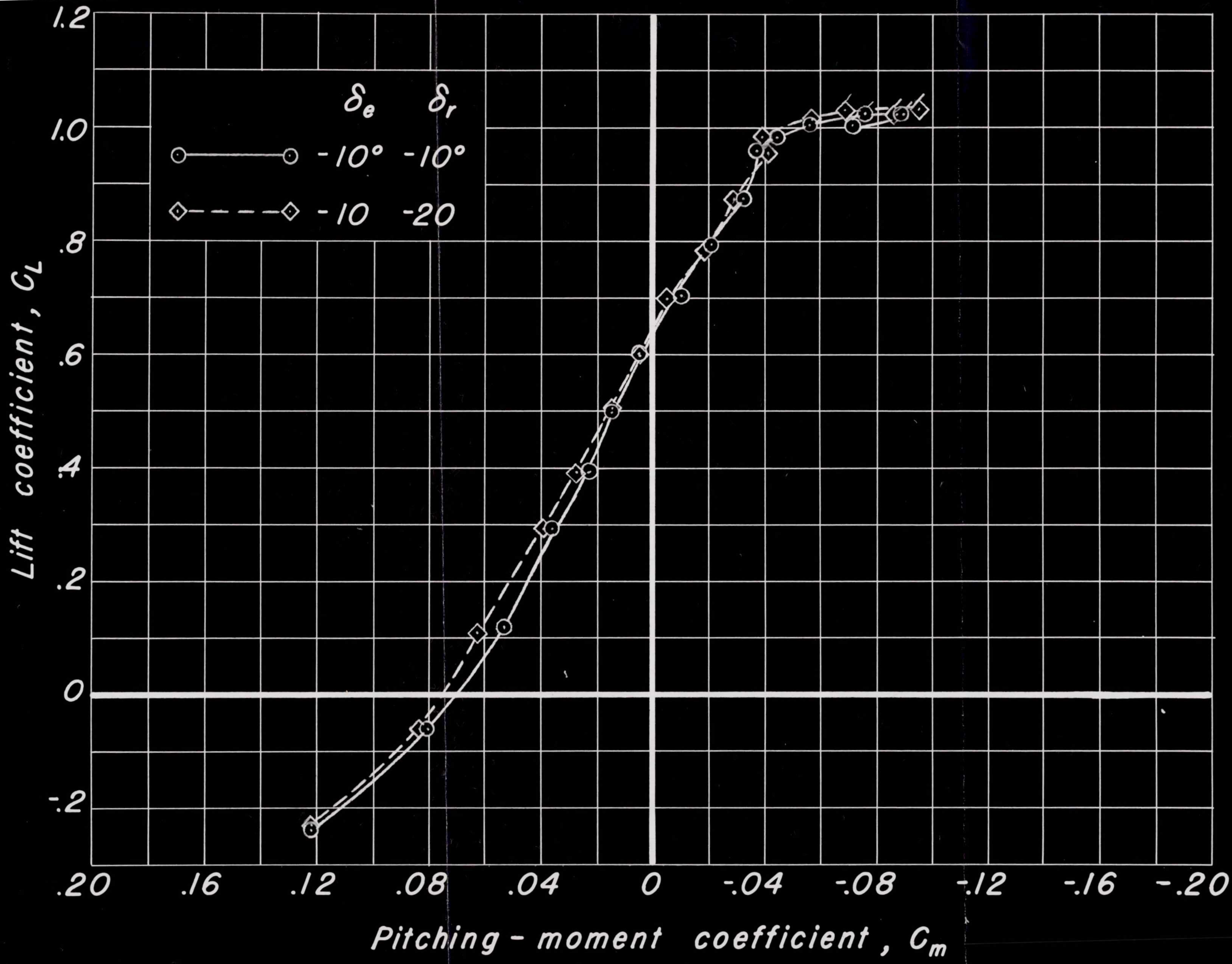

Figure 12.– Continued.

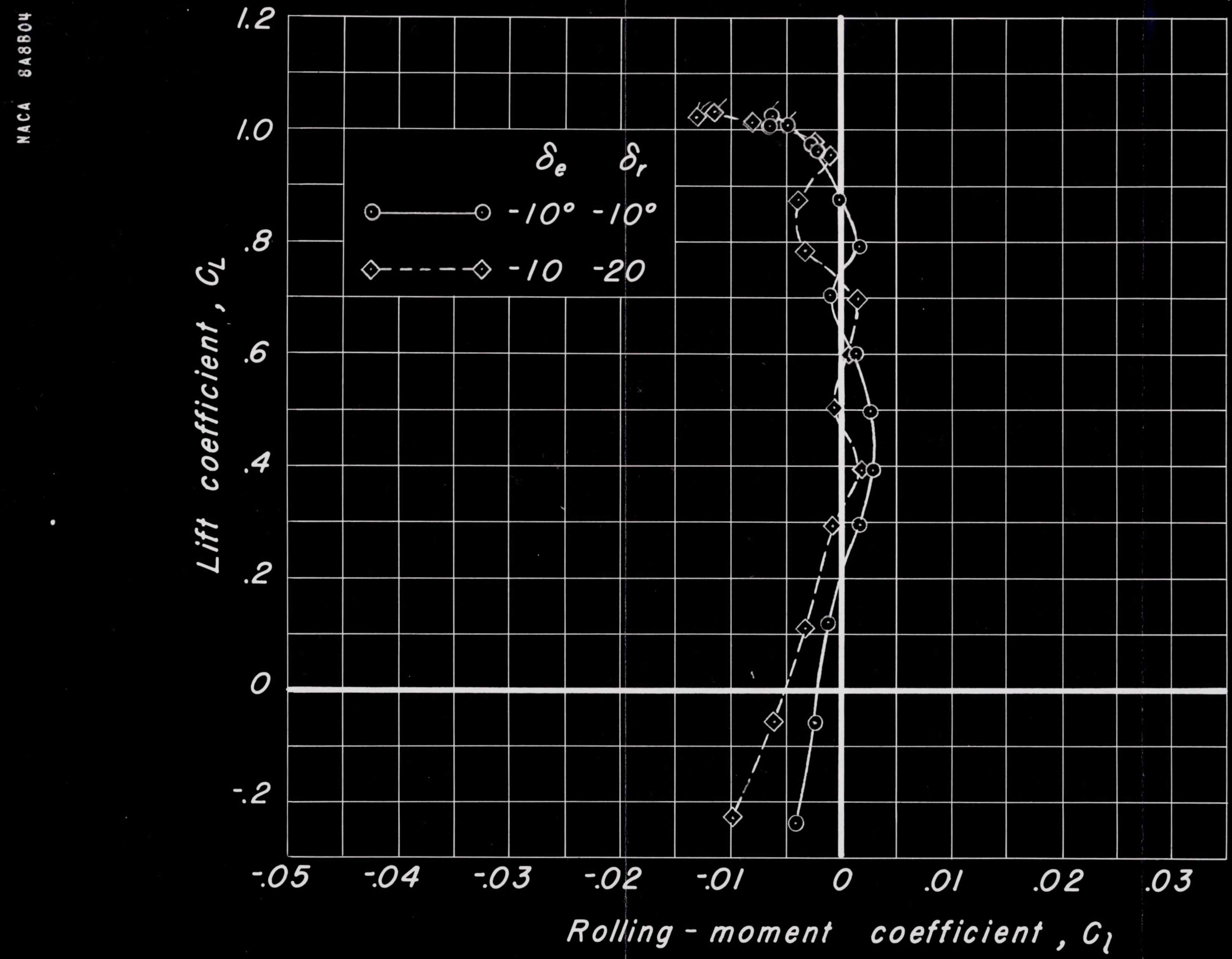

Figure 12.– Continued.

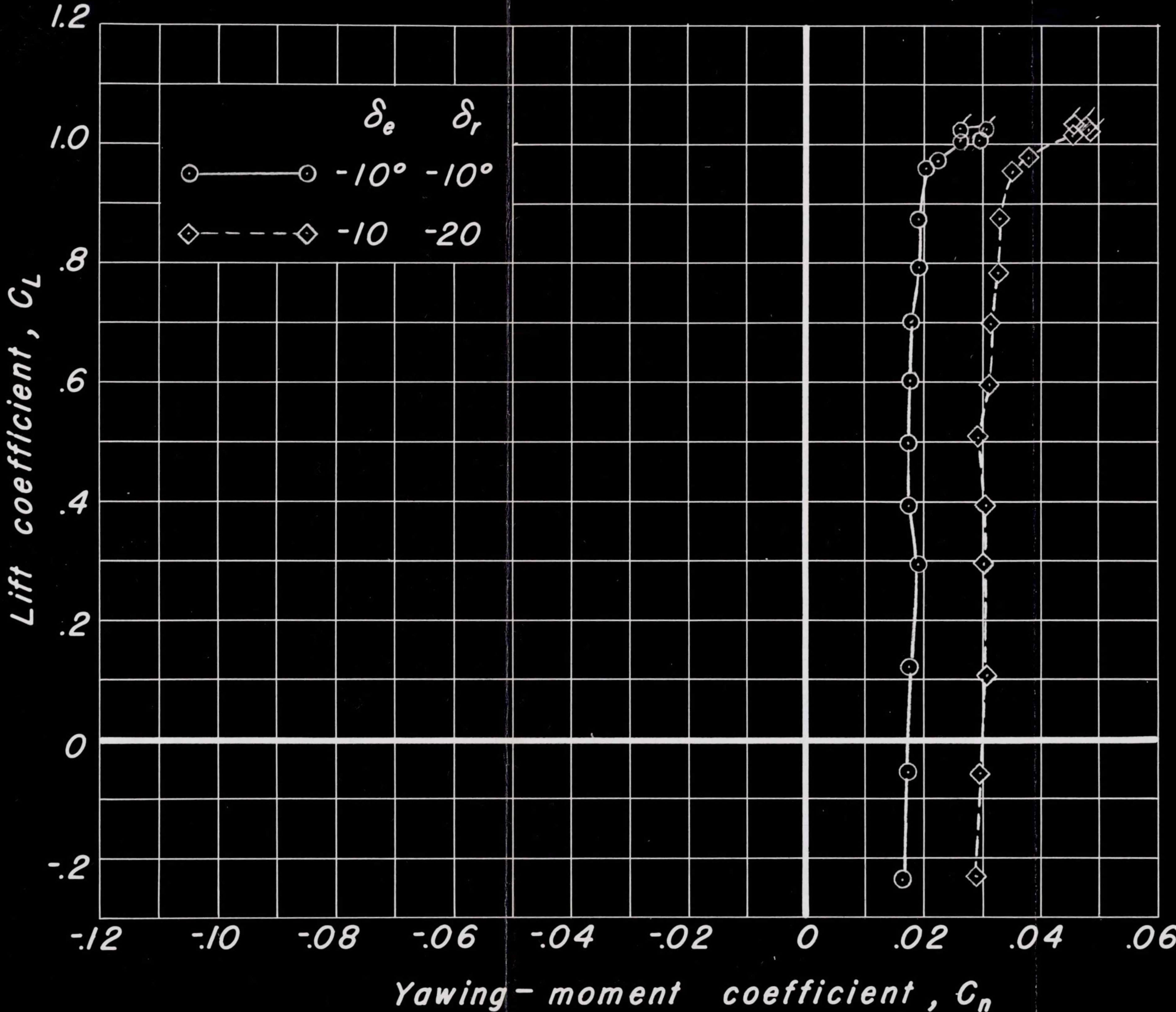

Figure 12.– Continued.

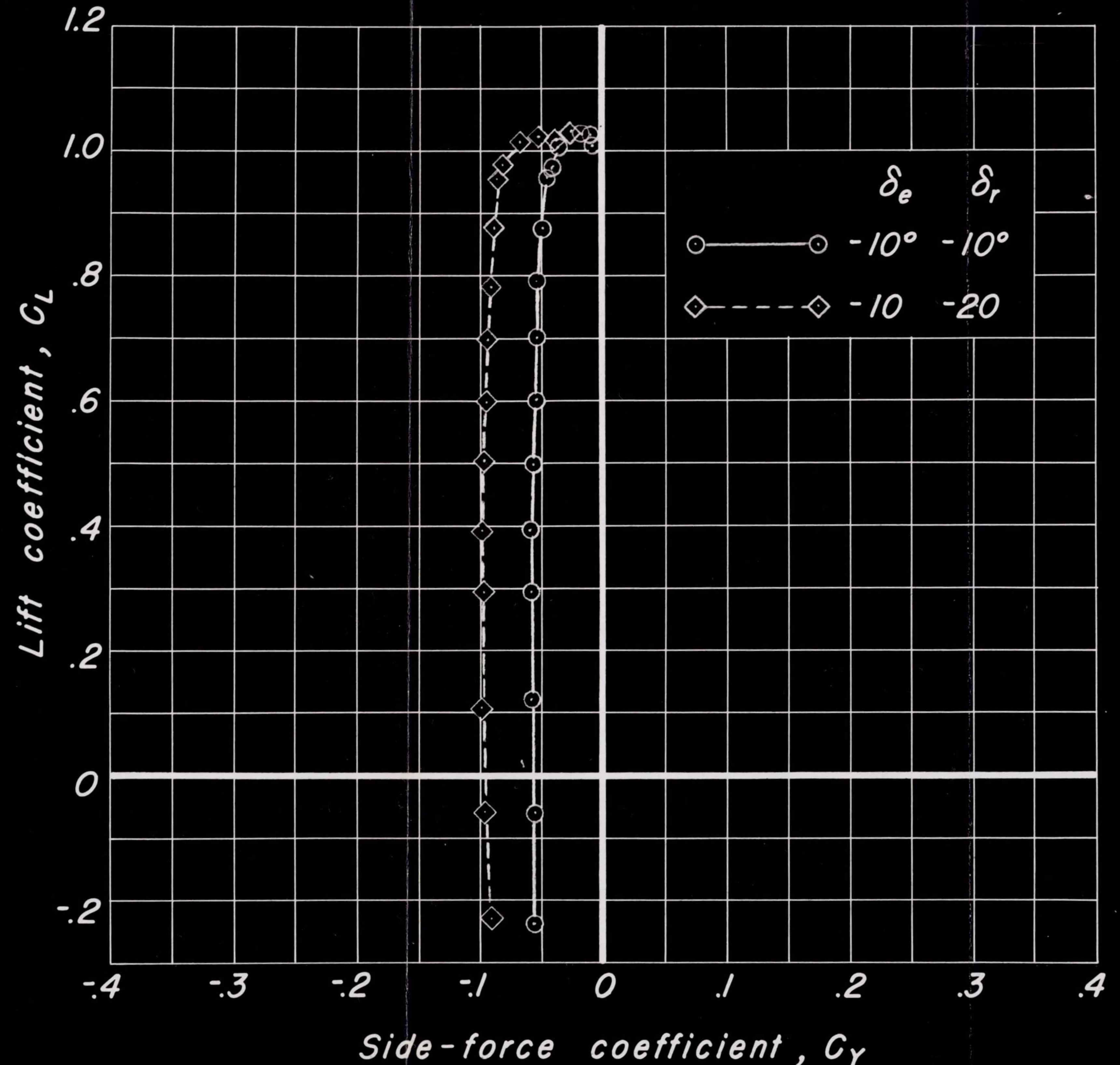

Figure 12.– Concluded.

NACA 8A8B04

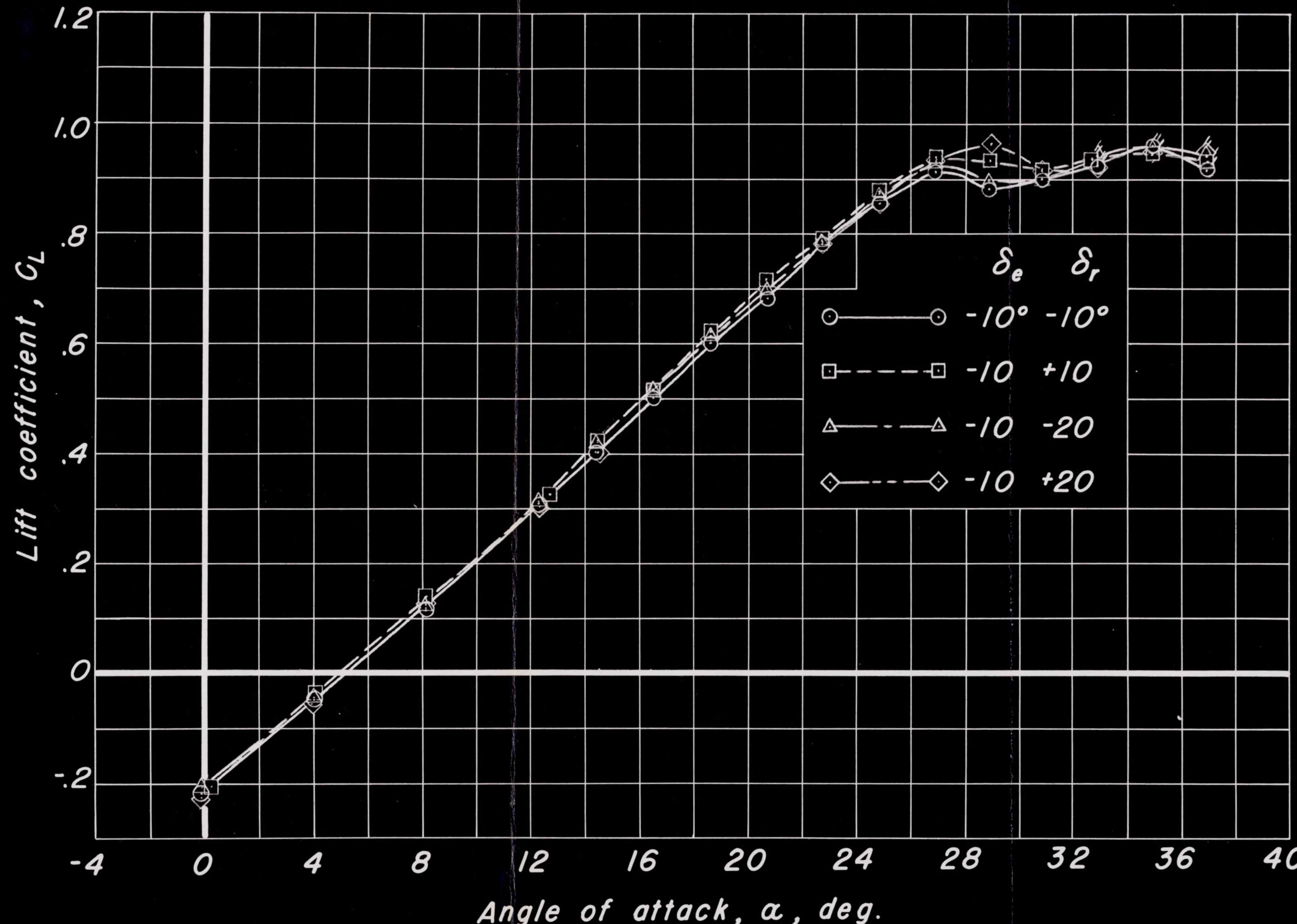

Figure 13.—Longitudinal and directional control effectiveness, β = -10.06°.

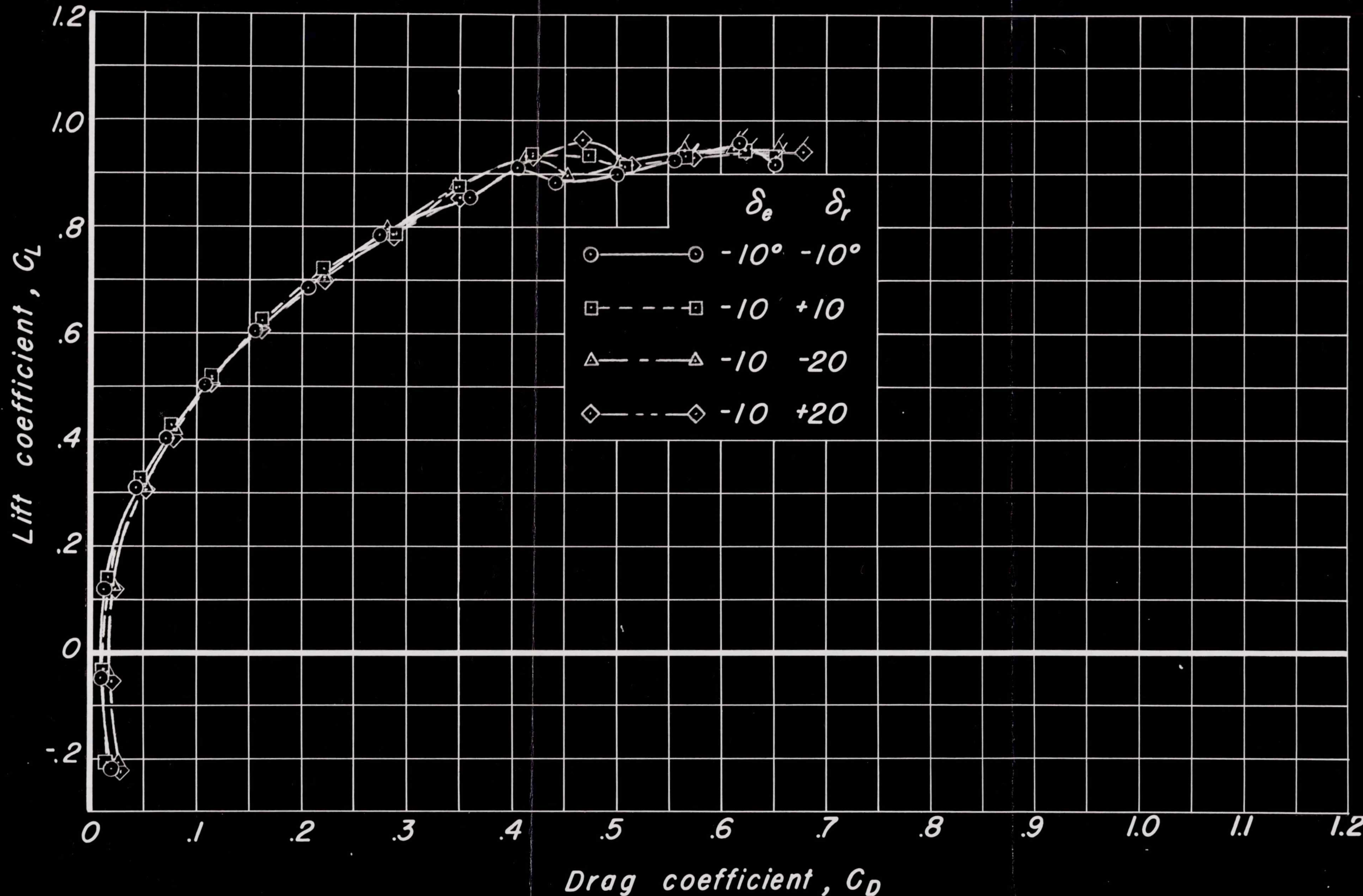

Figure 13.— Continued.

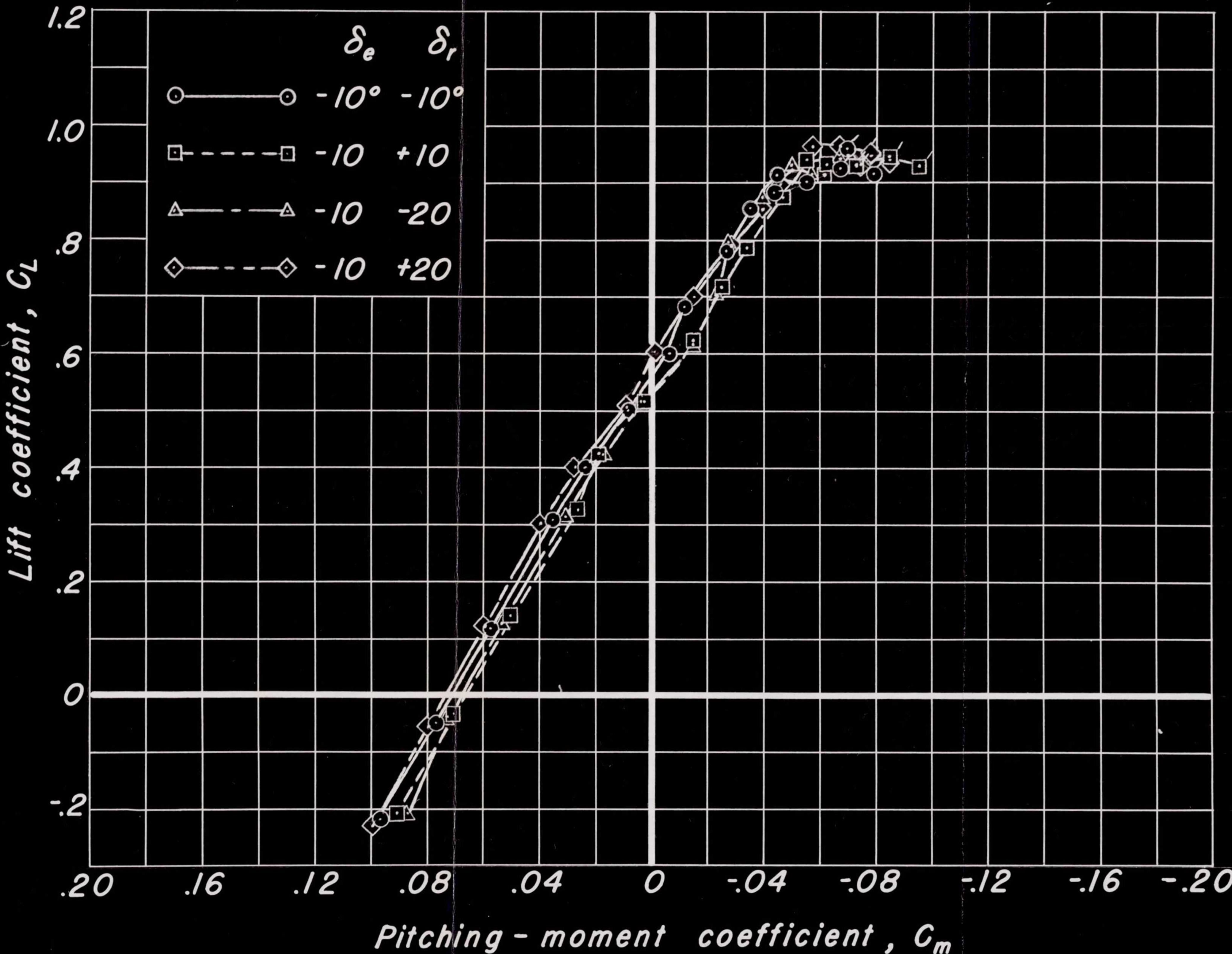

Figure 13.– Continued.

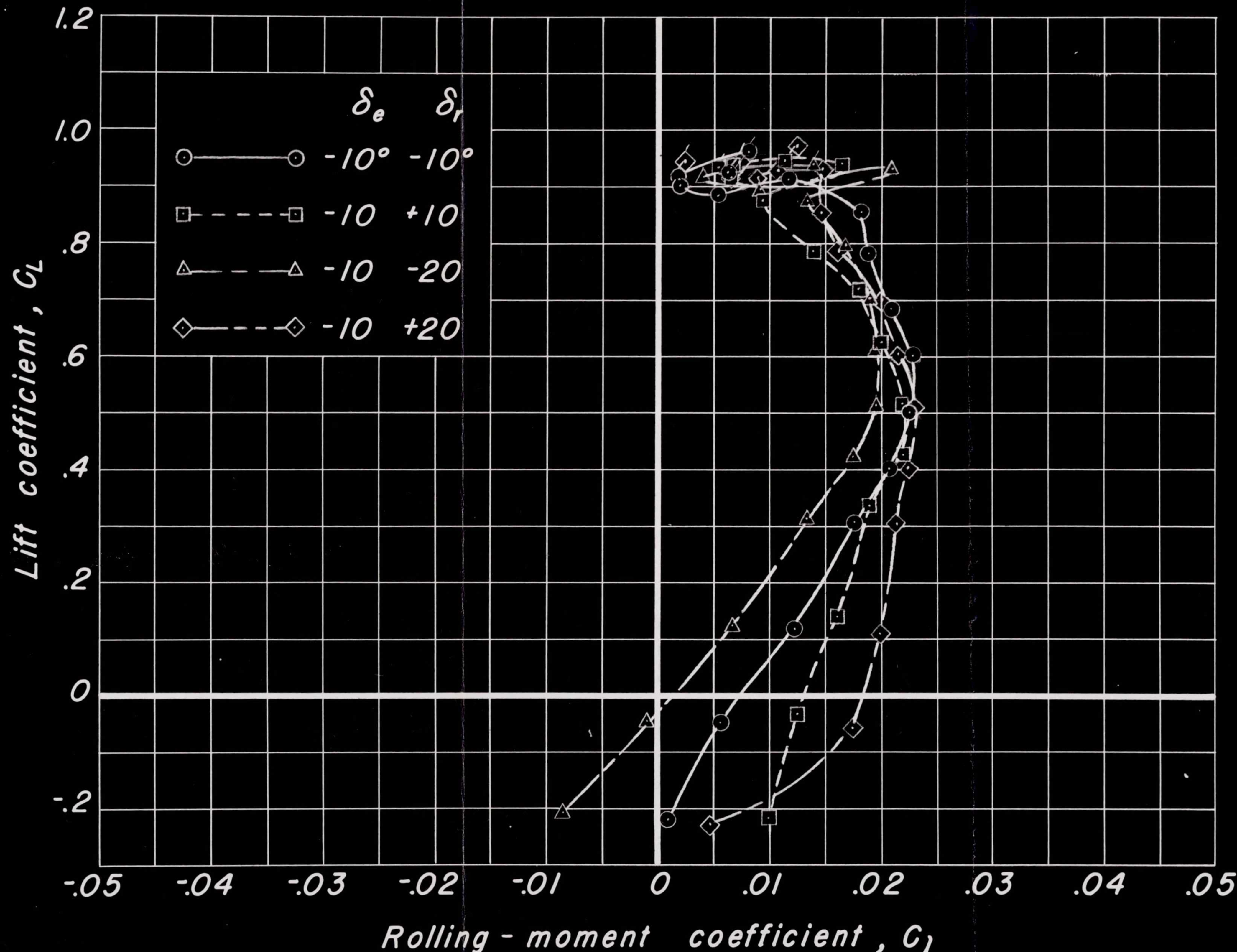

Figure 13.—Continued.

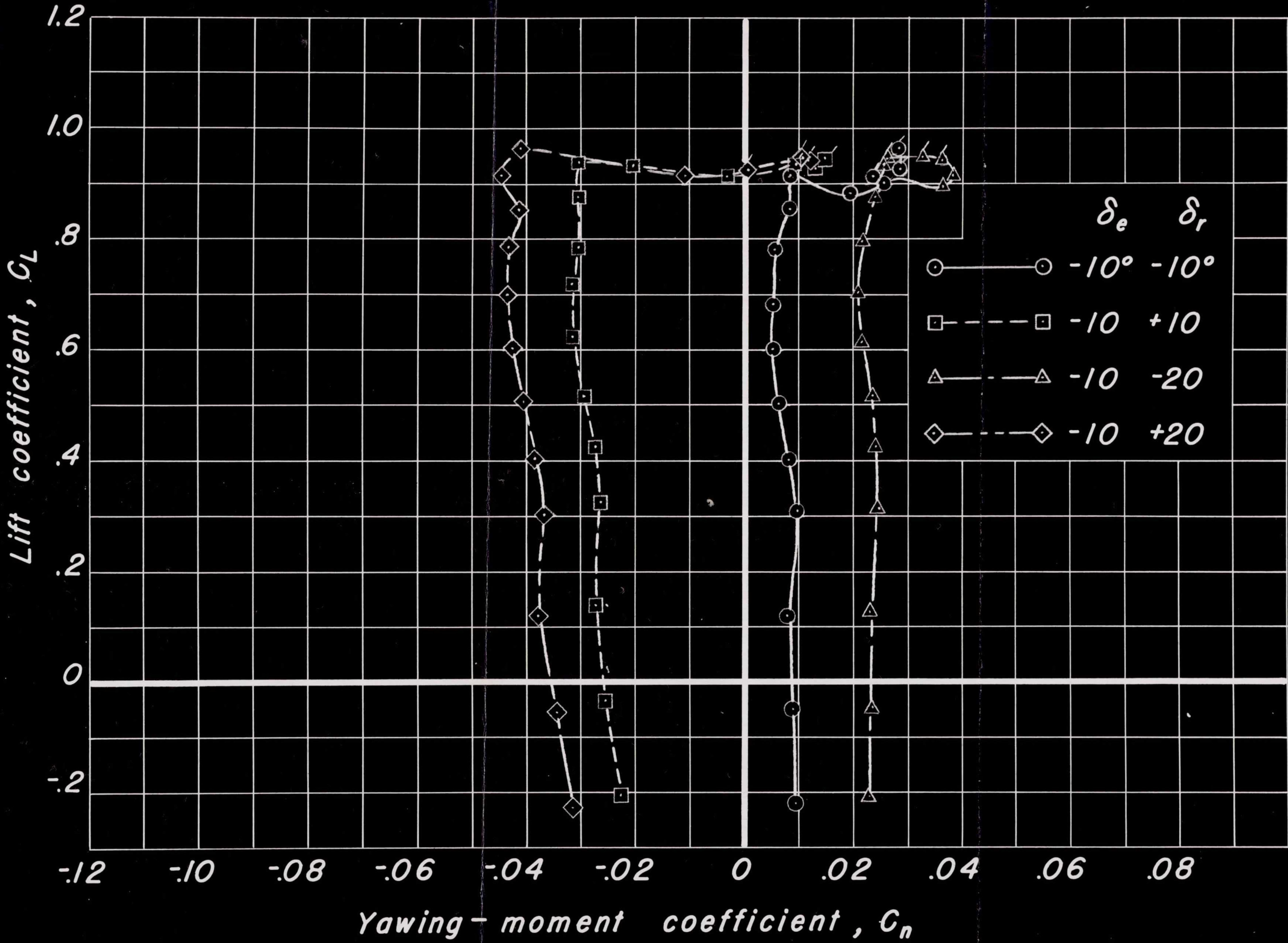

Figure 13.– Continued.

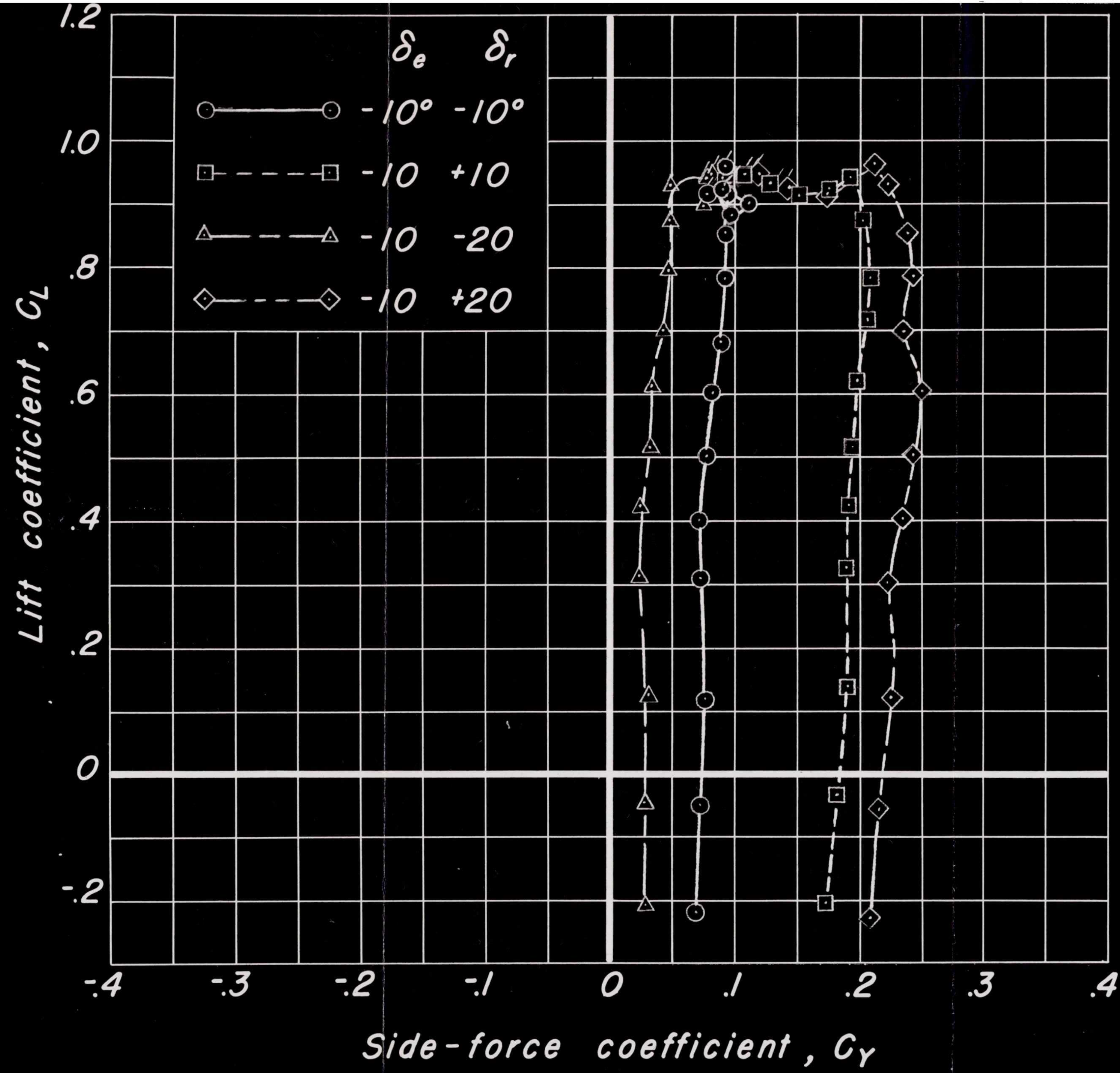

Figure 13.– Concluded.

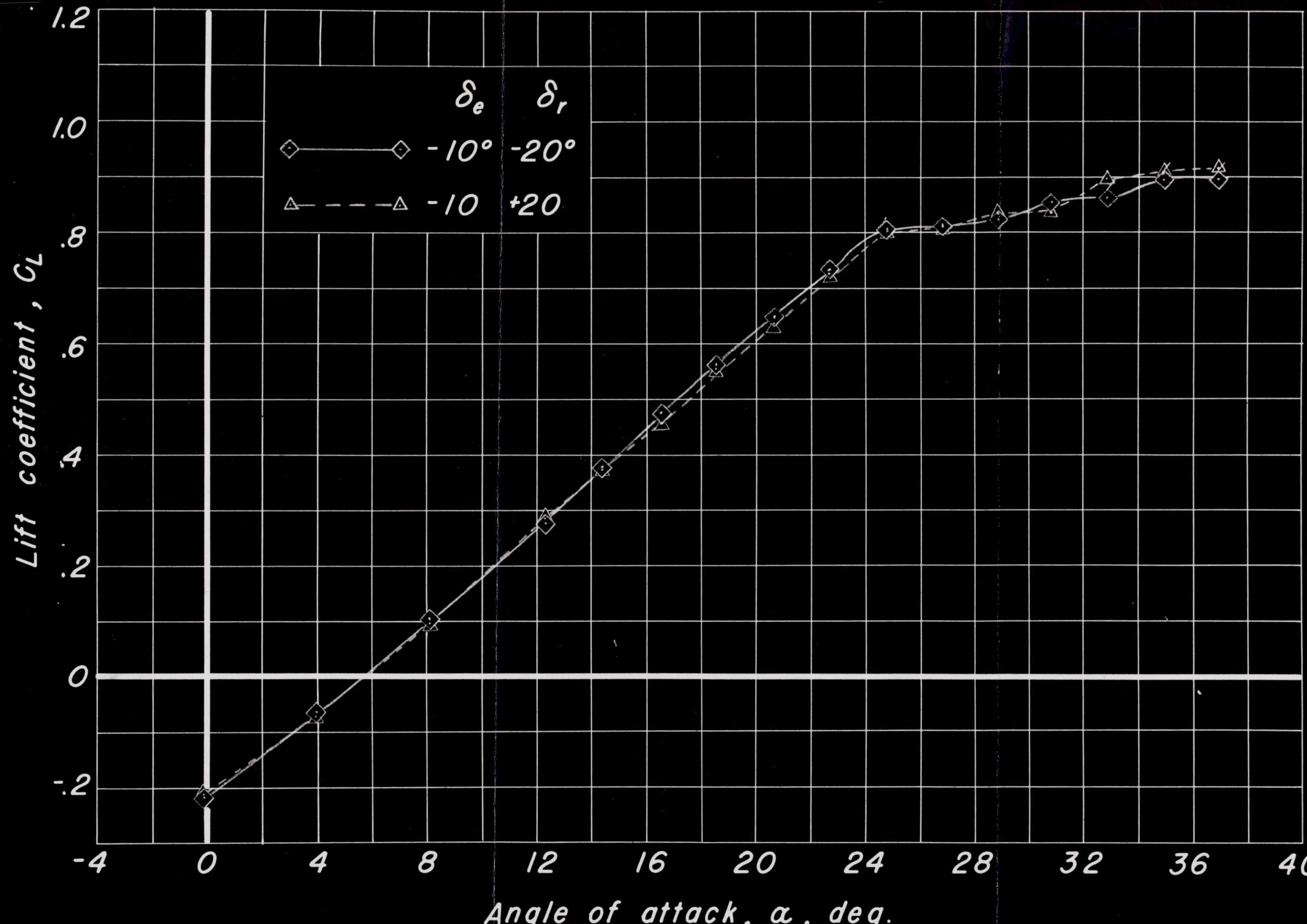

Figure 14.—Longitudinal and directional control effectiveness, $\beta = -20.20°$

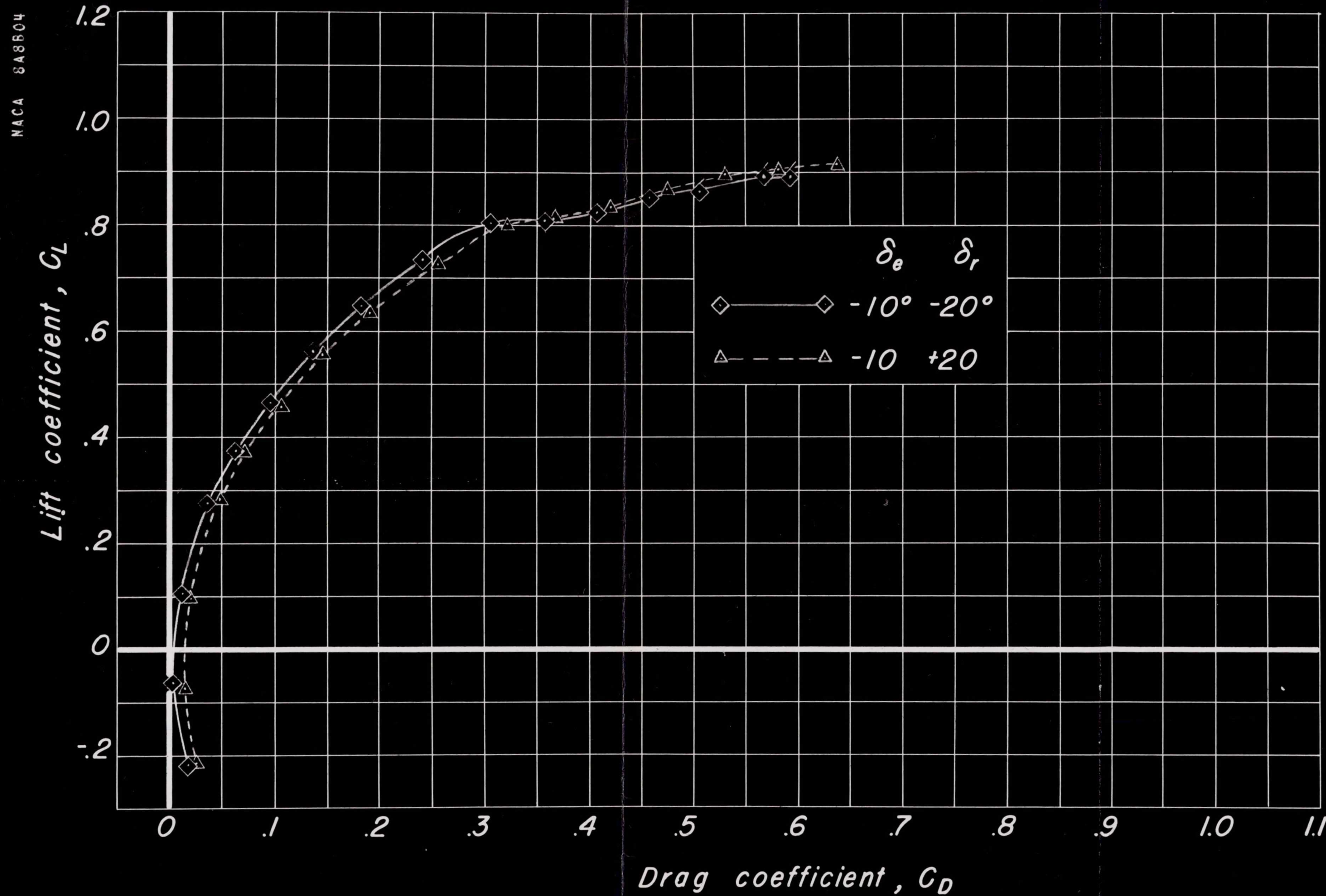

Figure 14.- Continued.

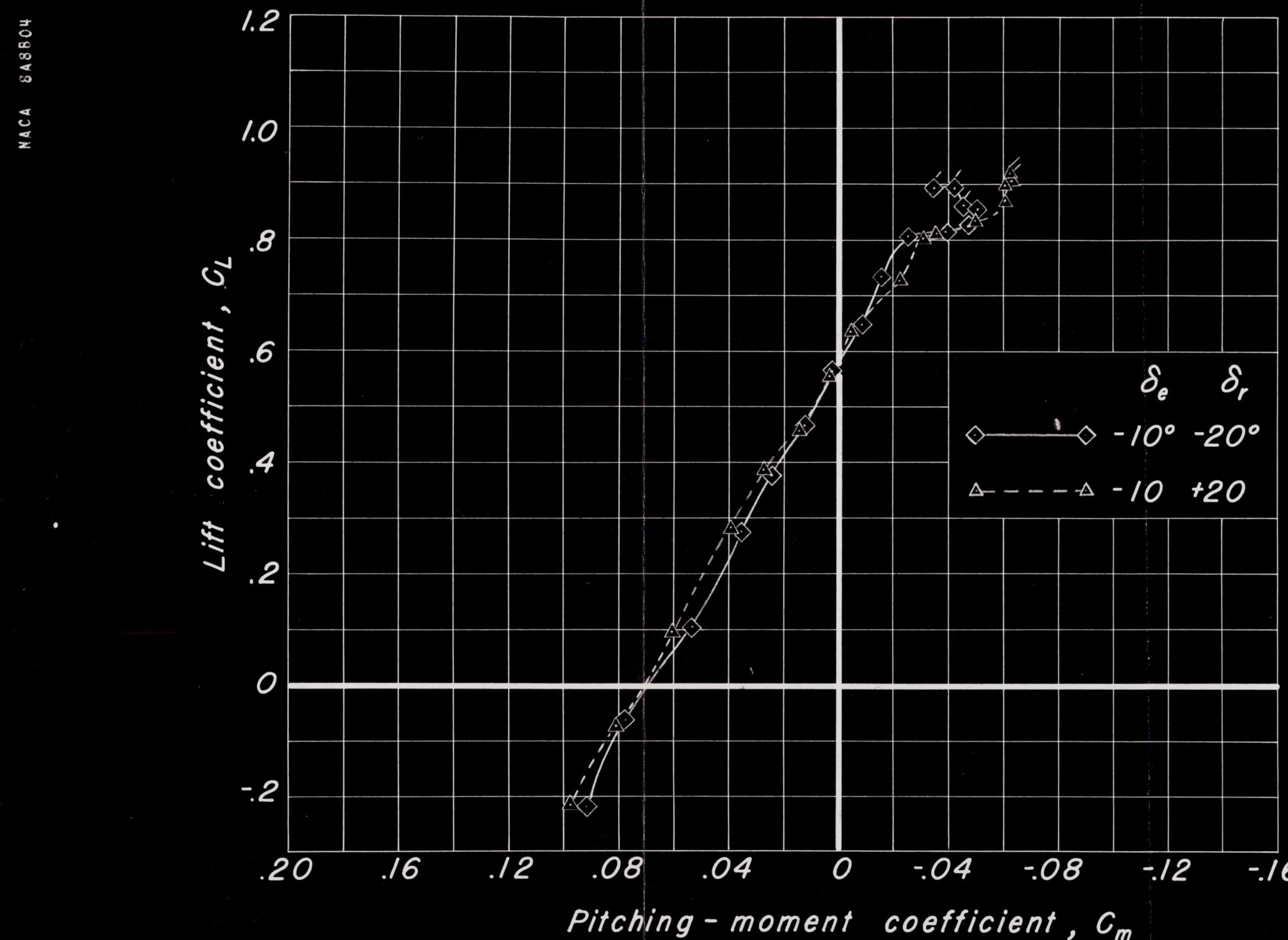

Figure 14.– Continued.

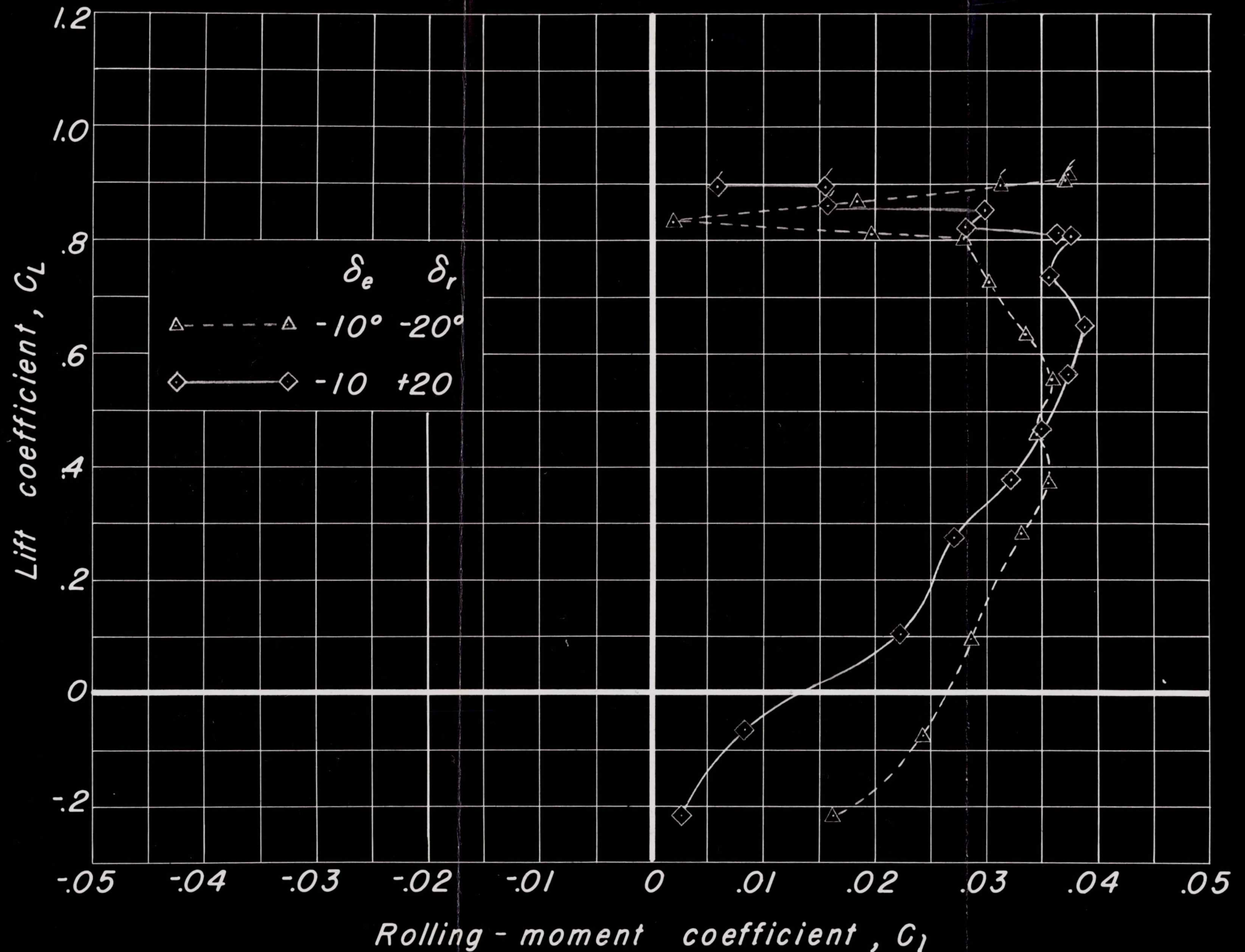

Figure 14.– Continued.

Figure 14.– Continued.

Figure 14.— Concluded.

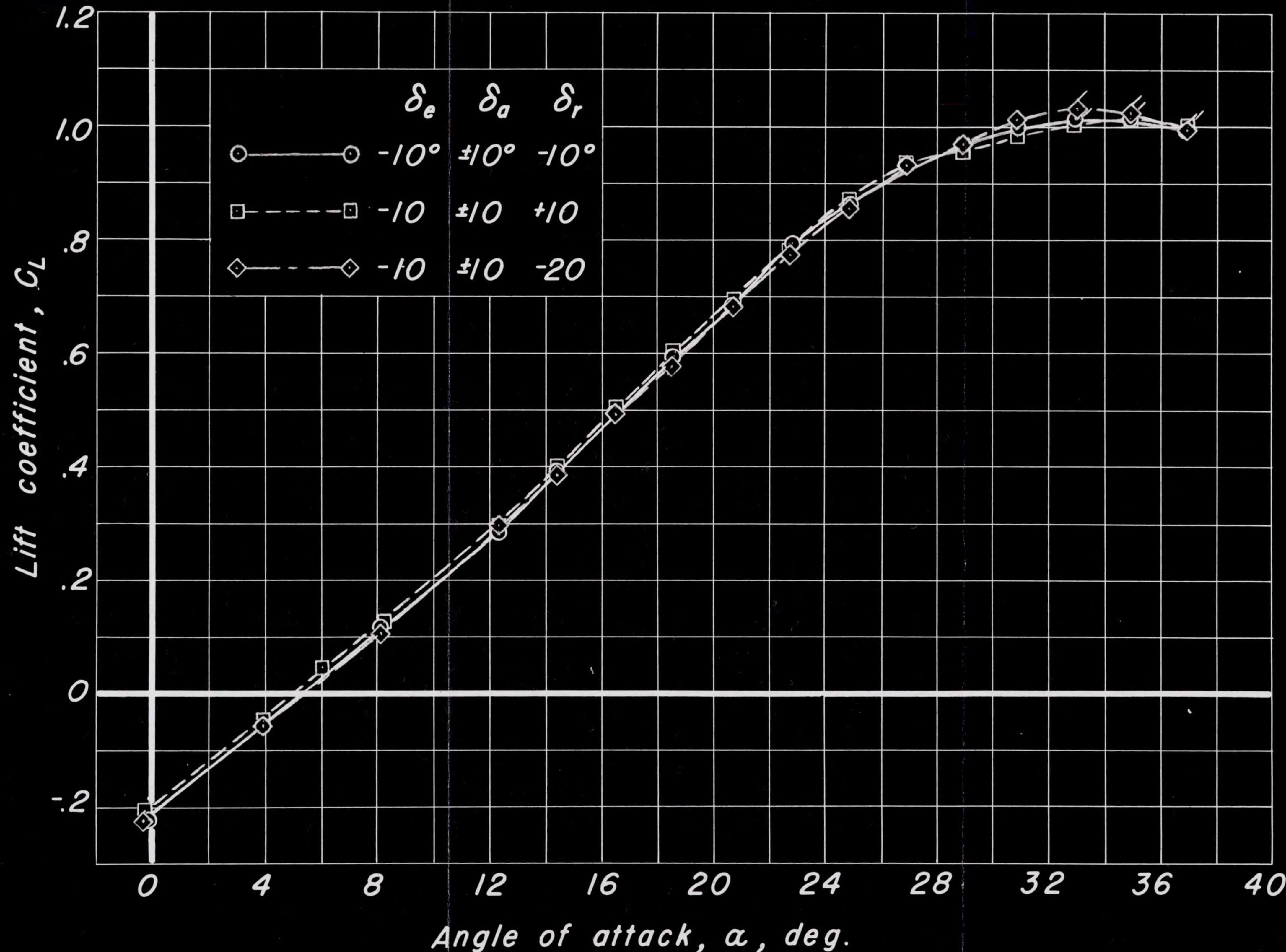

Figure 15.– Longitudinal, lateral and directional control effectiveness, $\beta = 0.13°$.

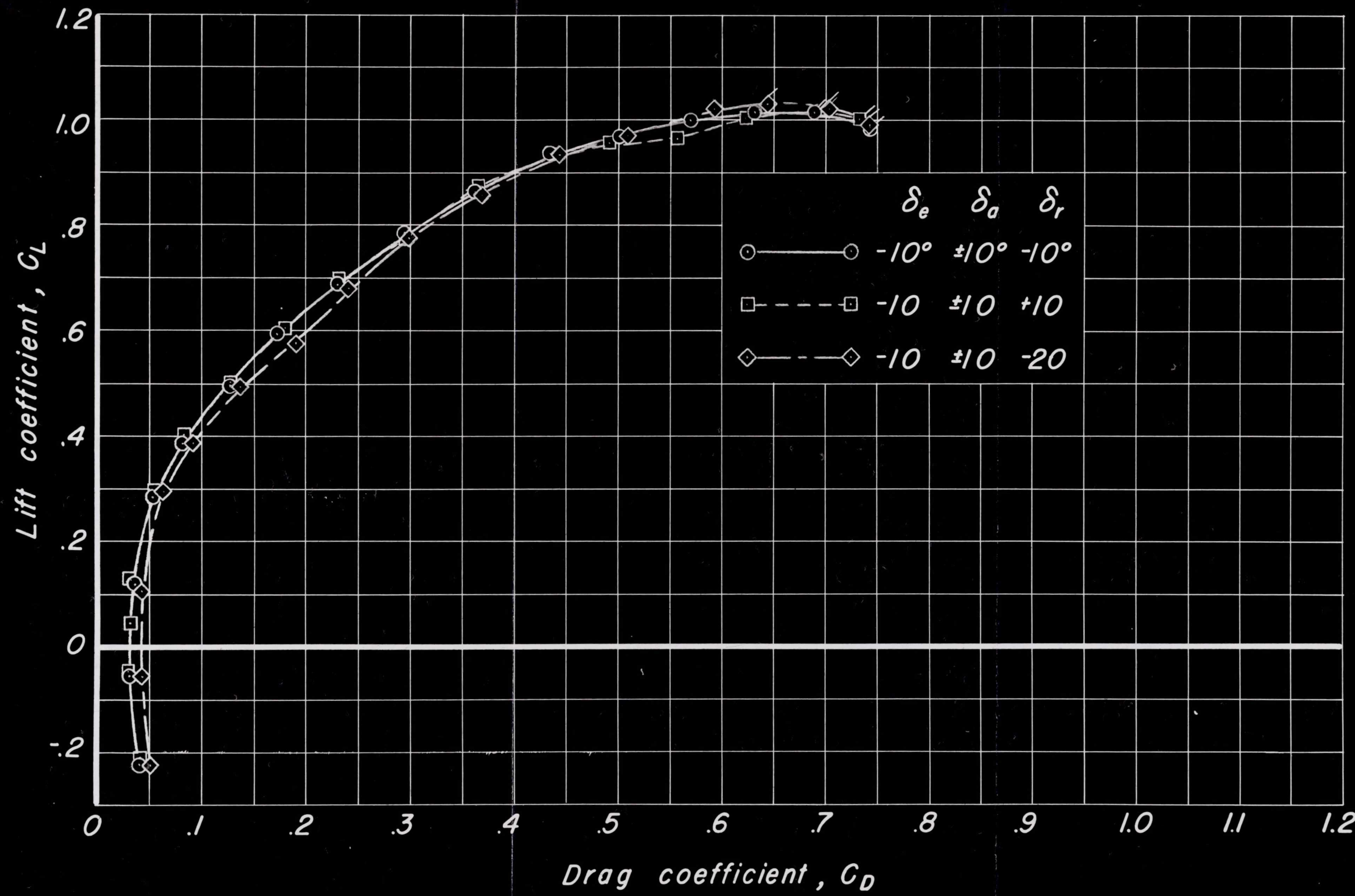

Figure 15.- Continued.

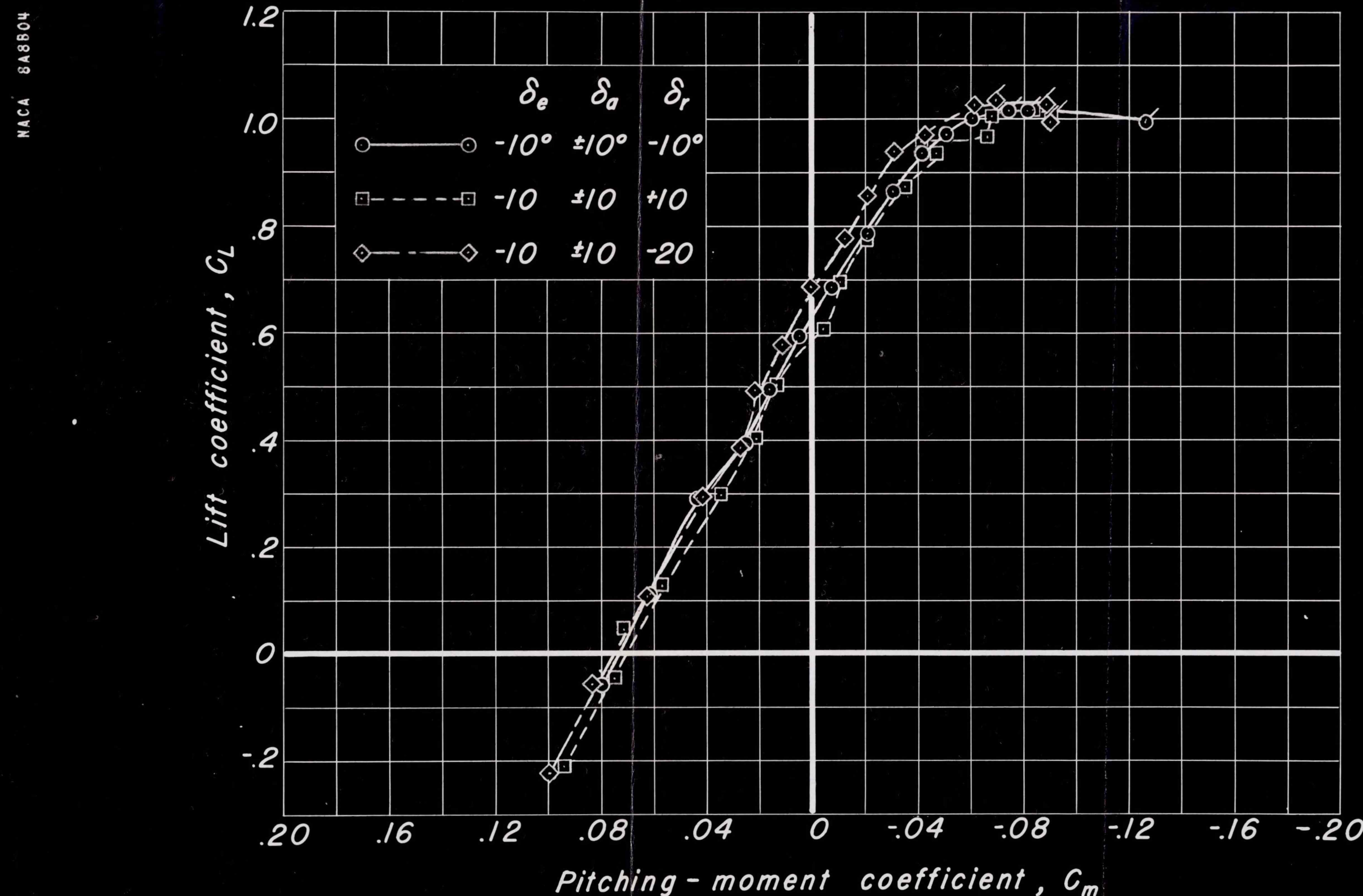

Figure 15.- Continued.

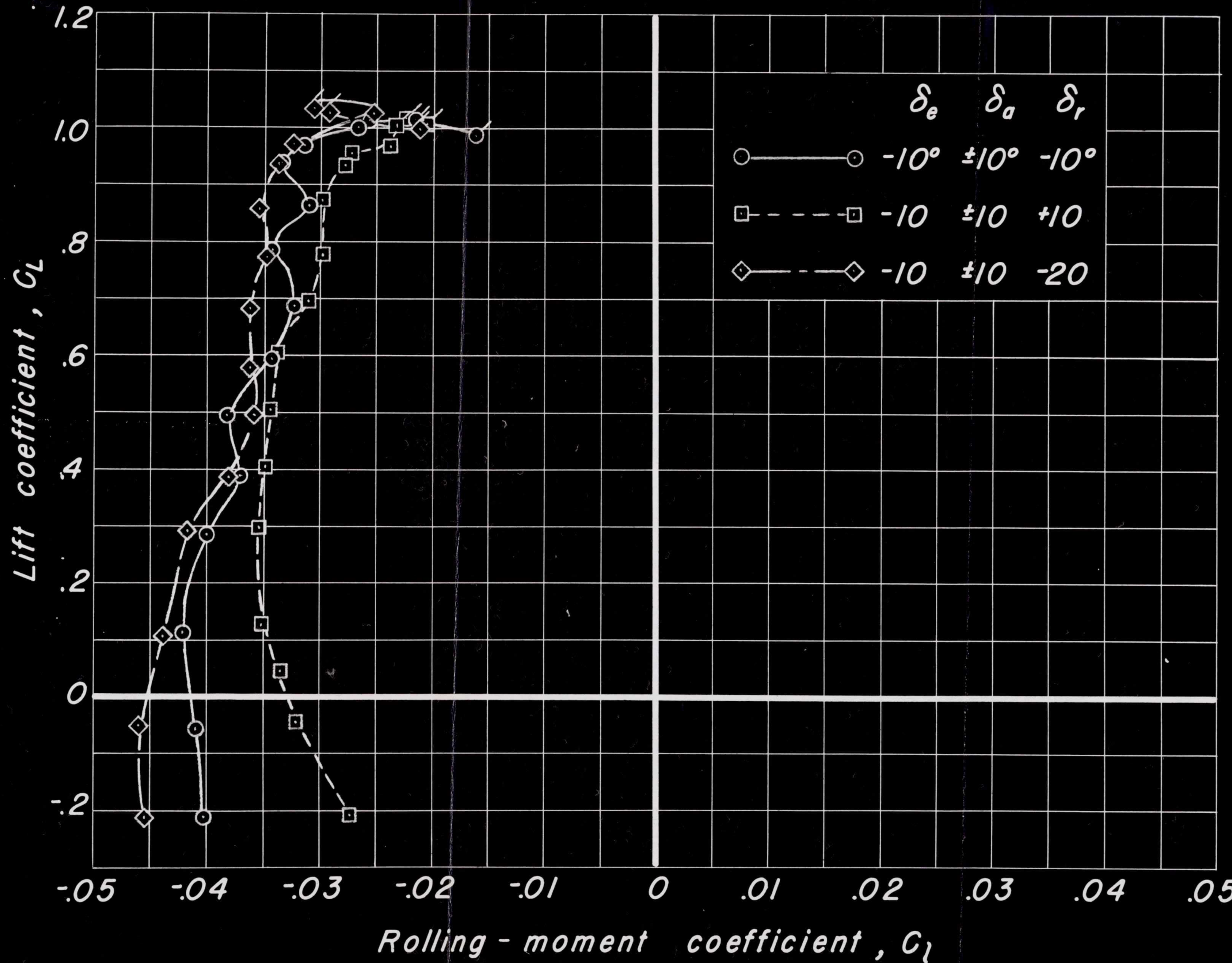

Figure 15. — Continued.

Figure 15.- Continued.

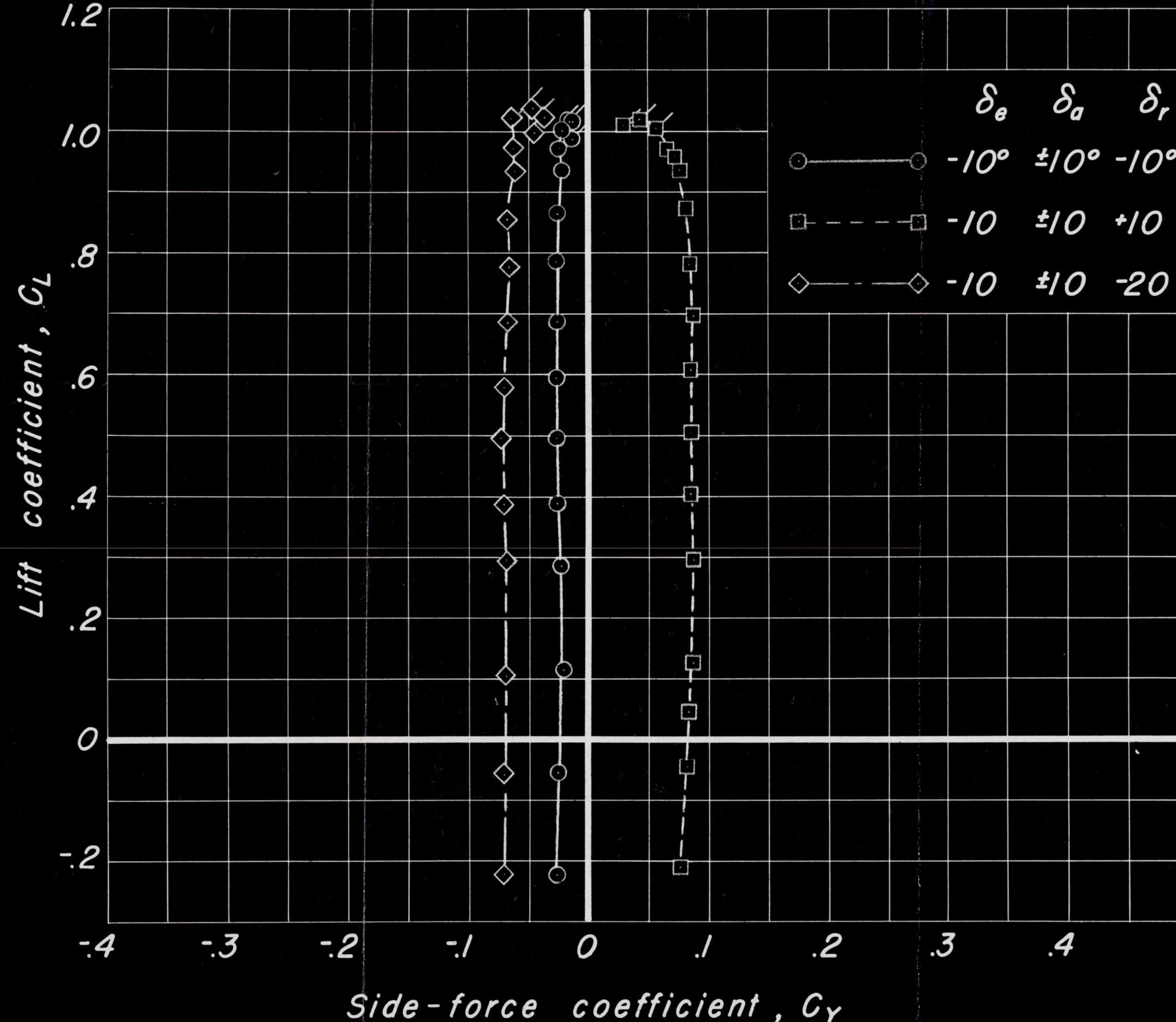

Figure 15.– Concluded.

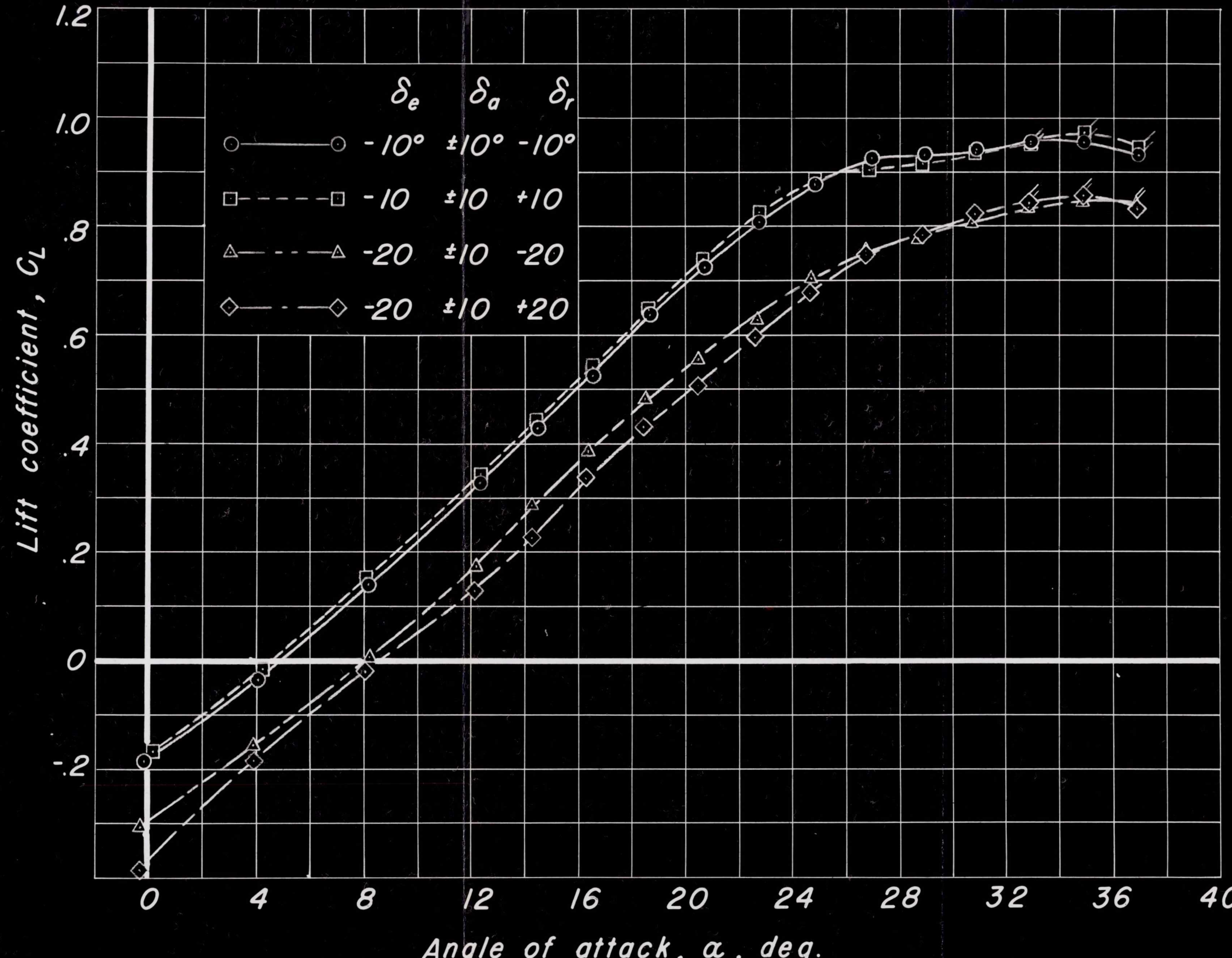

Figure 16.– Longitudinal, lateral and directional control effectiveness, $\beta = -10.06°$.

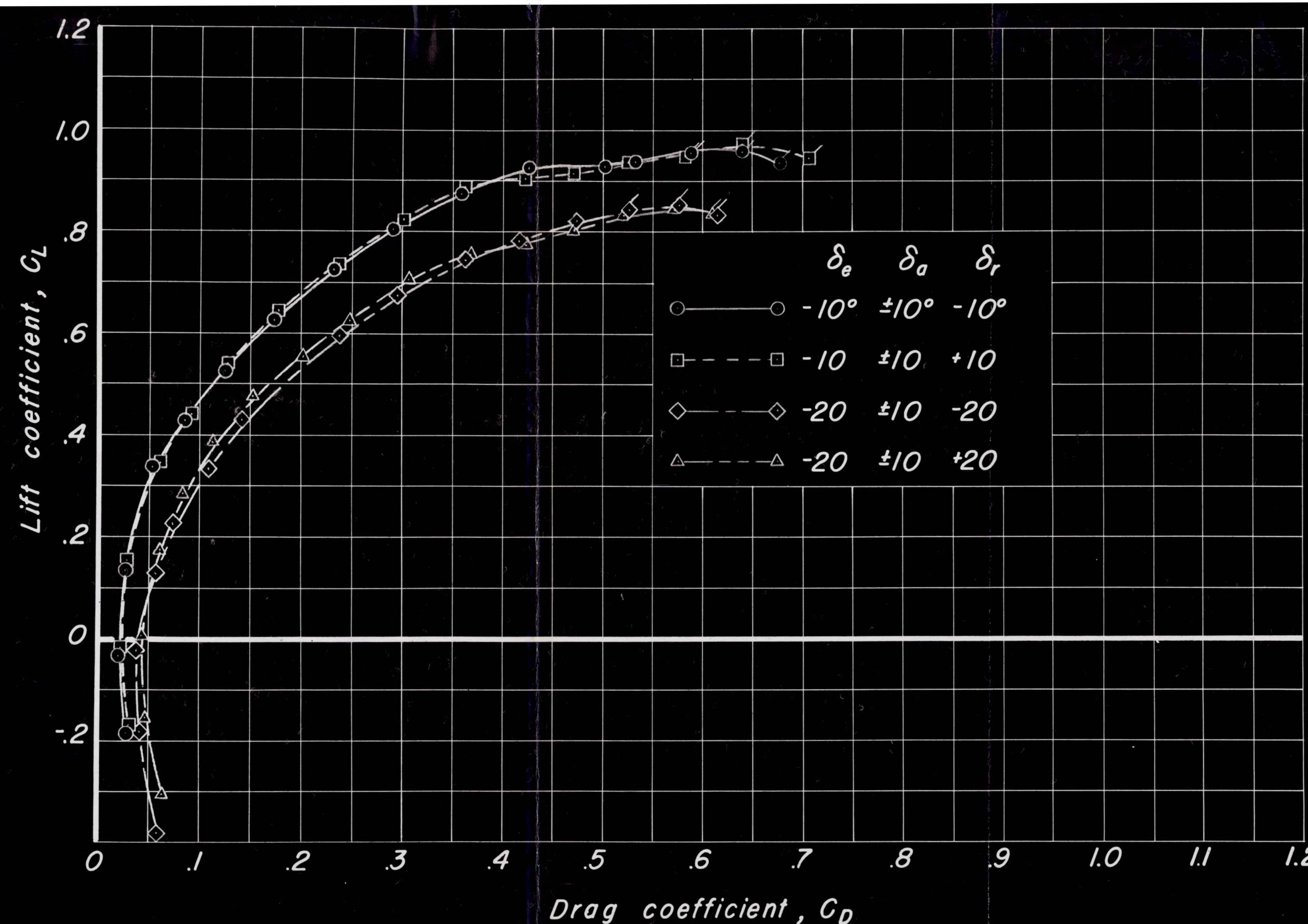

Figure 16.- Continued.

CONFIDENTIAL

NACA RM SA8B04

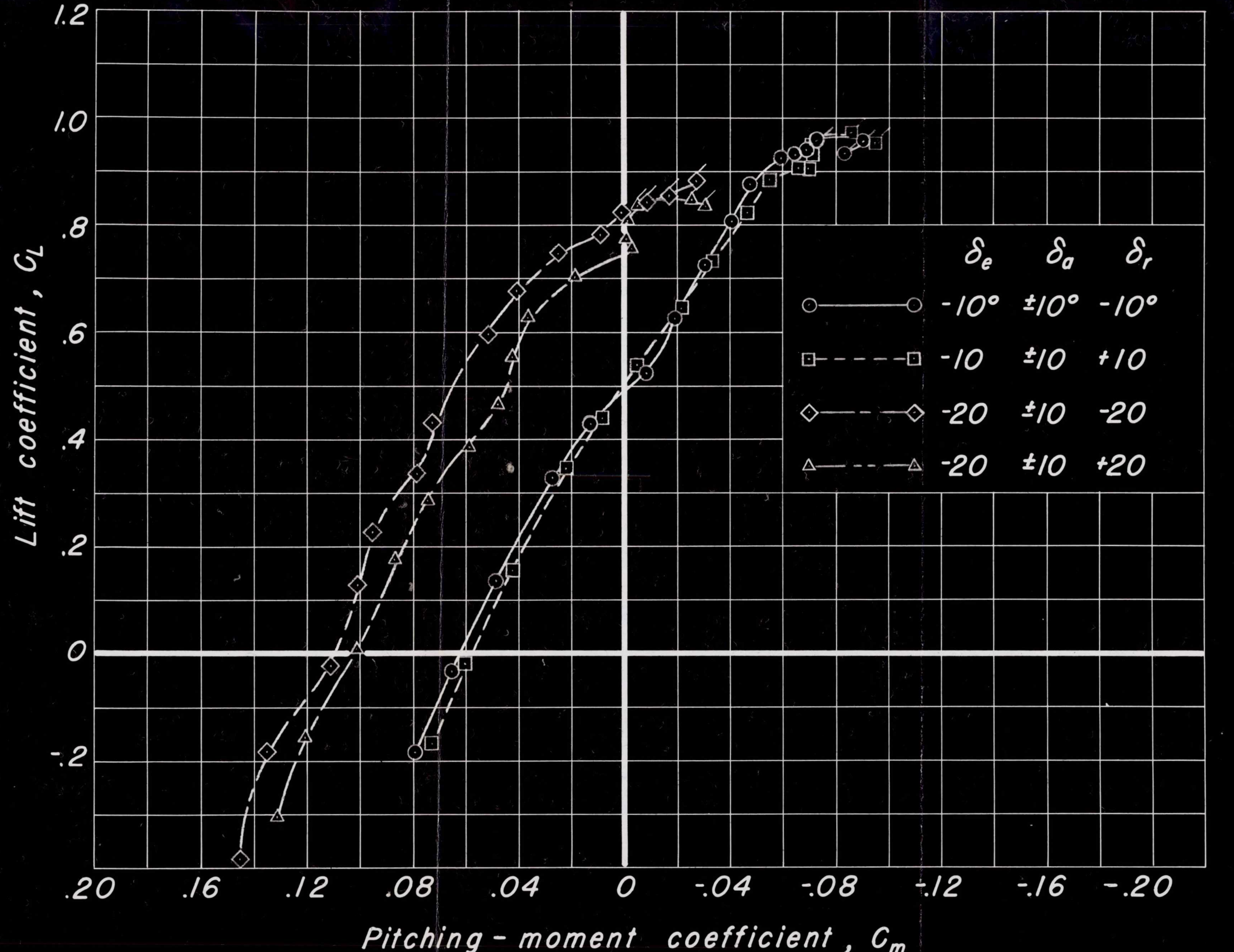

Figure 16.– Continued.

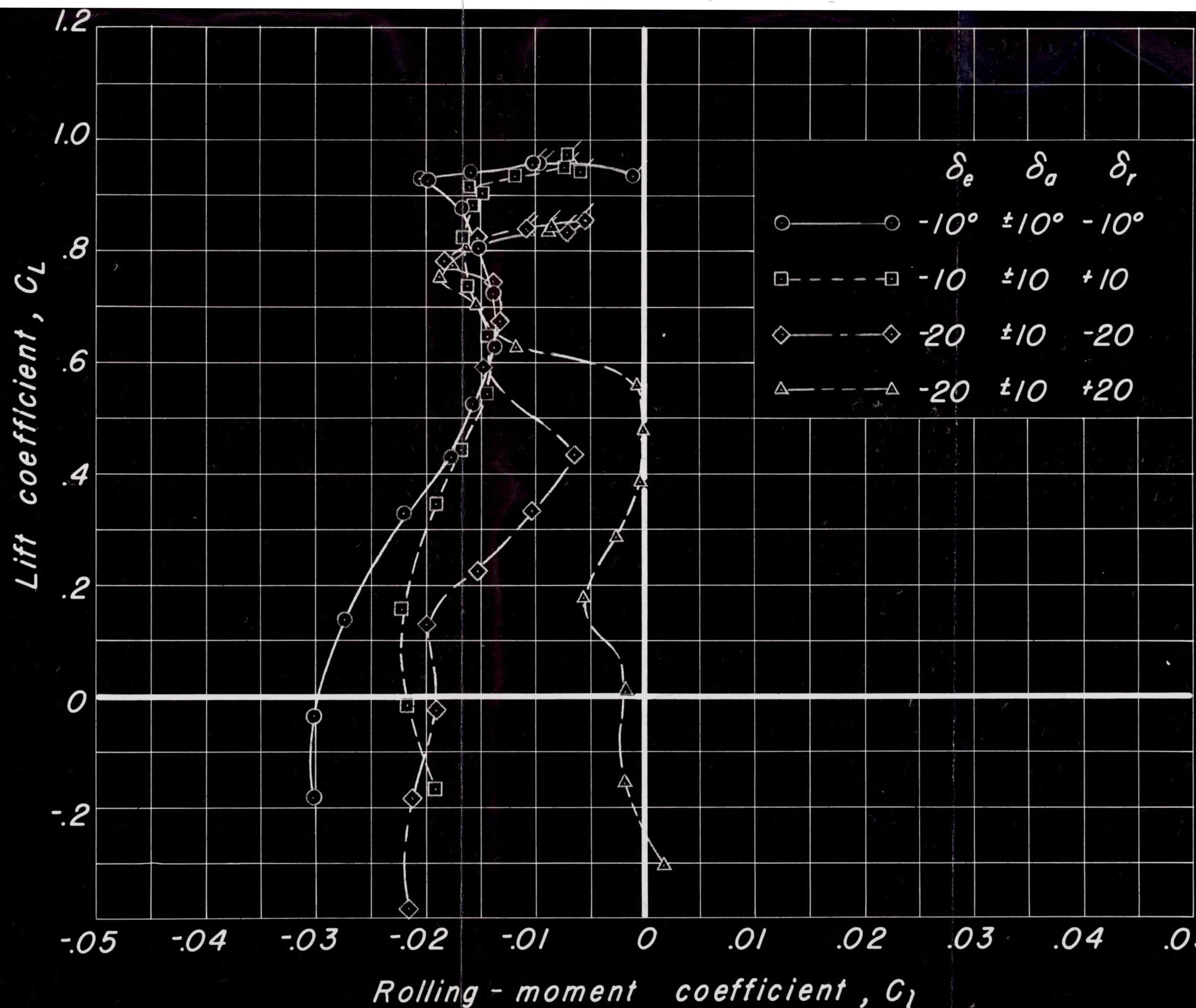

Figure 16. — Continued.

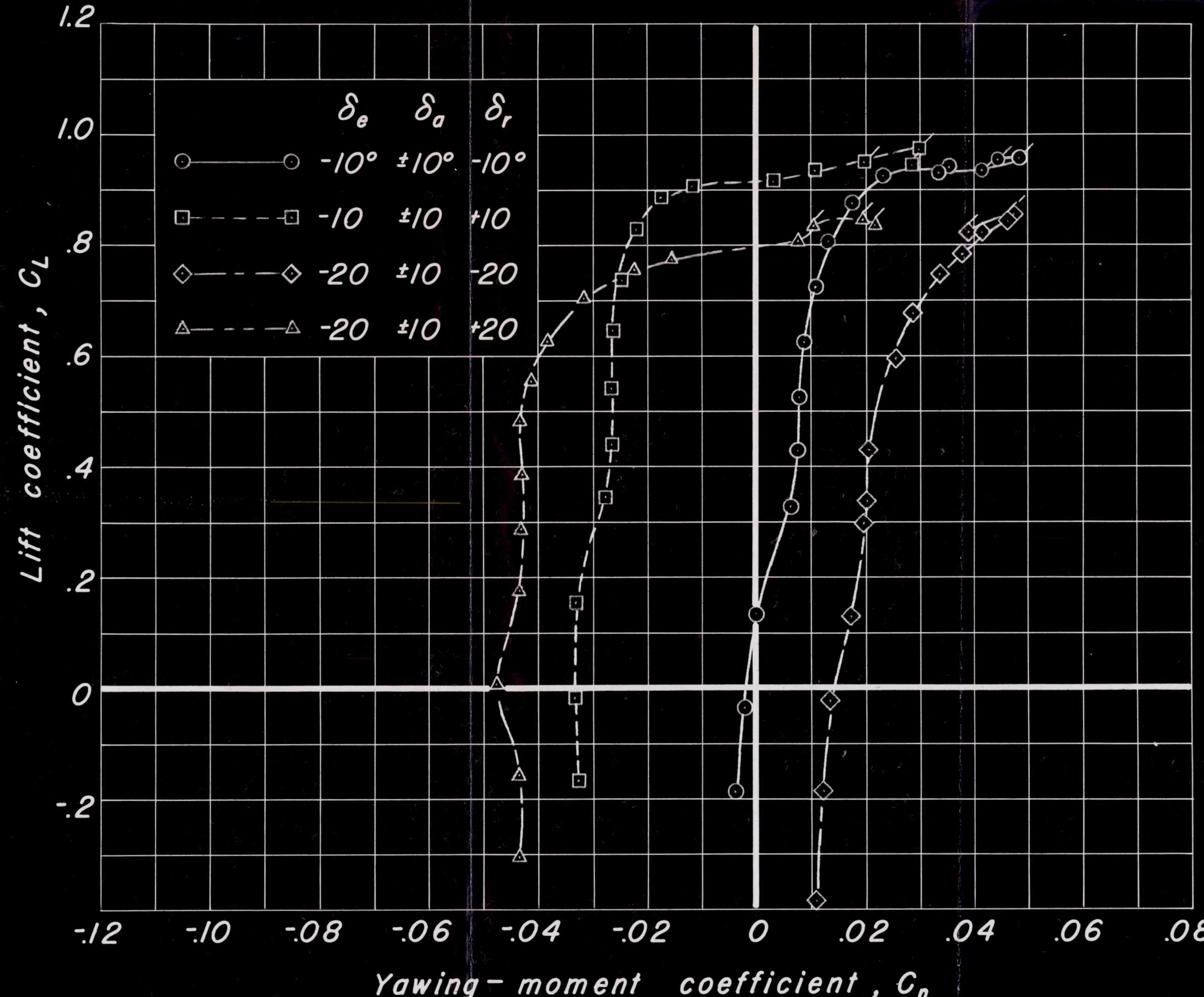

Figure 16.- Continued.

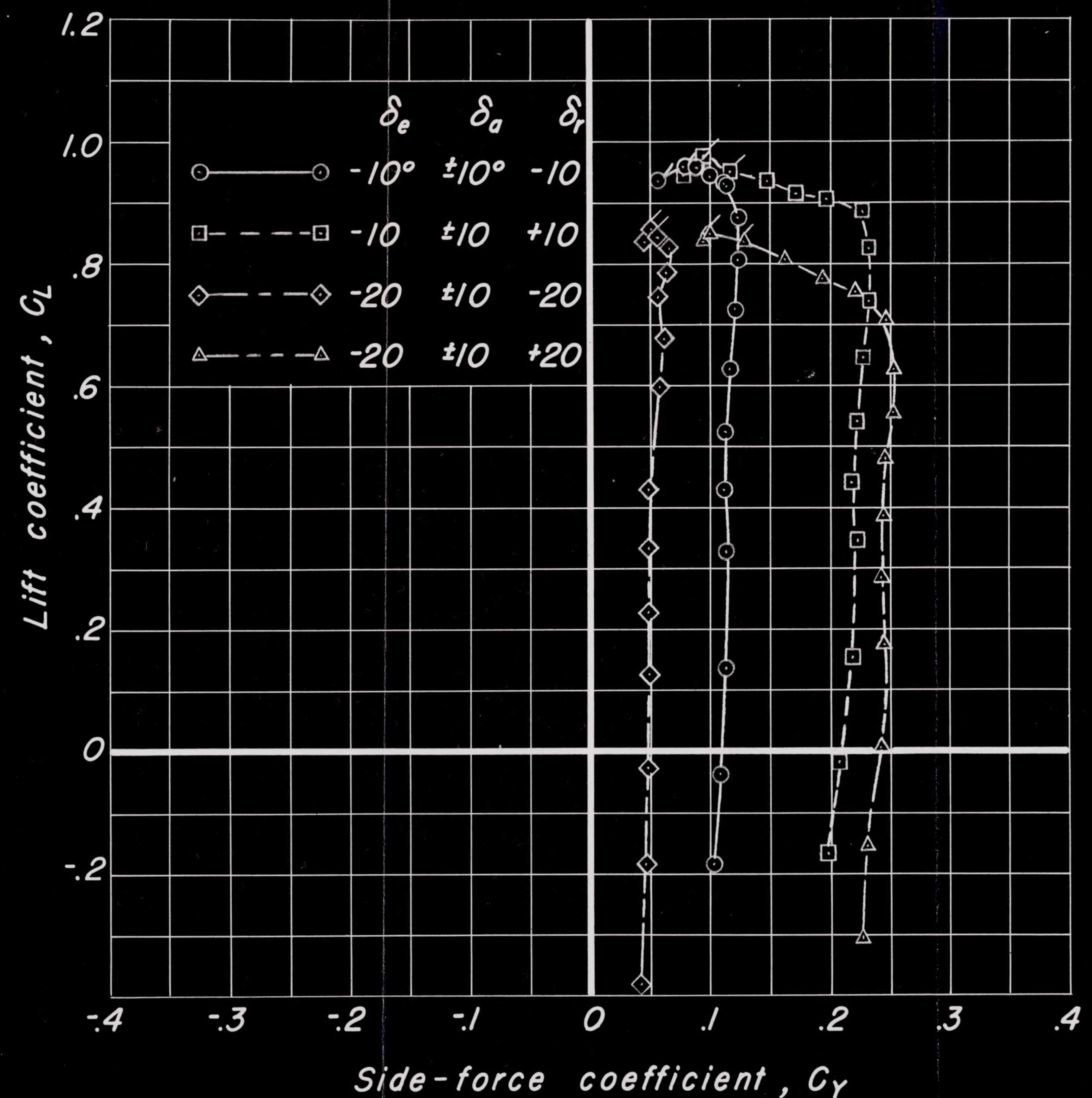

Figure 16.— Concluded.

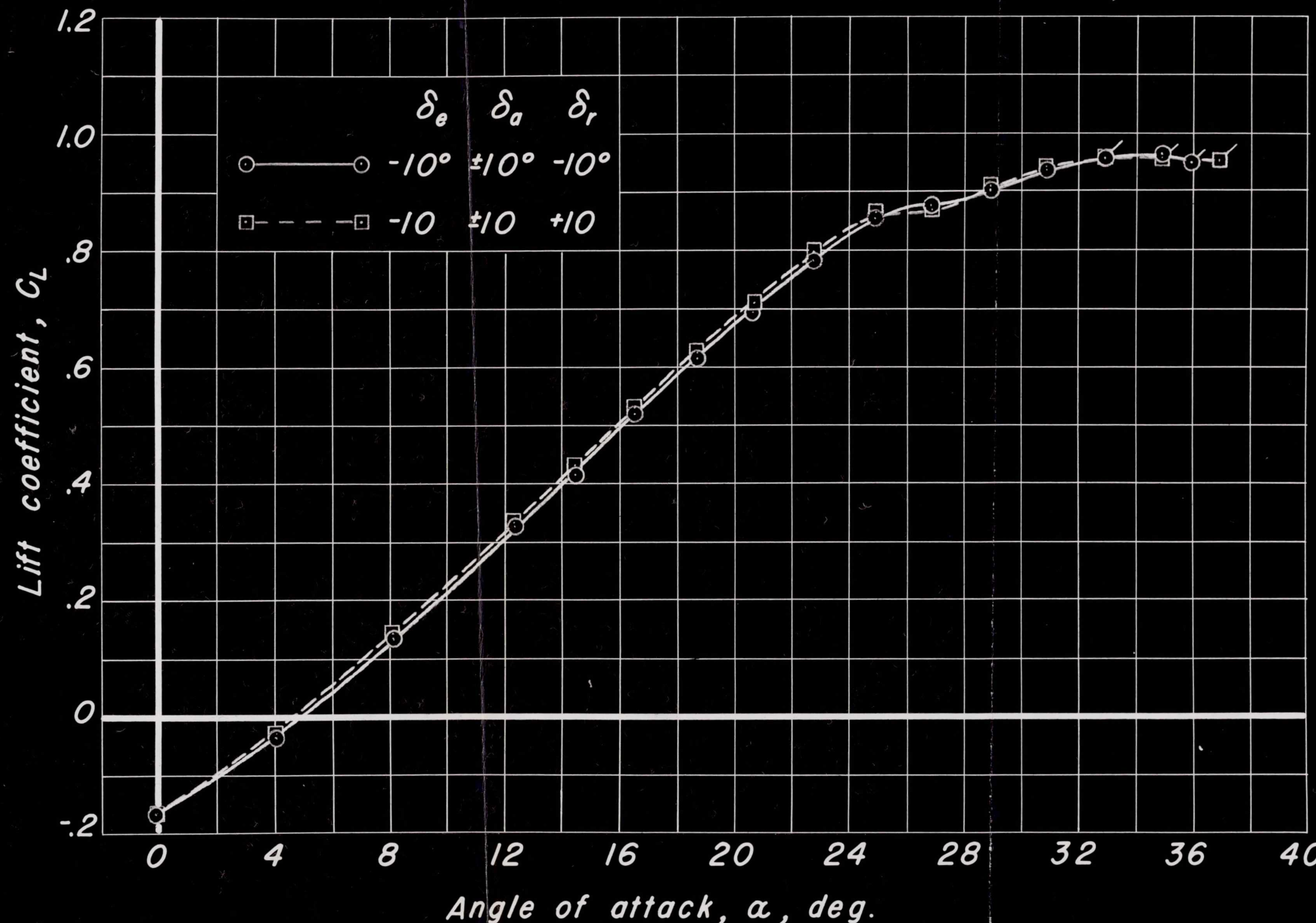

Figure 17.—Longitudinal, lateral and directional control effectiveness, $\beta = -20.20°$.

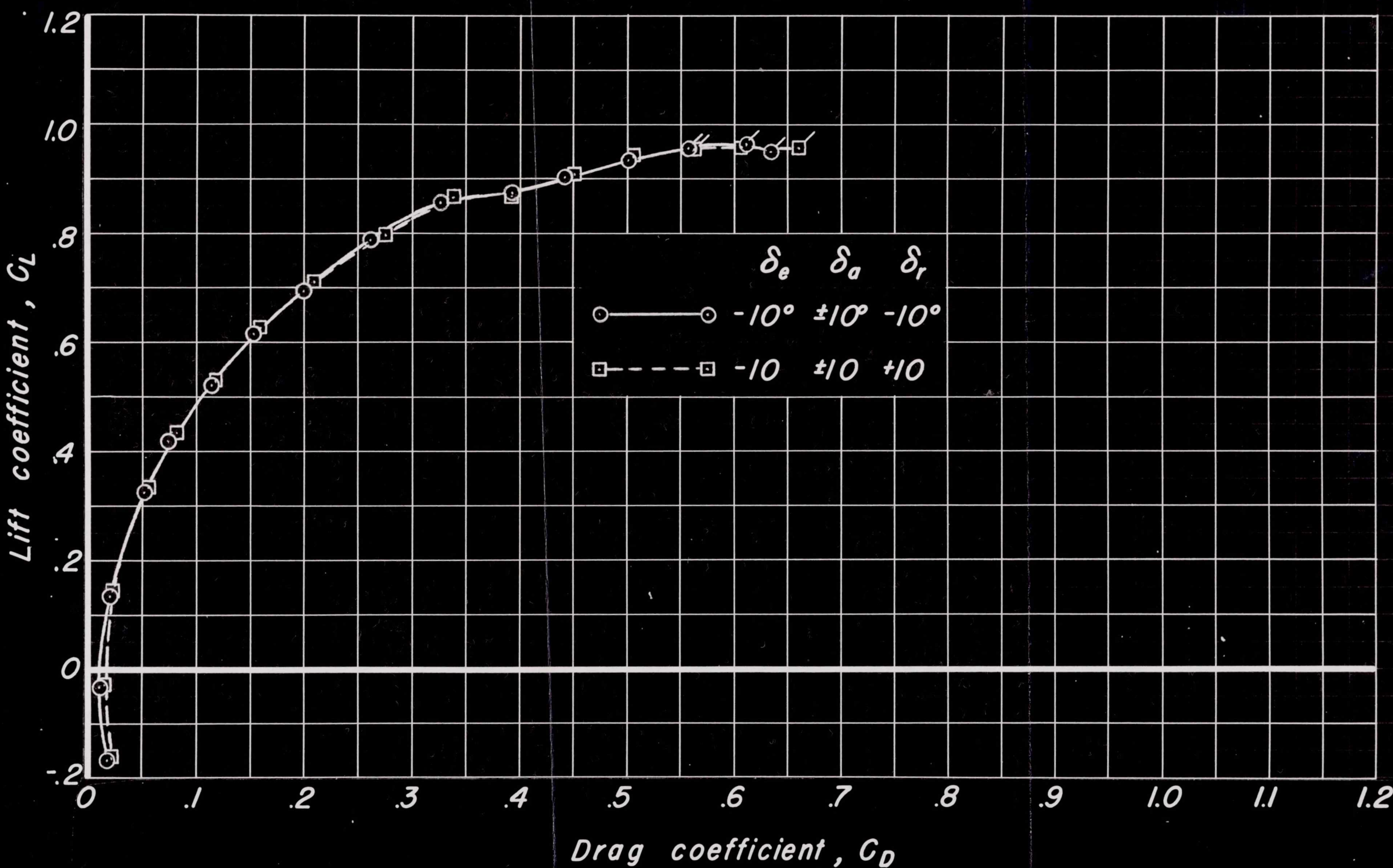

Figure 17.—Continued.

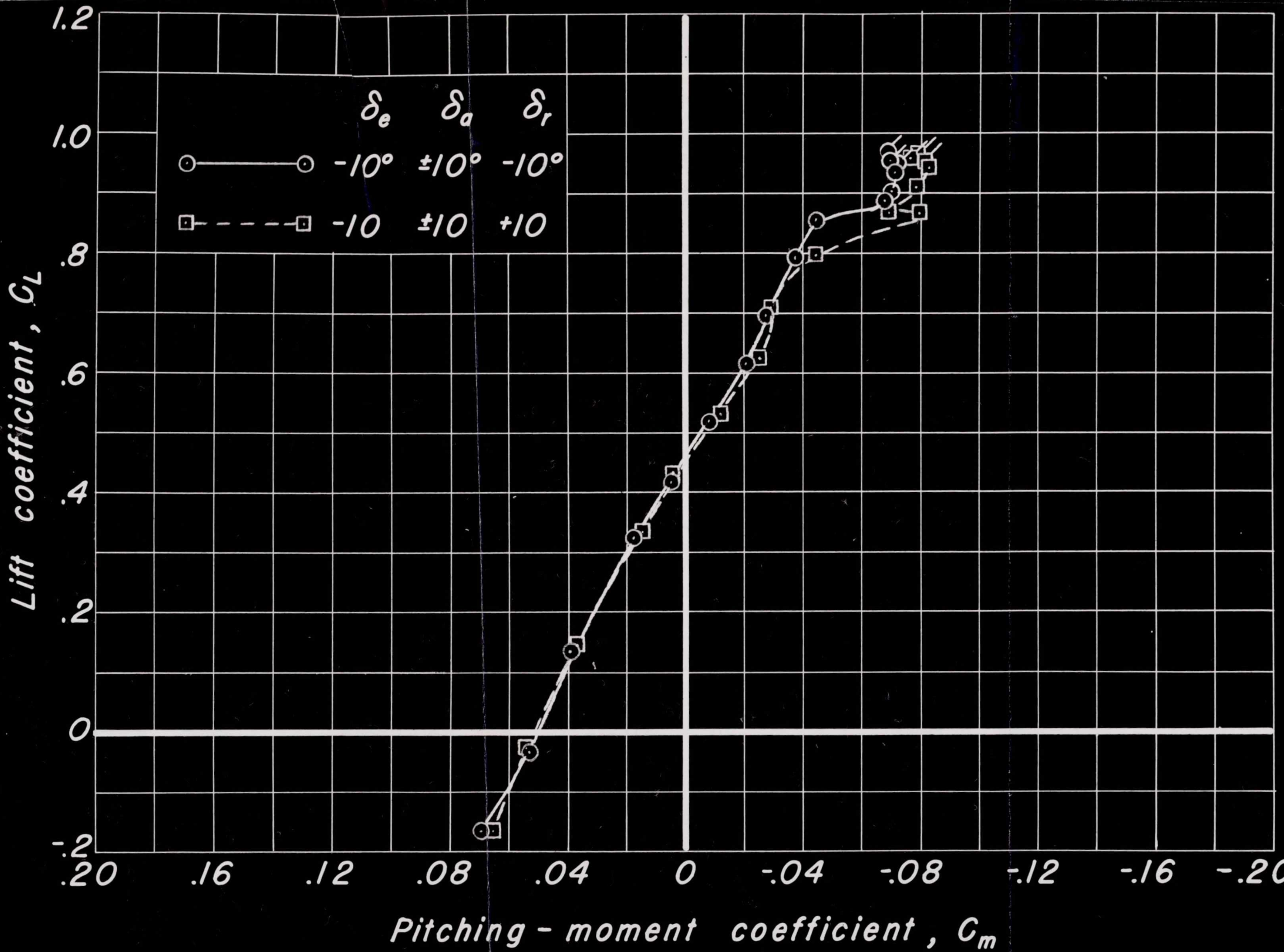

Figure 17.— Continued.

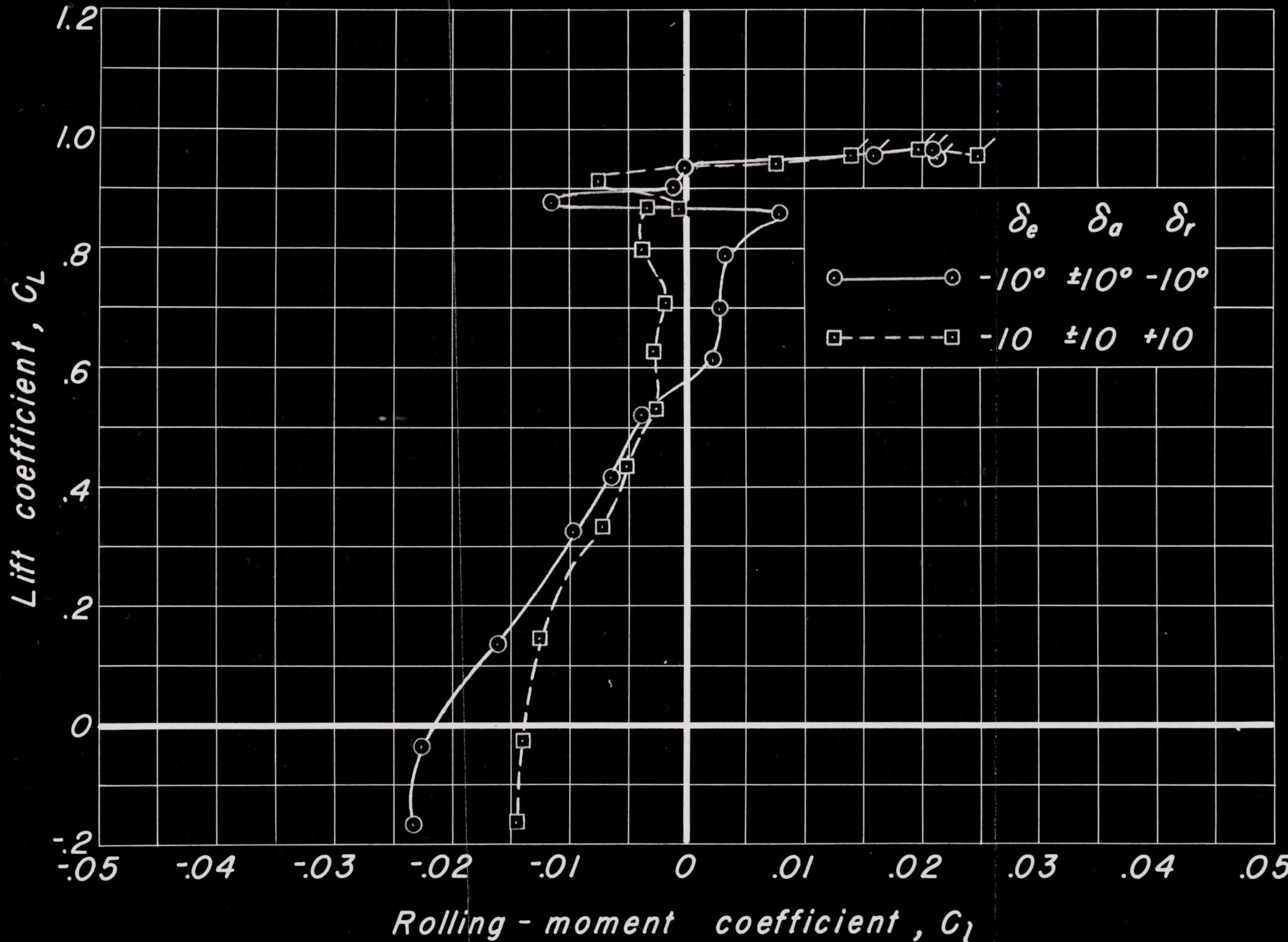

Figure 17.- Continued.

NACA SA8B04

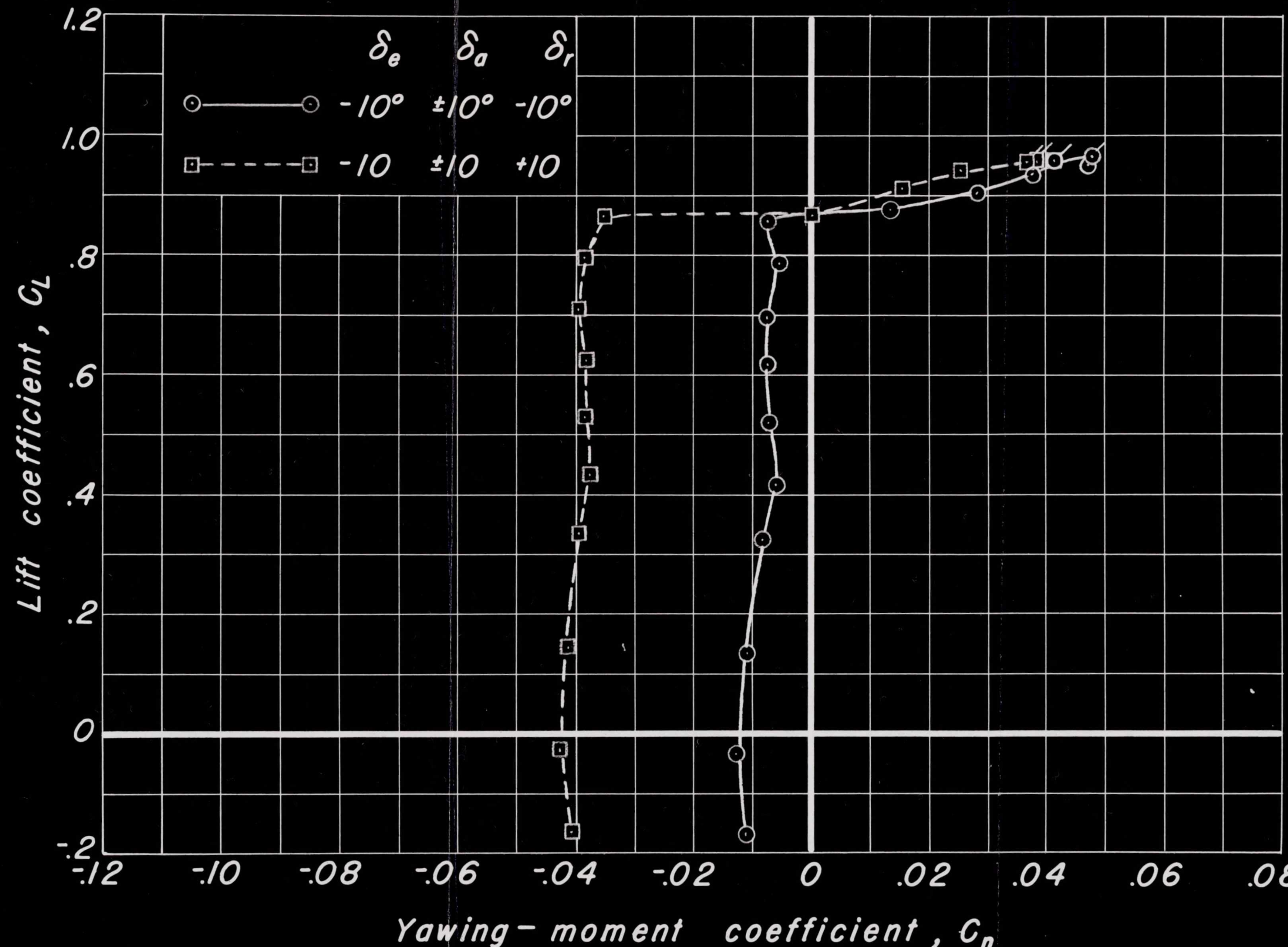

Figure 17.—Continued.

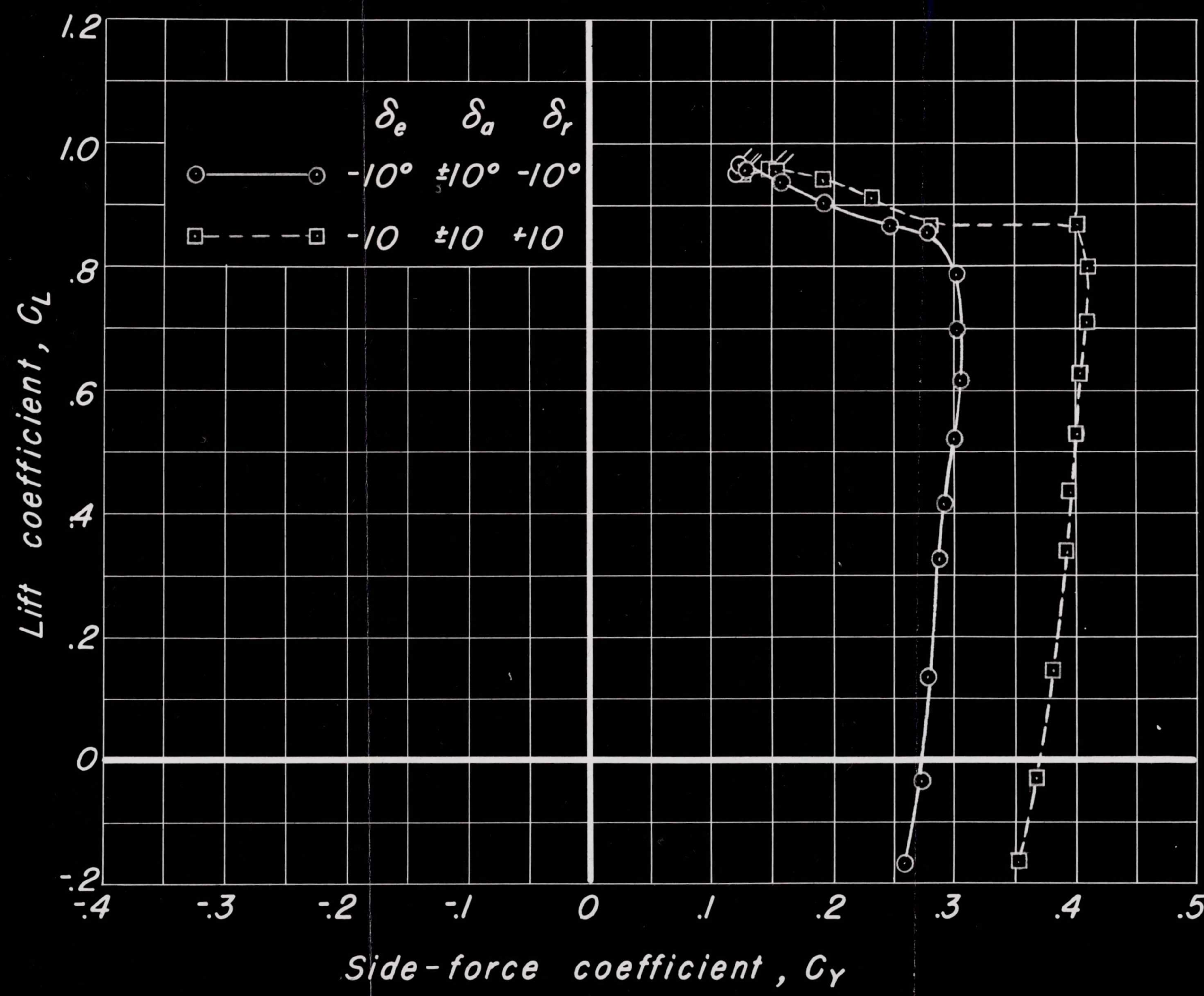

Figure 17. — Concluded.

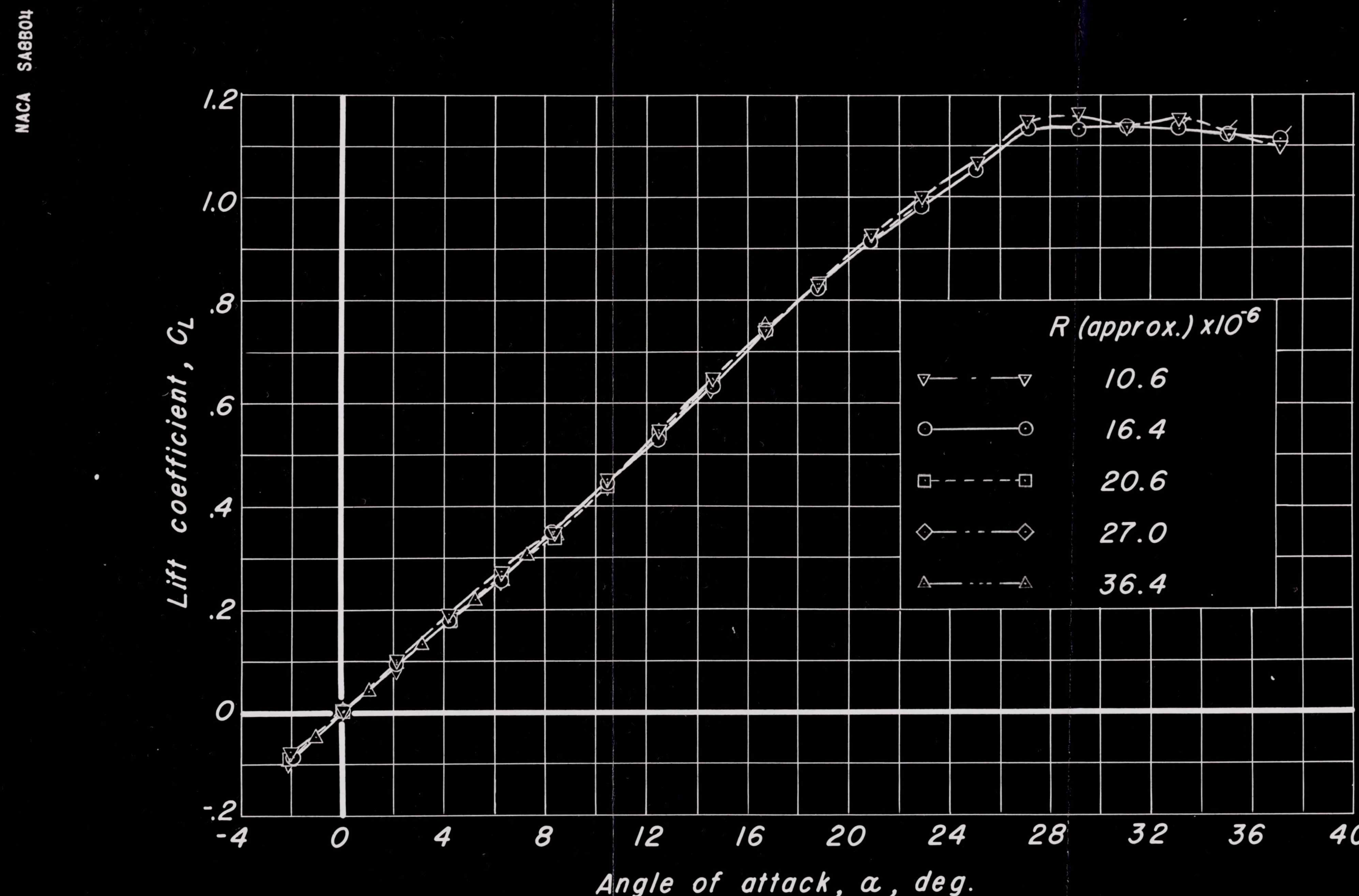

Figure 18.- Effect of Reynolds number on longitudinal characteristics with controls neutral.

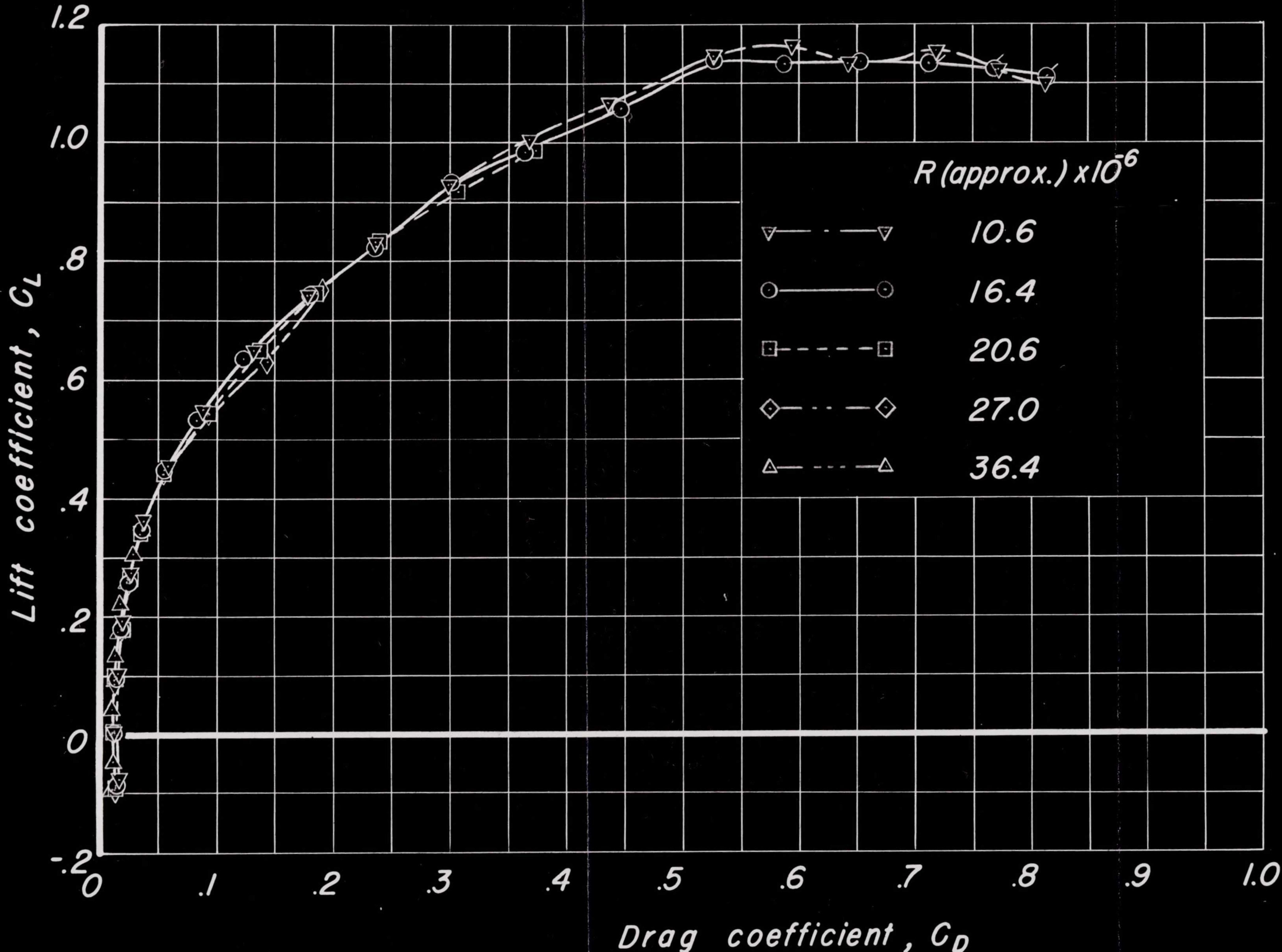

Figure 18. — Continued.

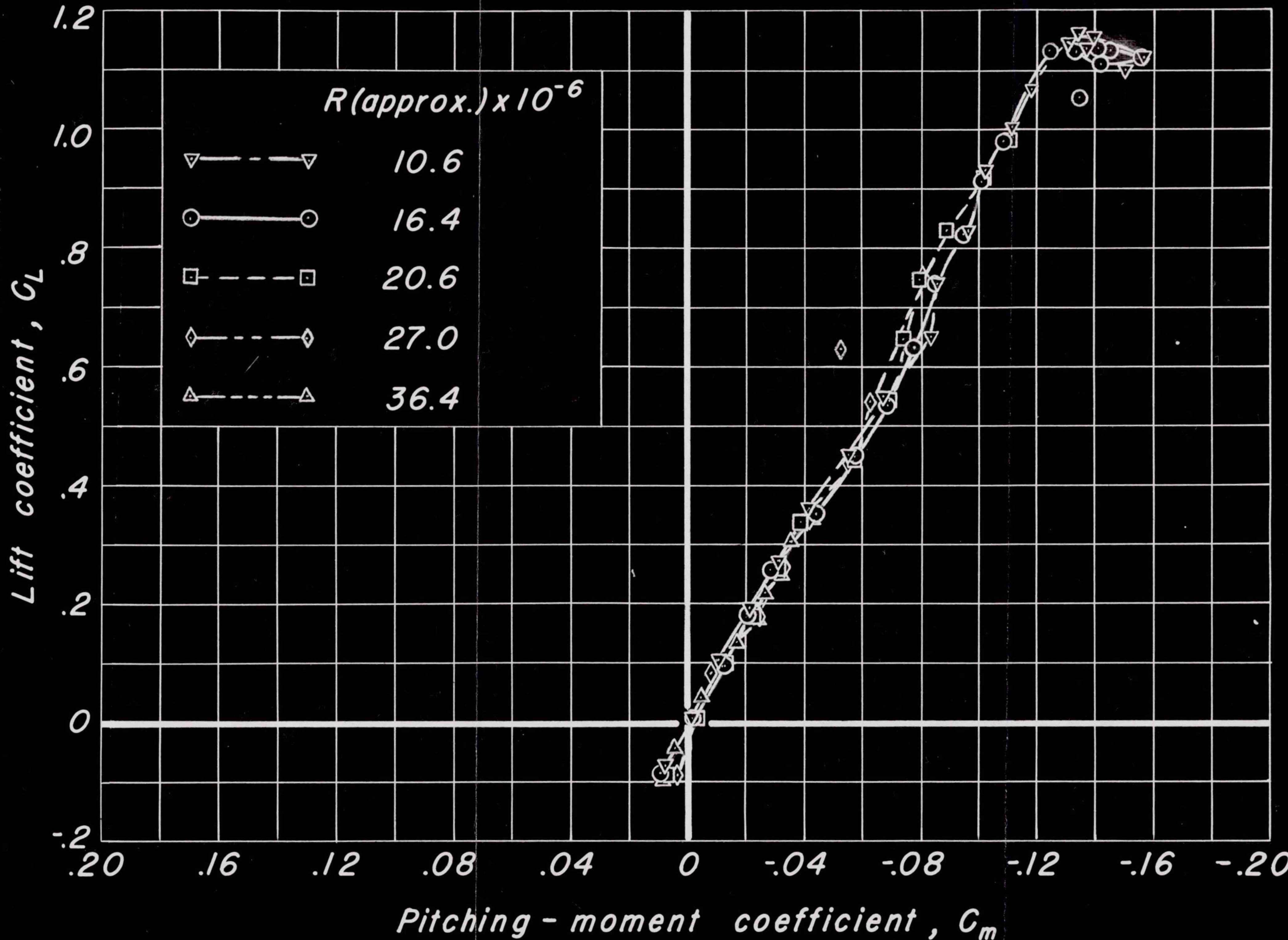

Figure 18. - Concluded.

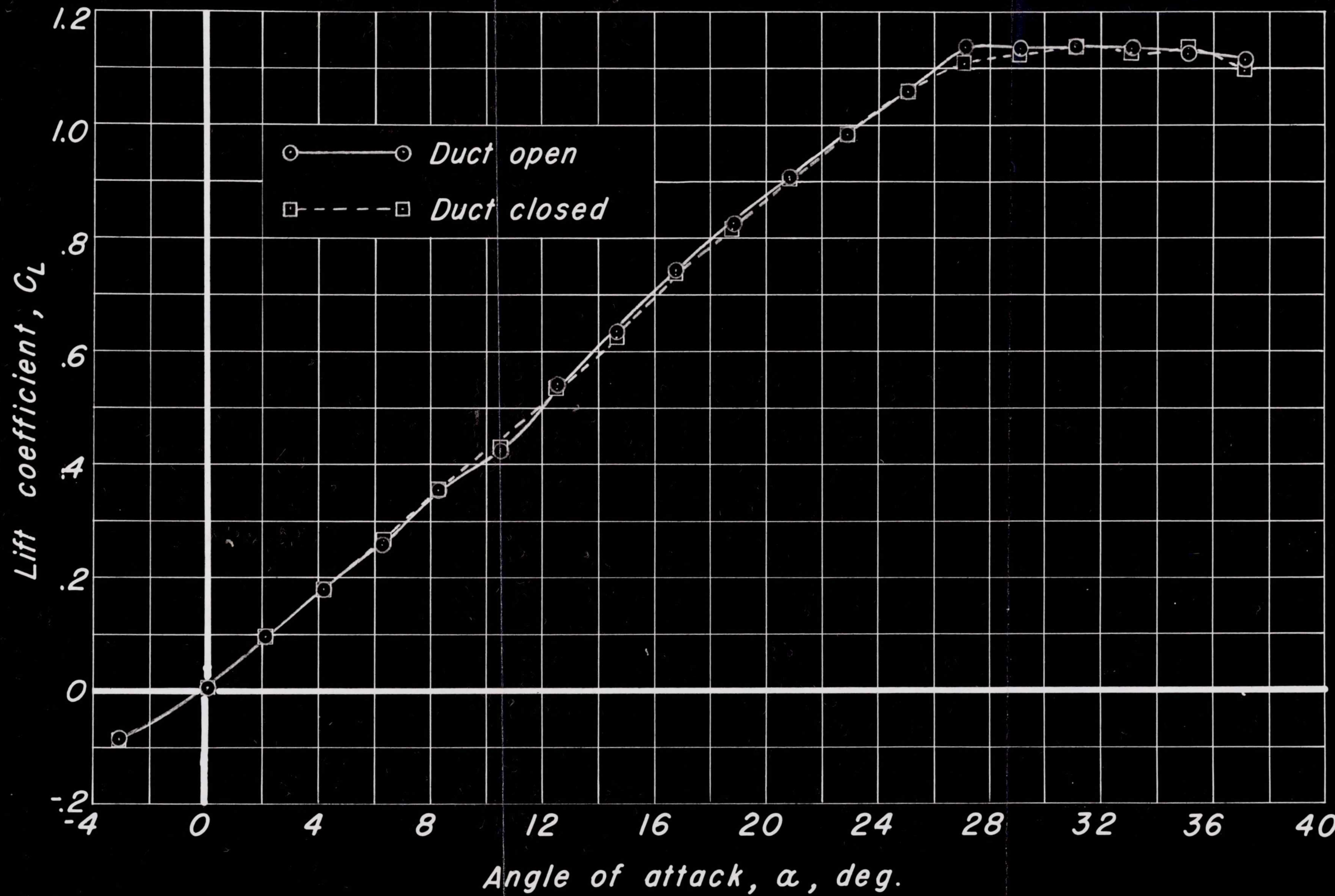

Figure 19.- Effect of internal flow through the ducted fuselage on longitudinal characteristics with controls neutral.

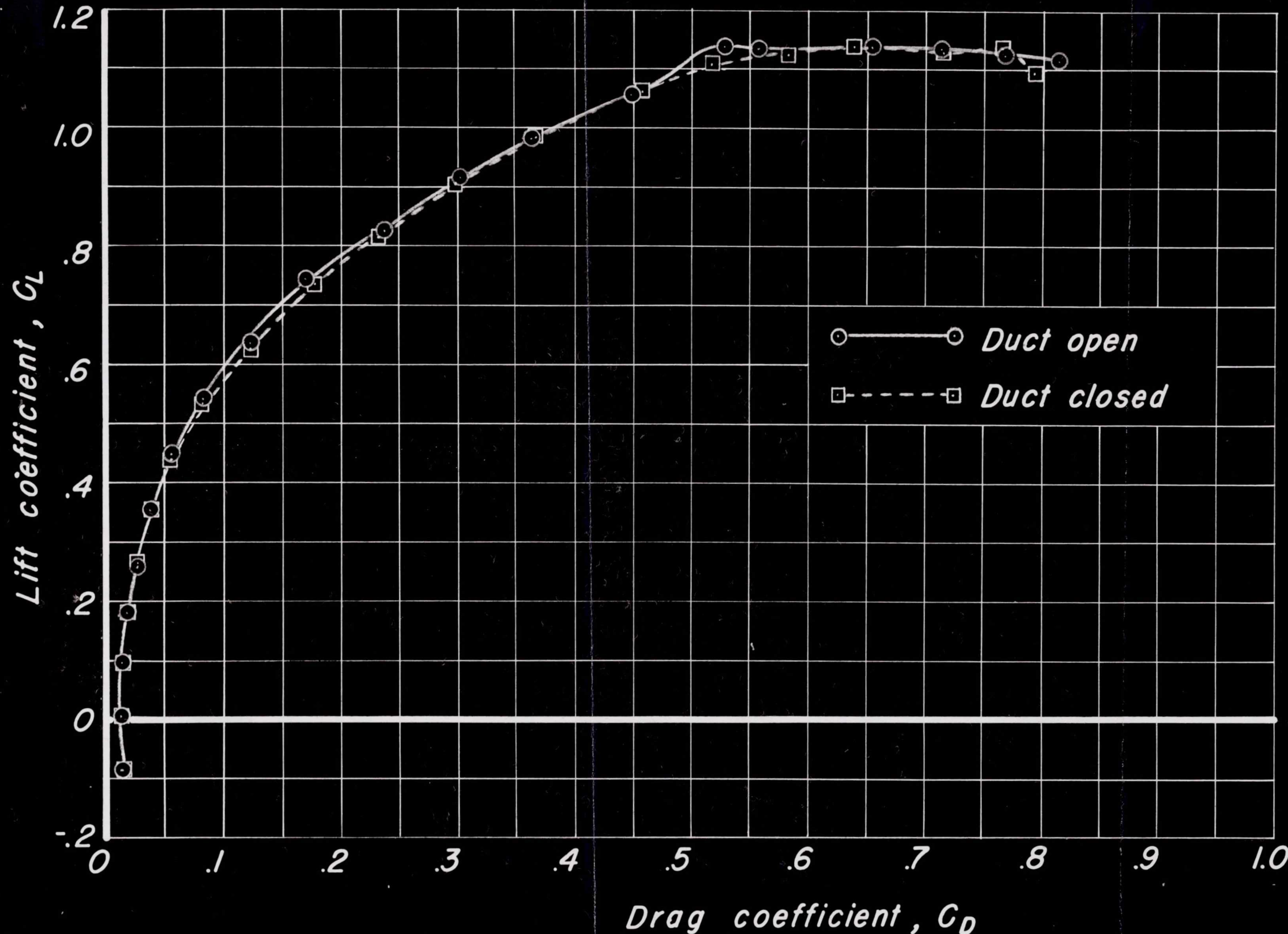

Figure 19.—Continued.

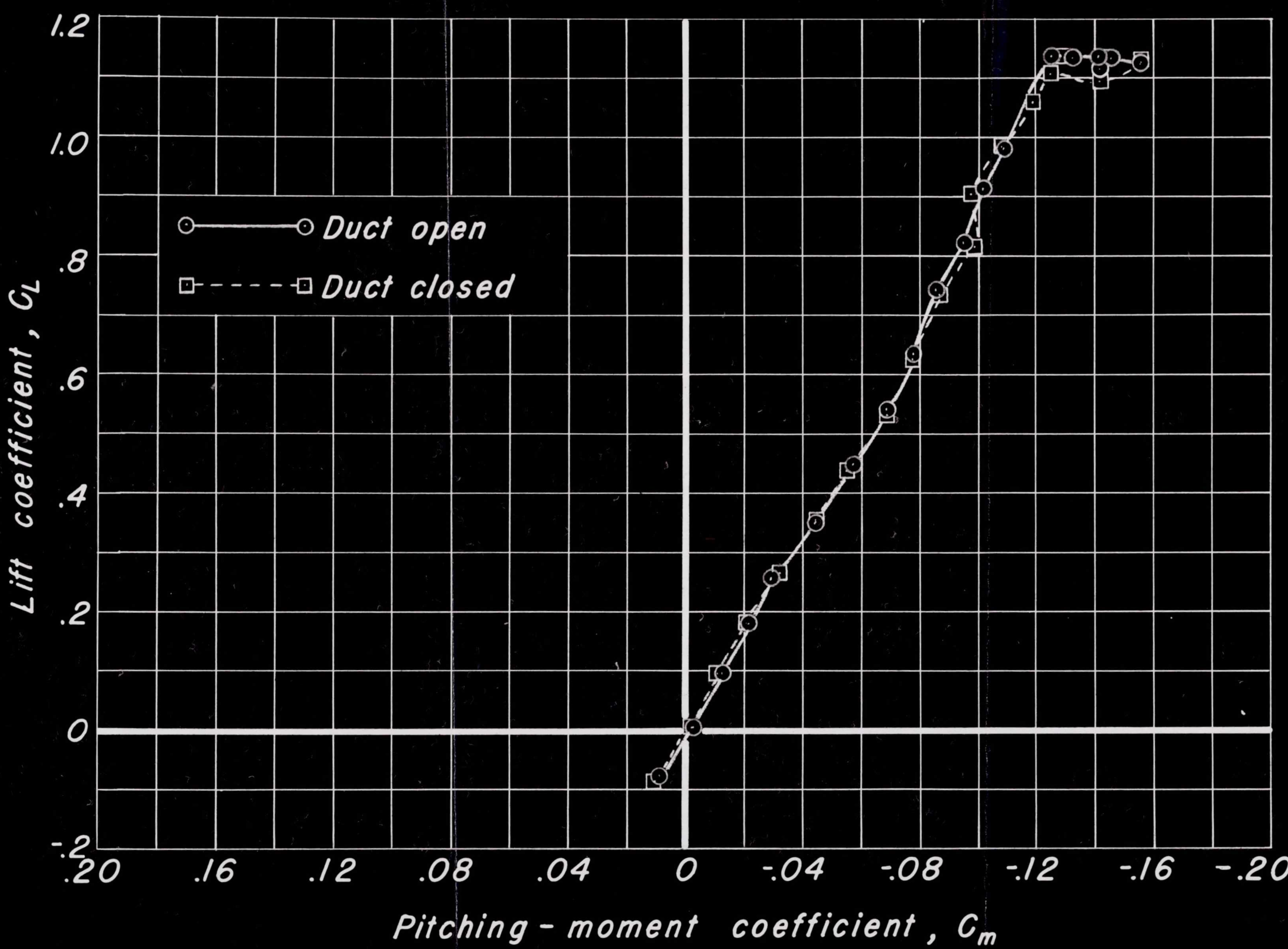

Figure 19.— Concluded.

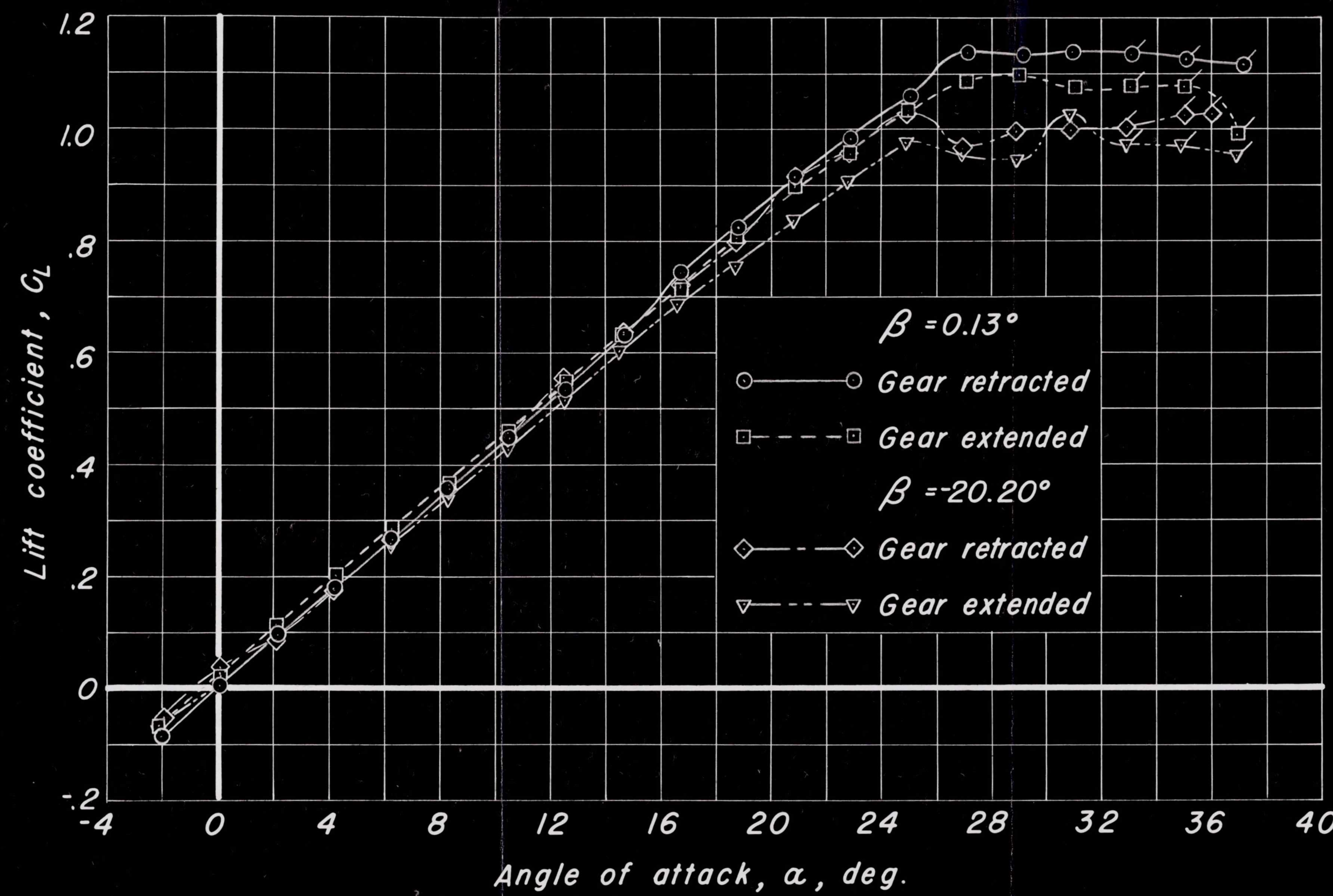

Figure 20. - Effects of extended landing gear on stability.

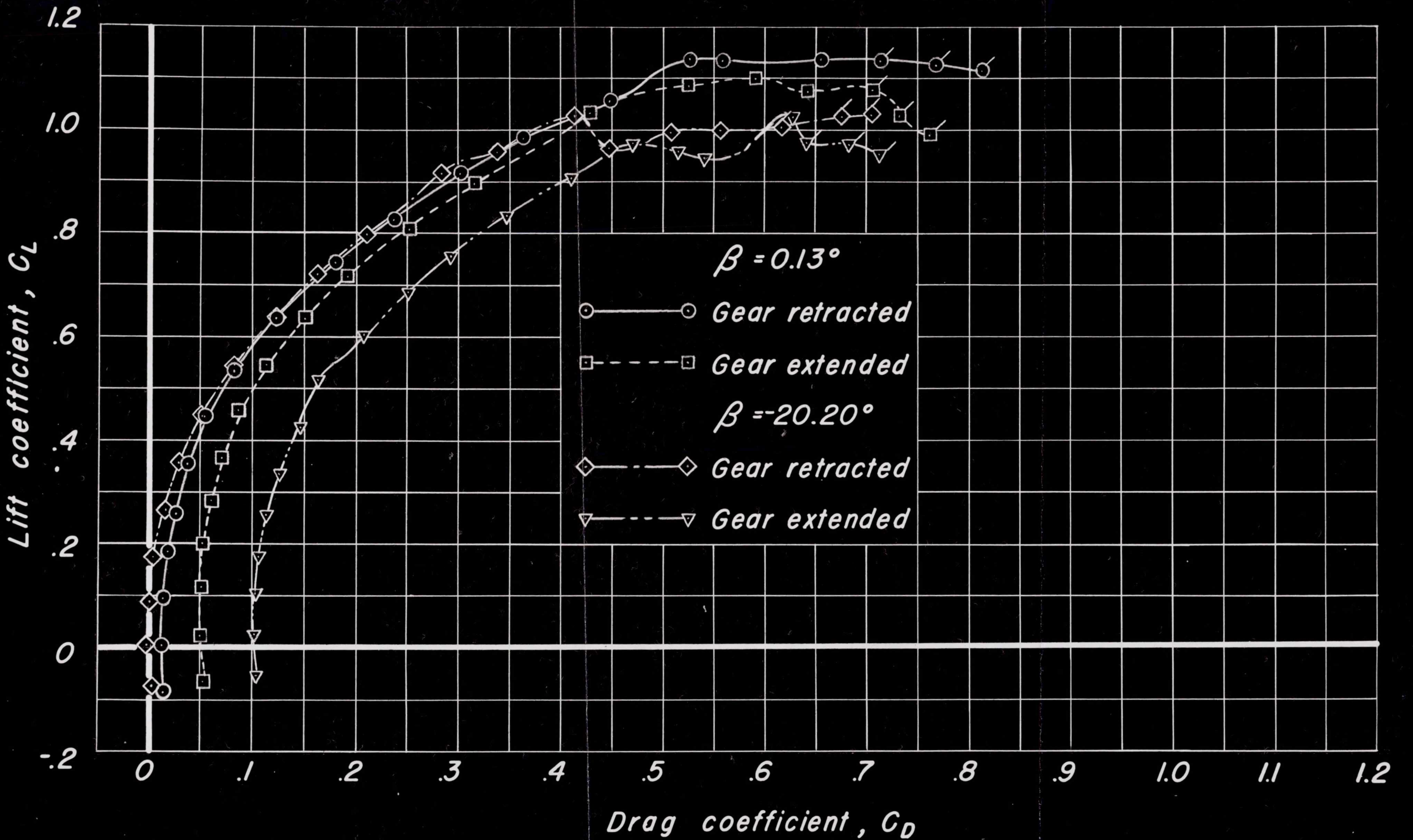

Figure 20.– Continued.

NACA SA8B04

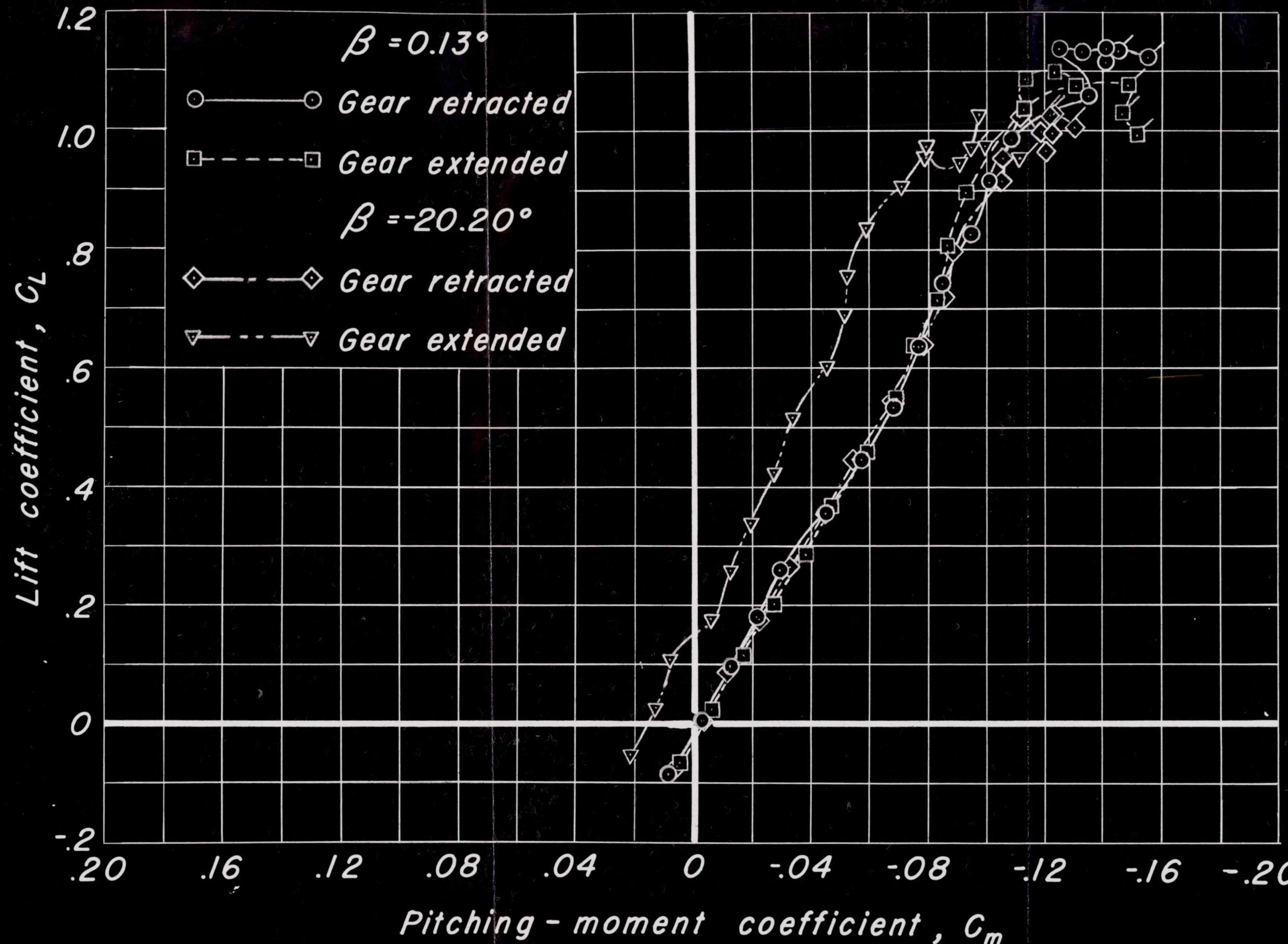

Figure 20.- Continued.

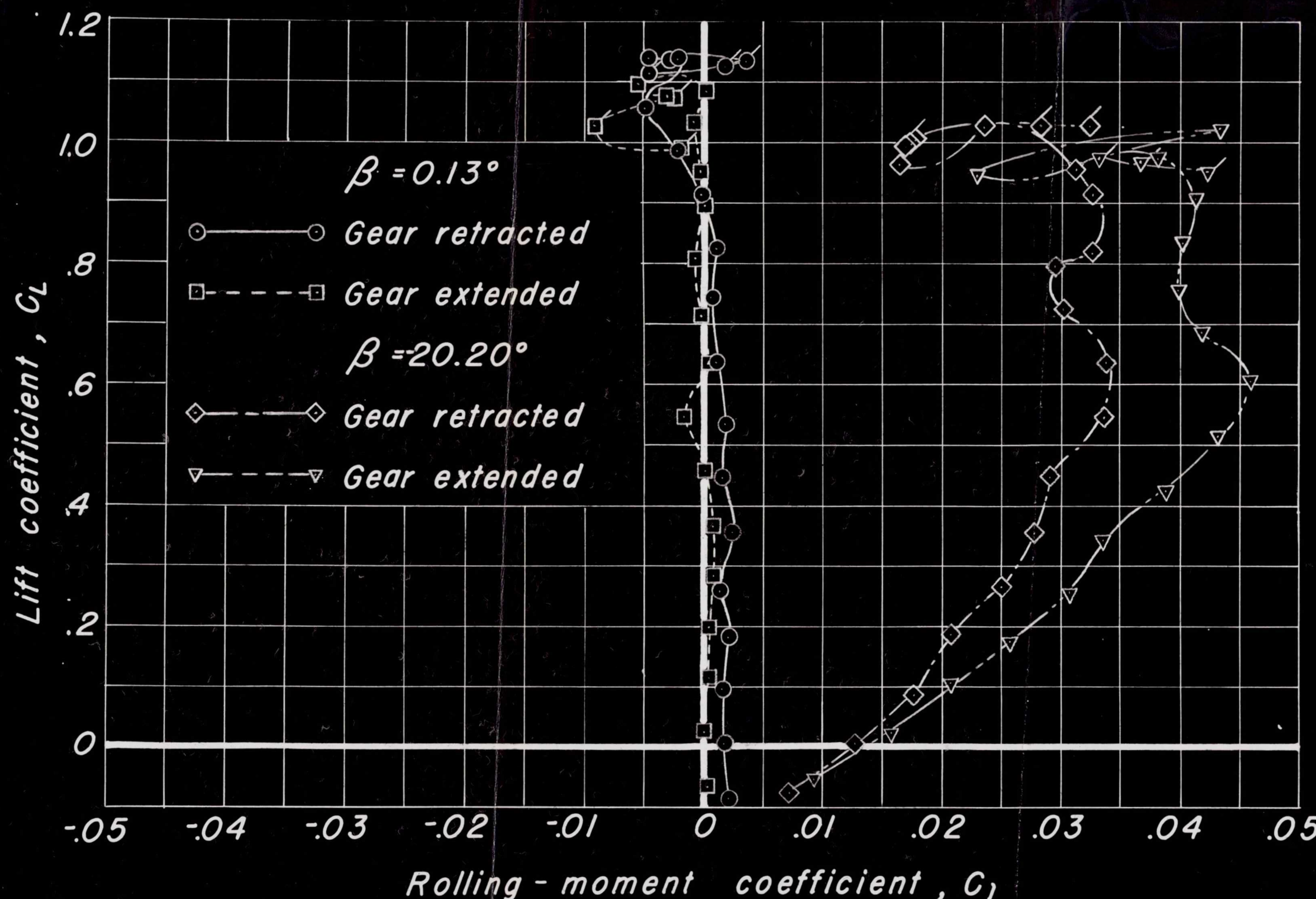

Figure 20. — Continued.

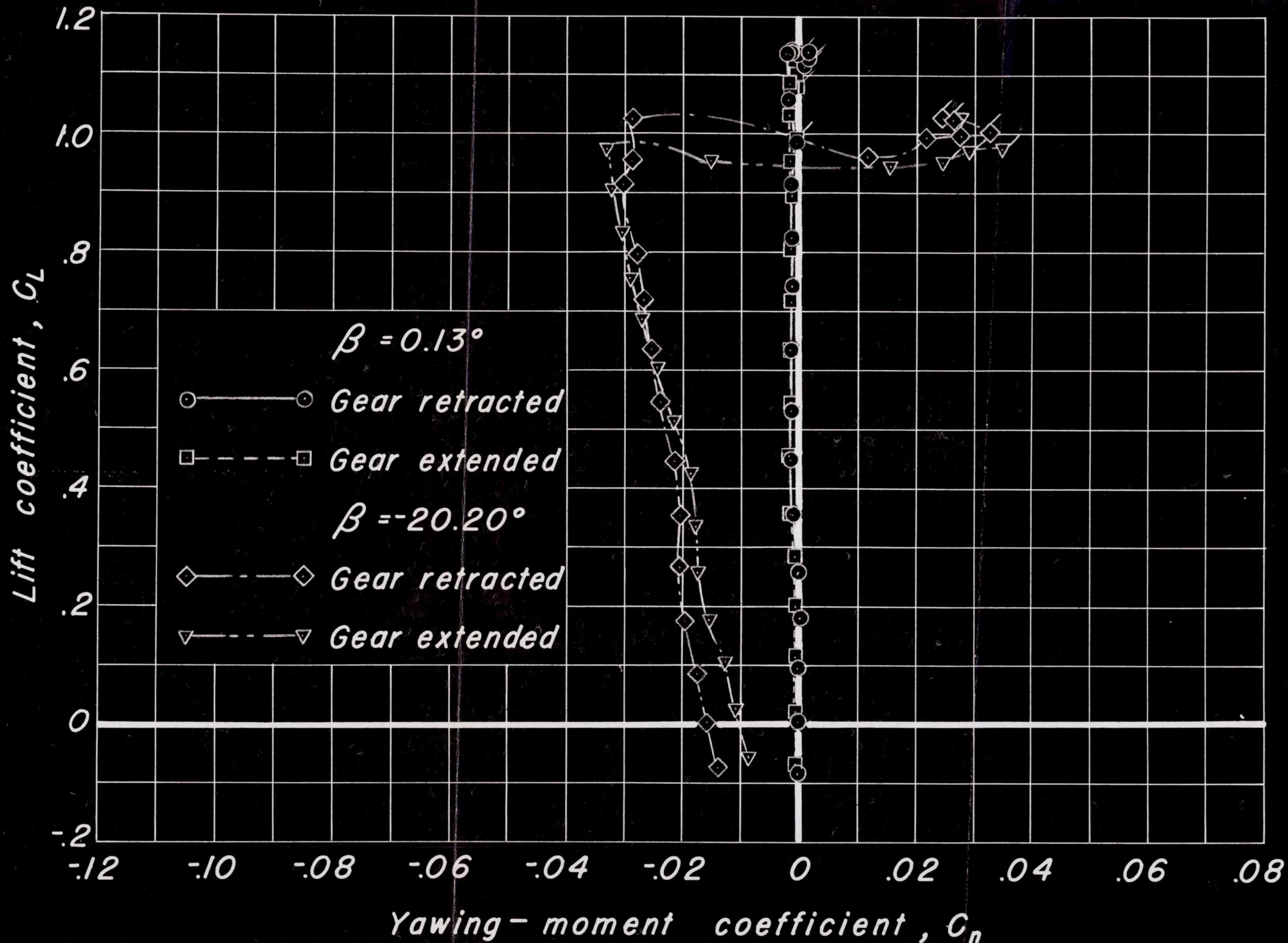

Figure 20.—Continued.

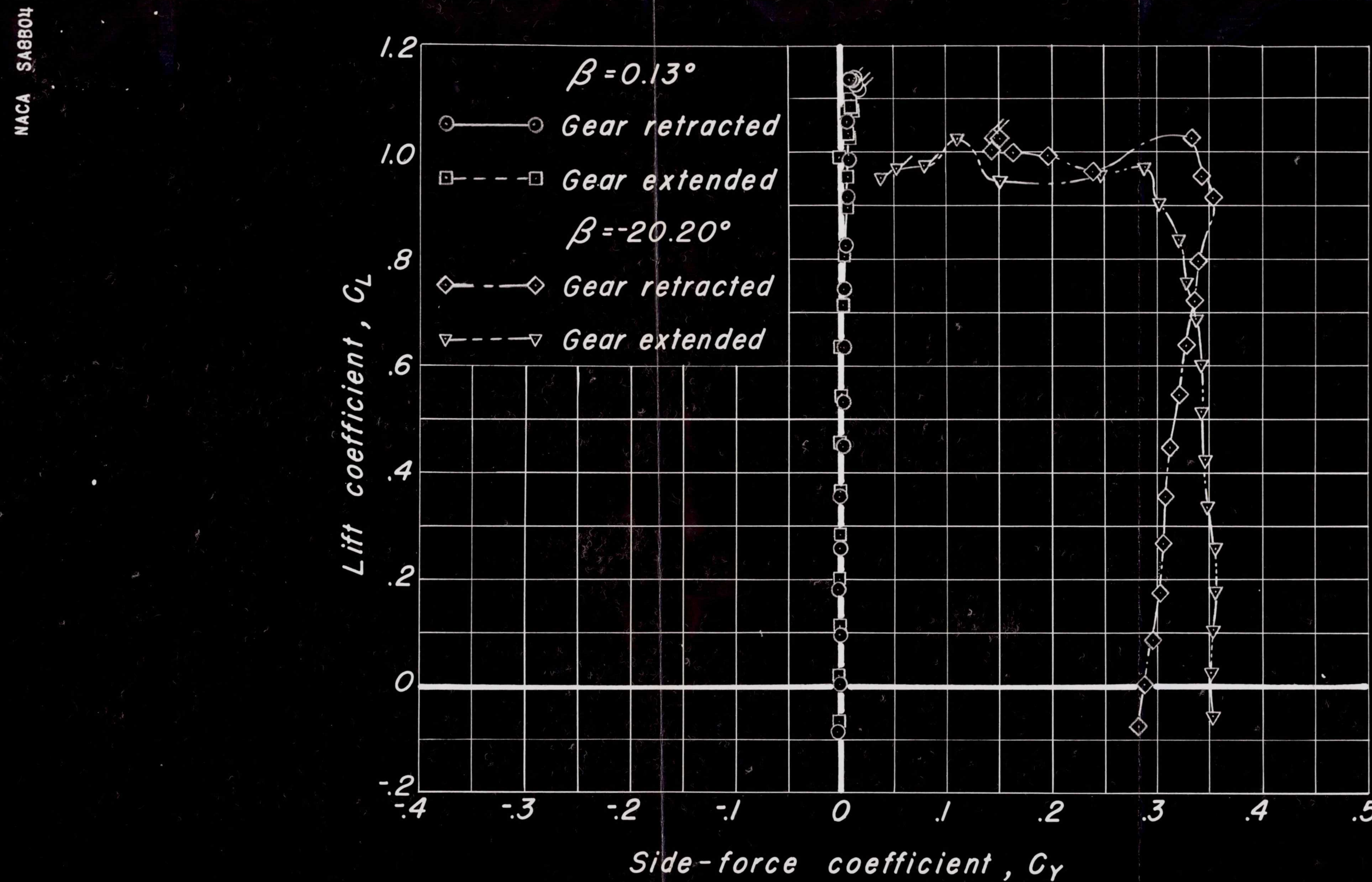

Figure 20. - Concluded.

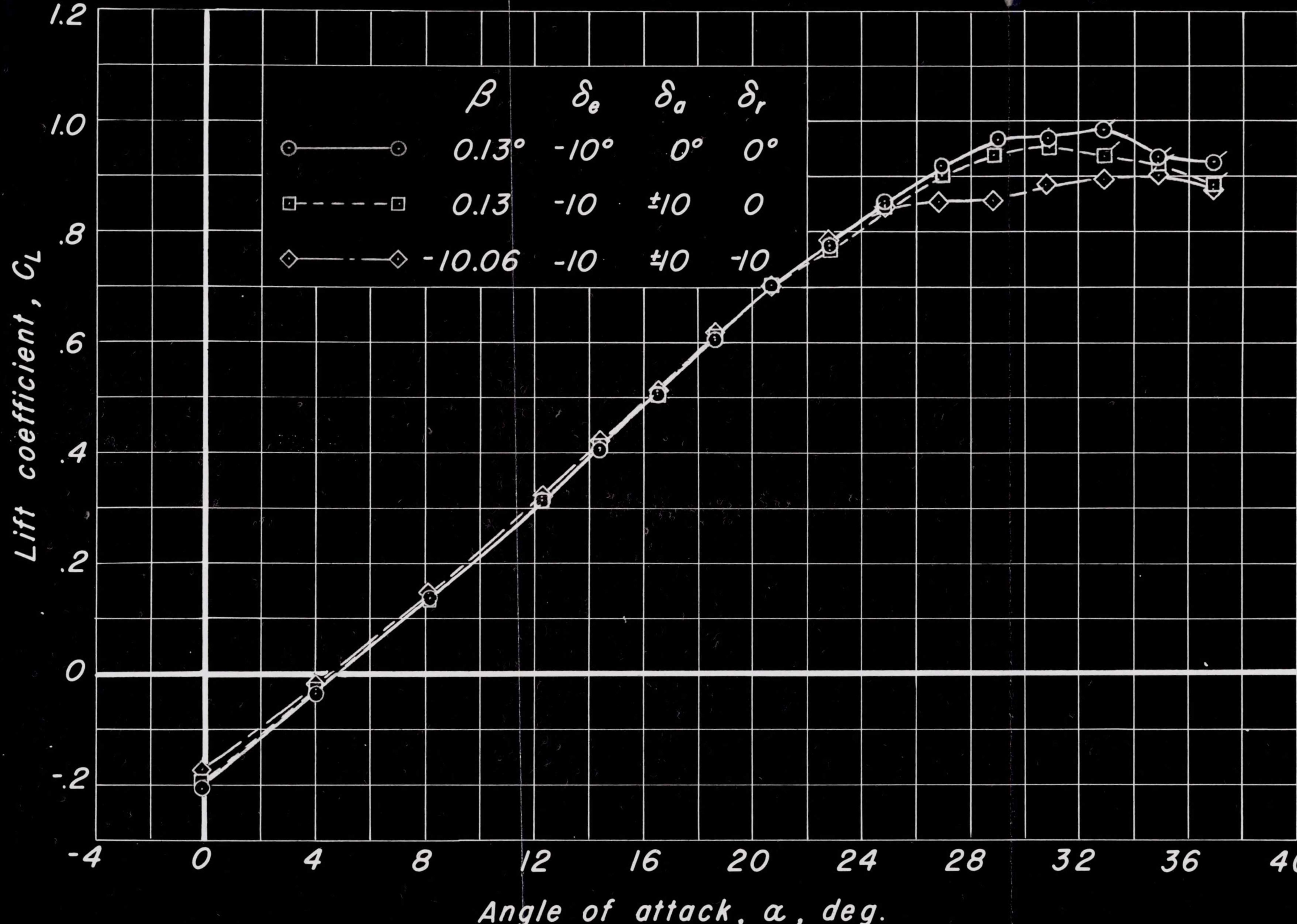

Figure 21. – Effects of extended landing gear on controls.

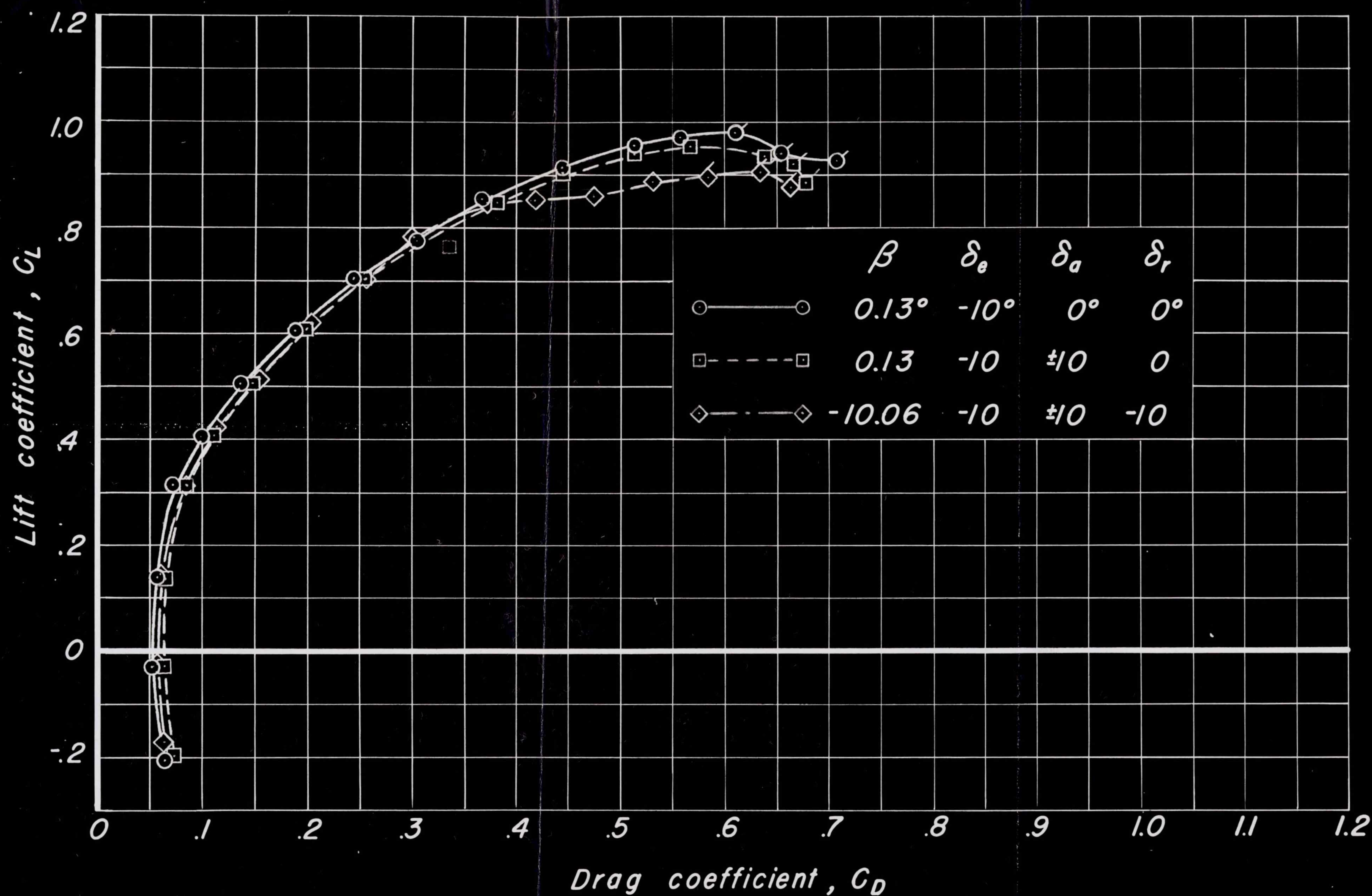

Figure 21. - Continued.

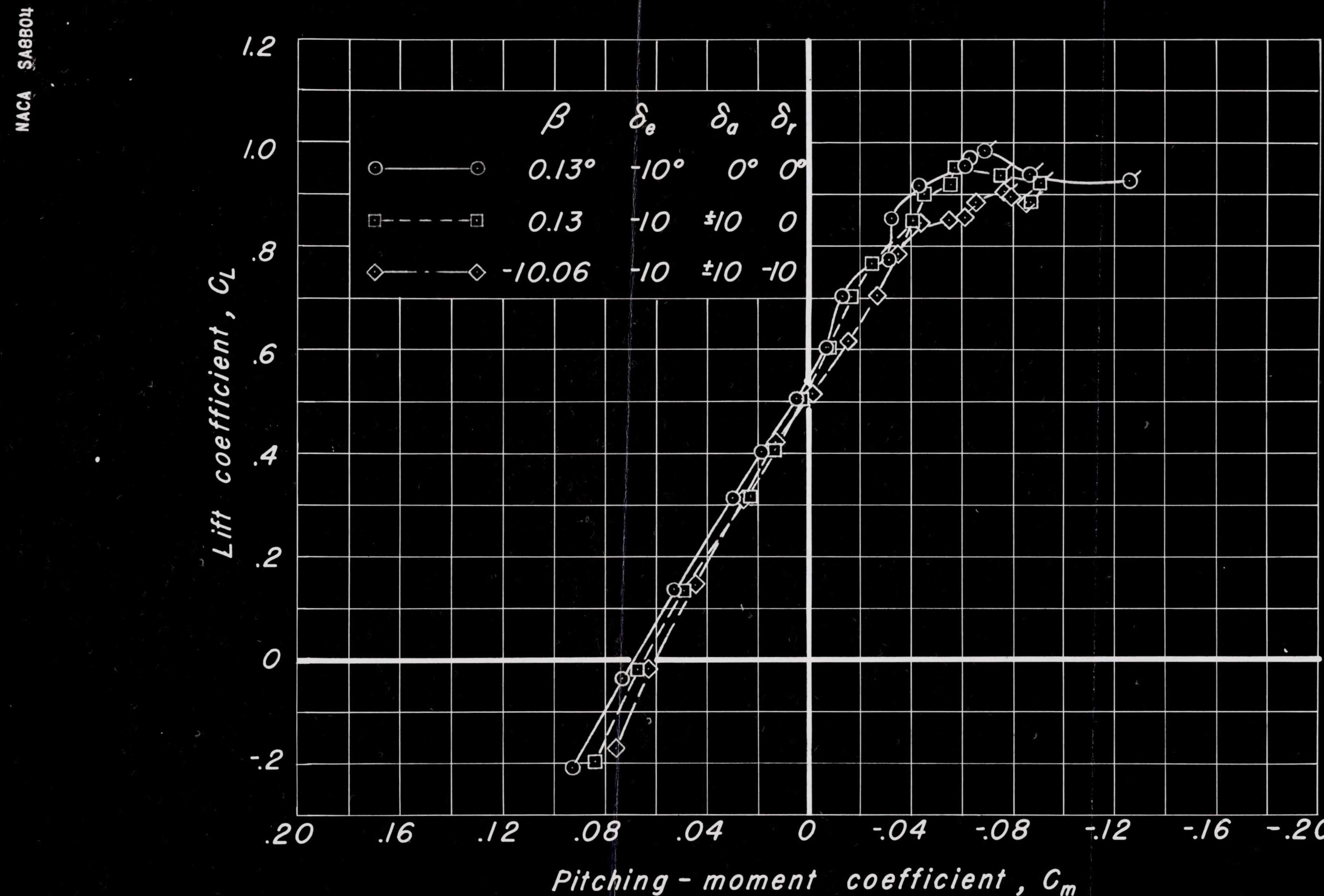

Figure 21. - Continued.

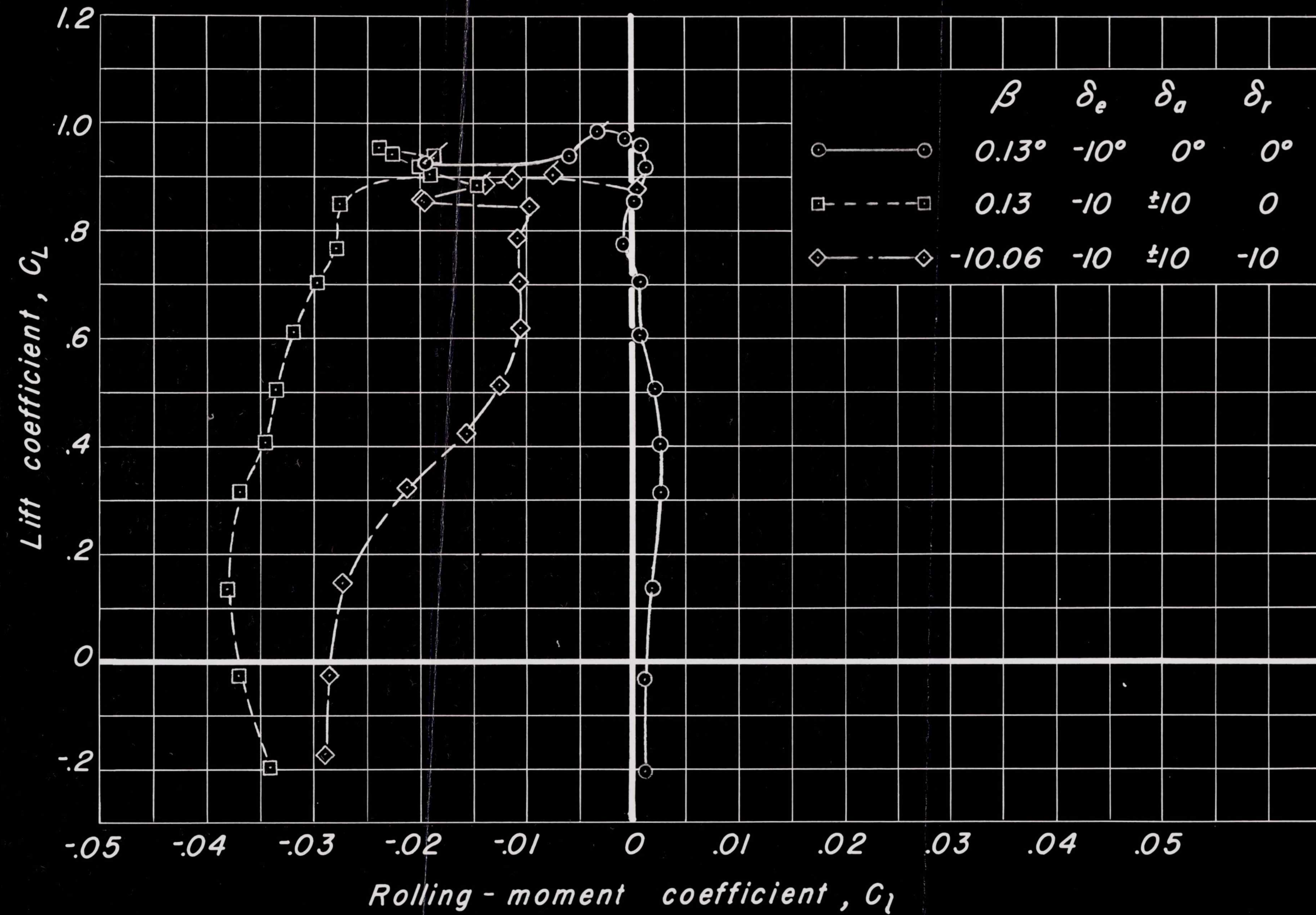

Figure 21. —Continued.

Figure 21. —Continued.

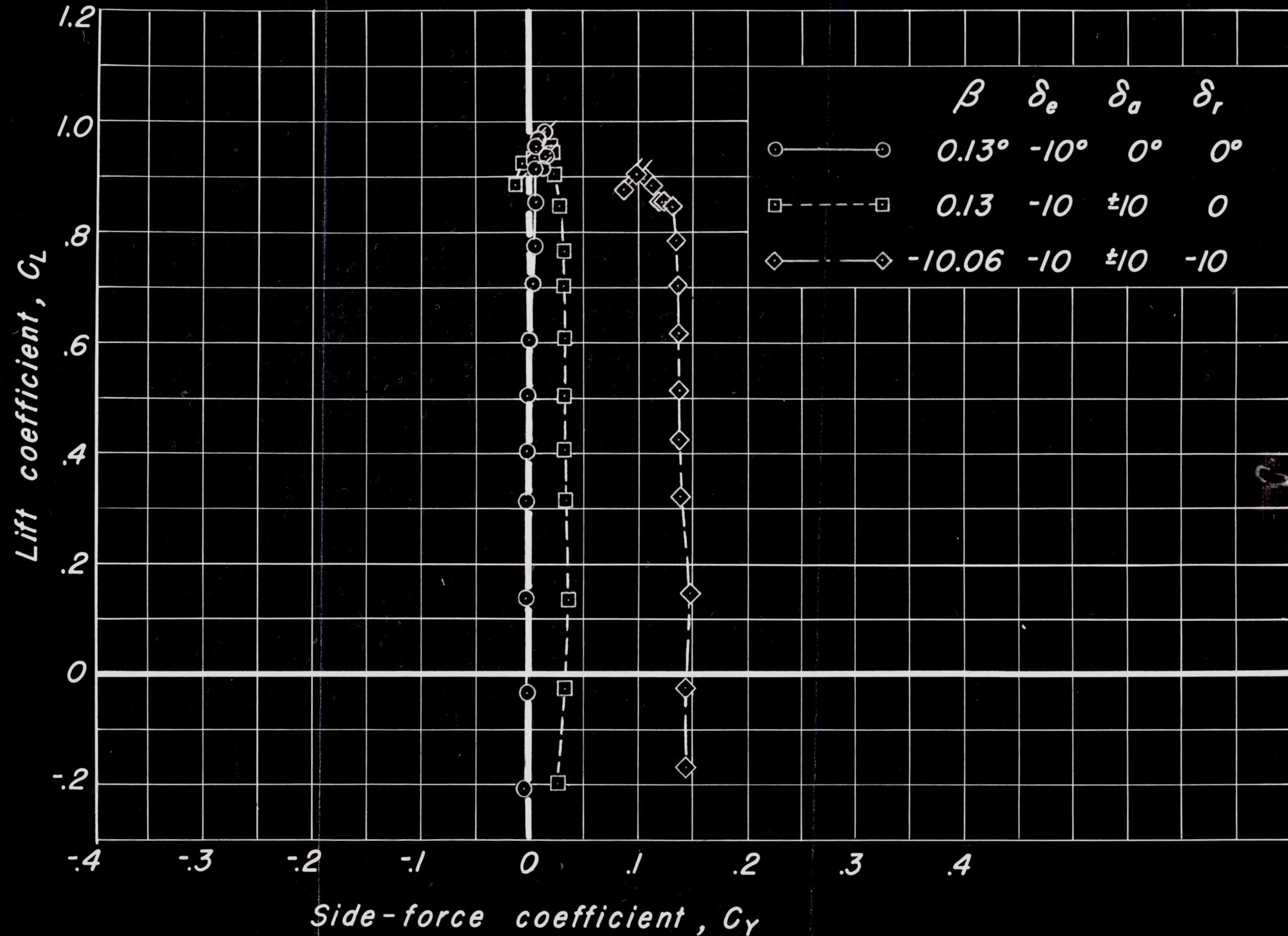

Figure 21. - Concluded.

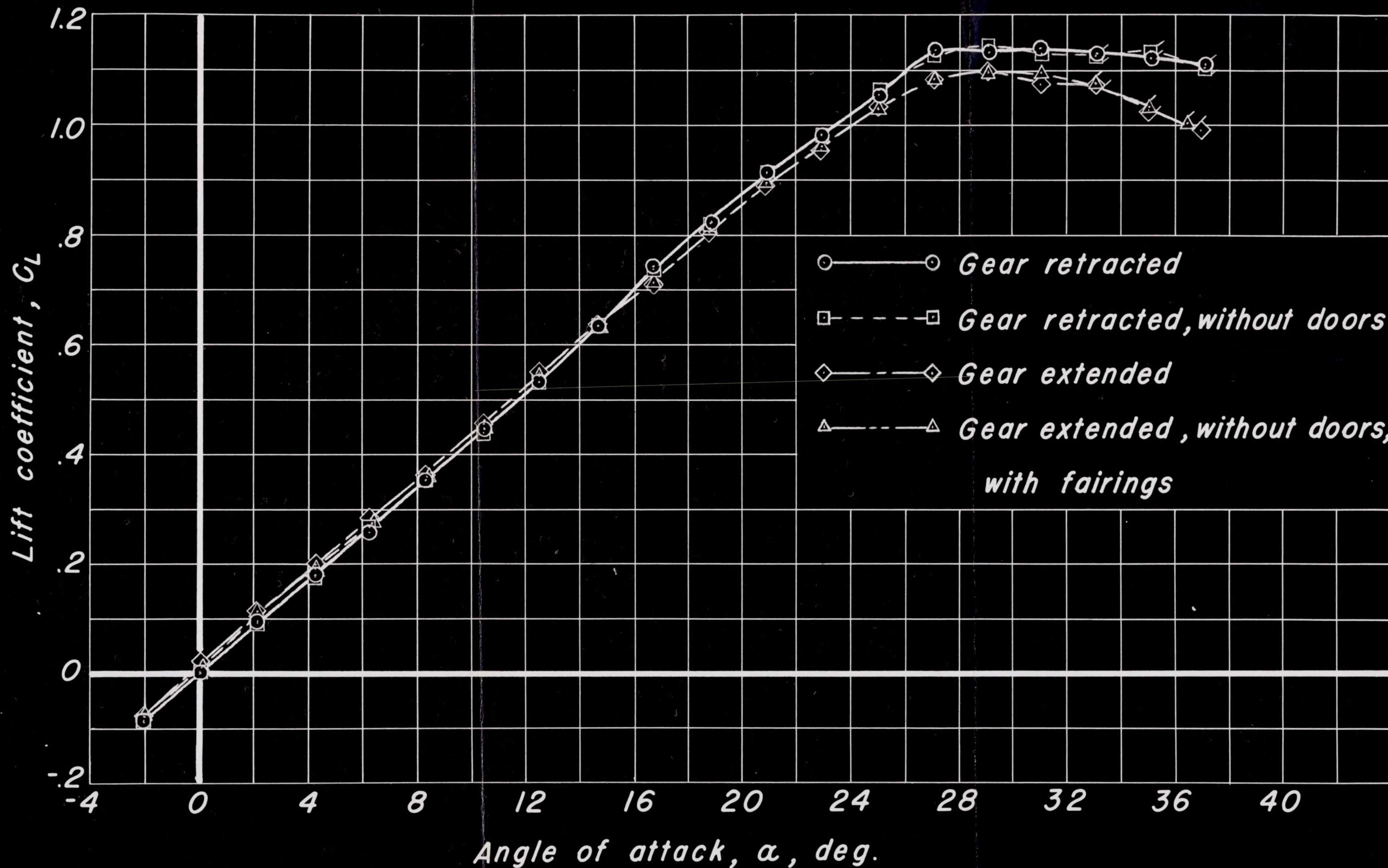

Figure 22.- Effects of various landing gear configurations on longitudinal characteristics with controls neutral.

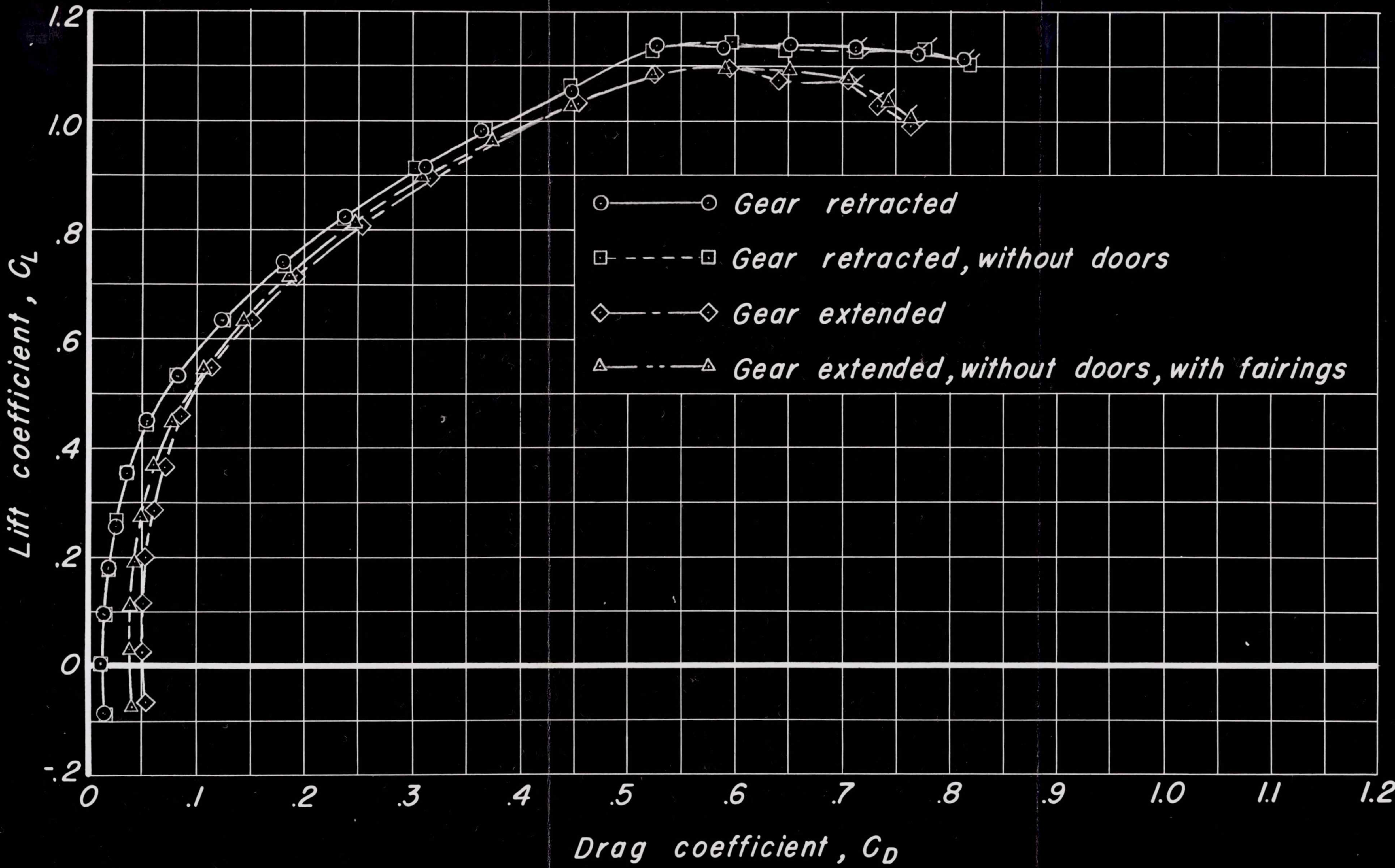

Figure 22.– Continued.

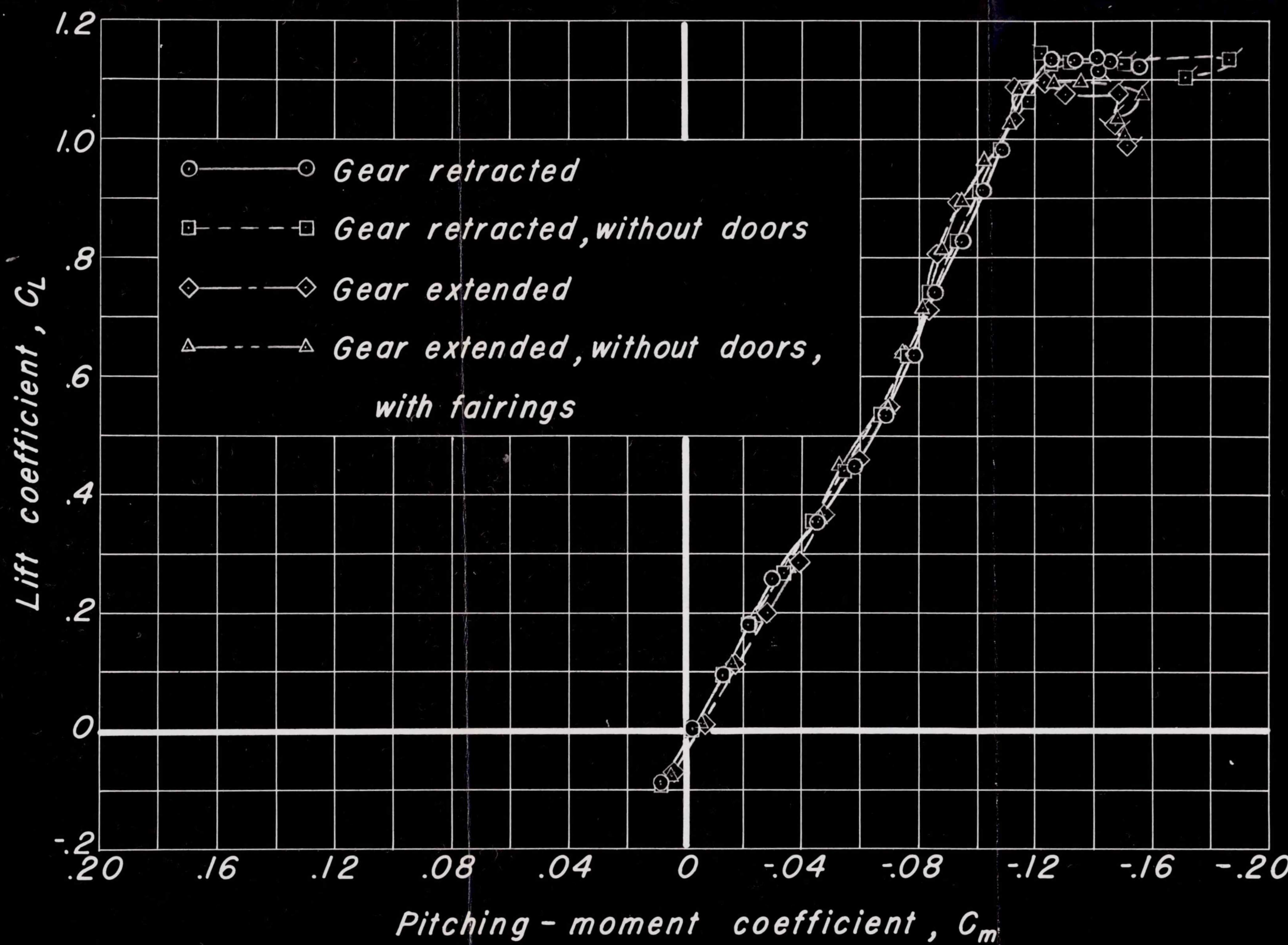

Figure 22.- Concluded.

NACA SA8B01

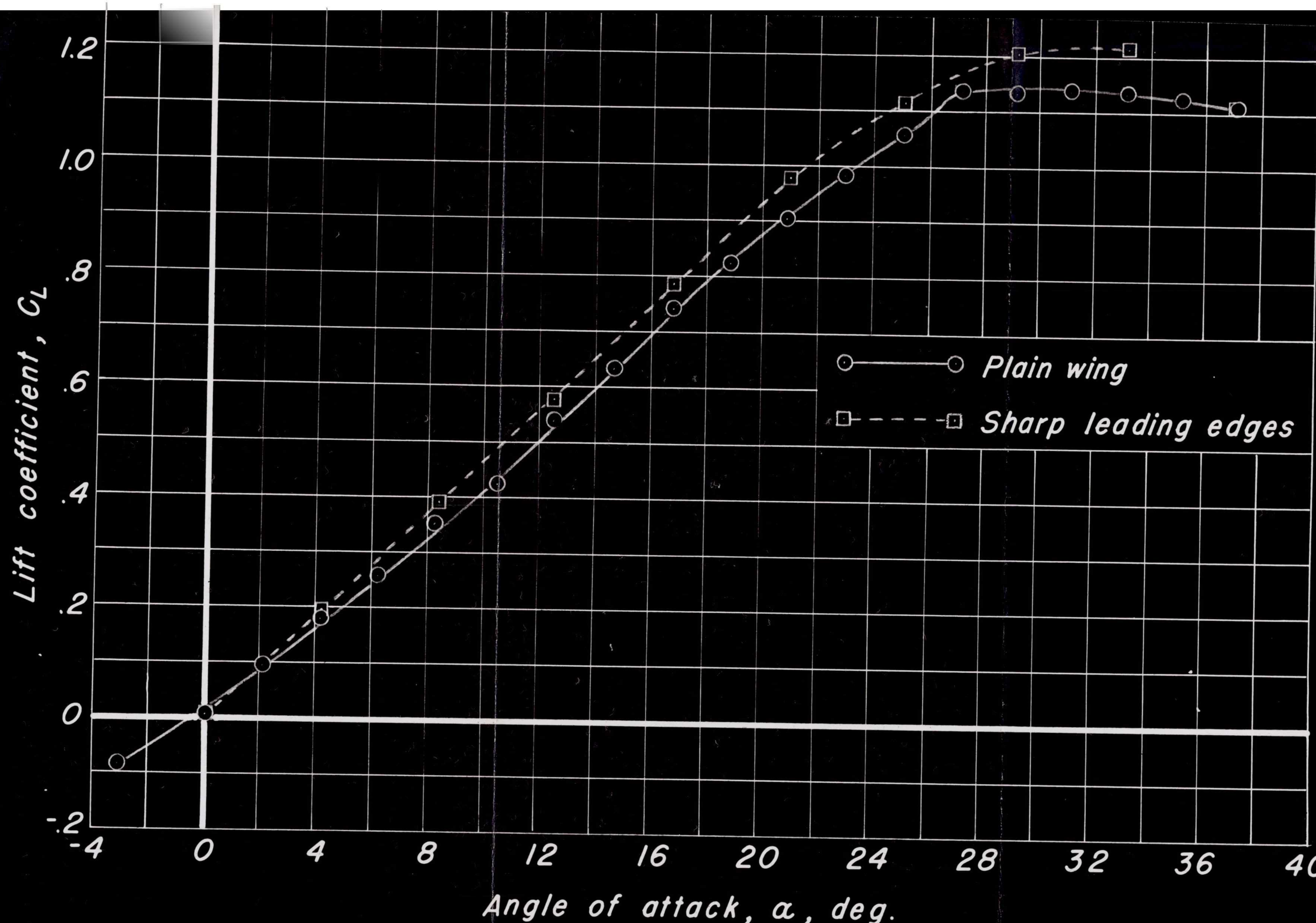

Figure 23.— Effect of sharp leading edges on longitudinal characteristics with controls neutral.

CONFIDENTIAL
NATIONAL ADVISORY COMMITTEE FOR AERONAUTICS

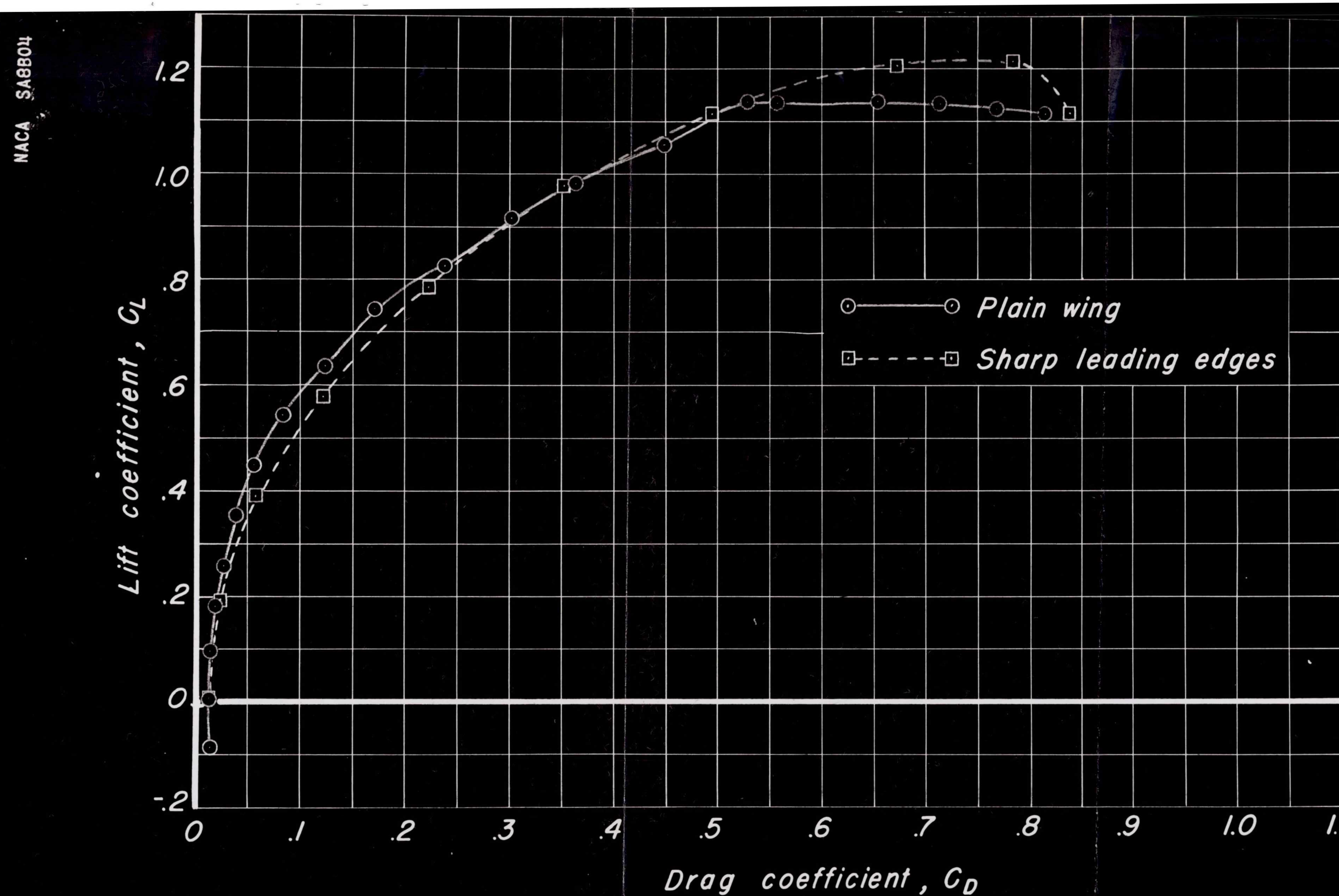

Figure 23.– Continued.

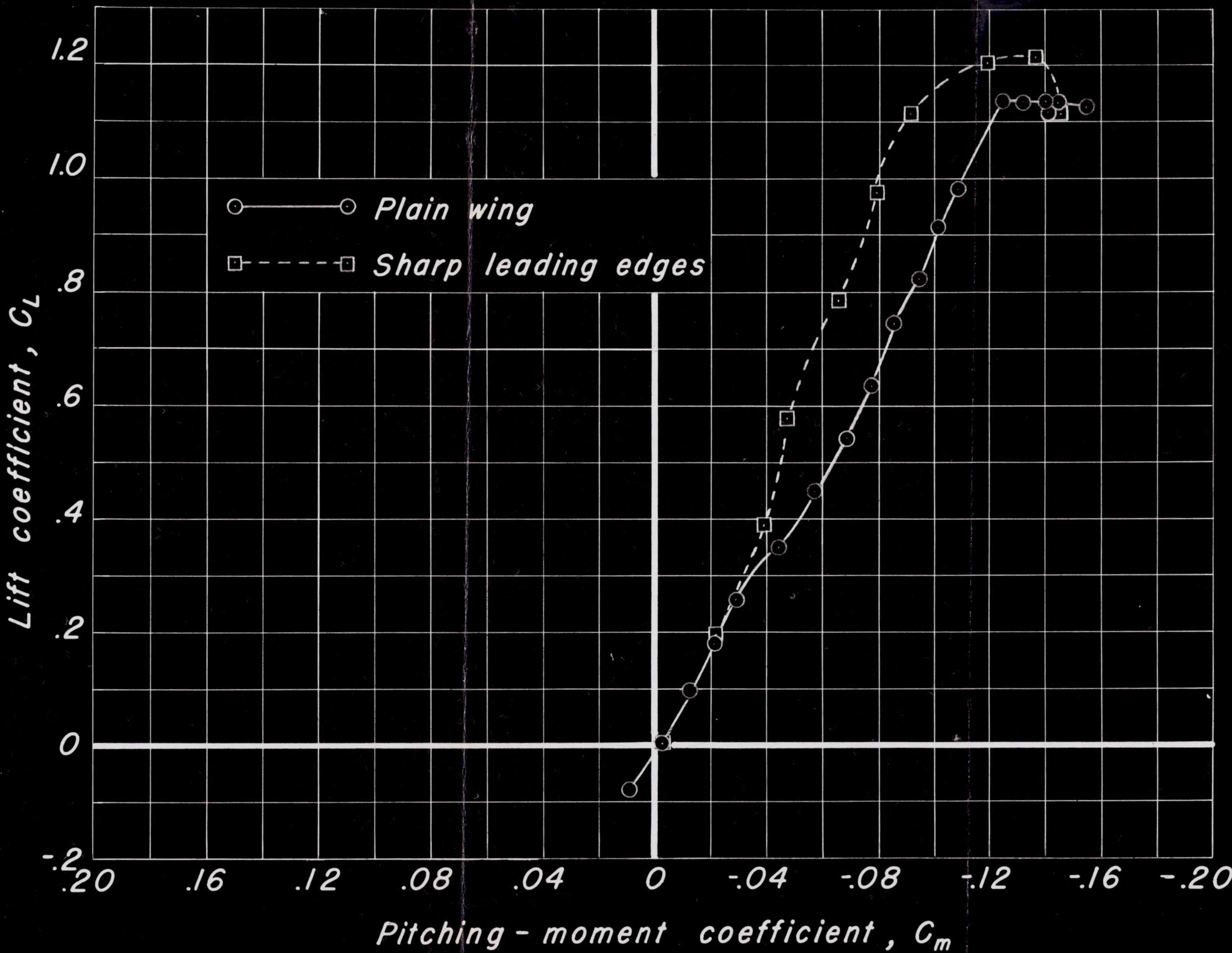

Figure 23.– Concluded.

NACA SA8B04

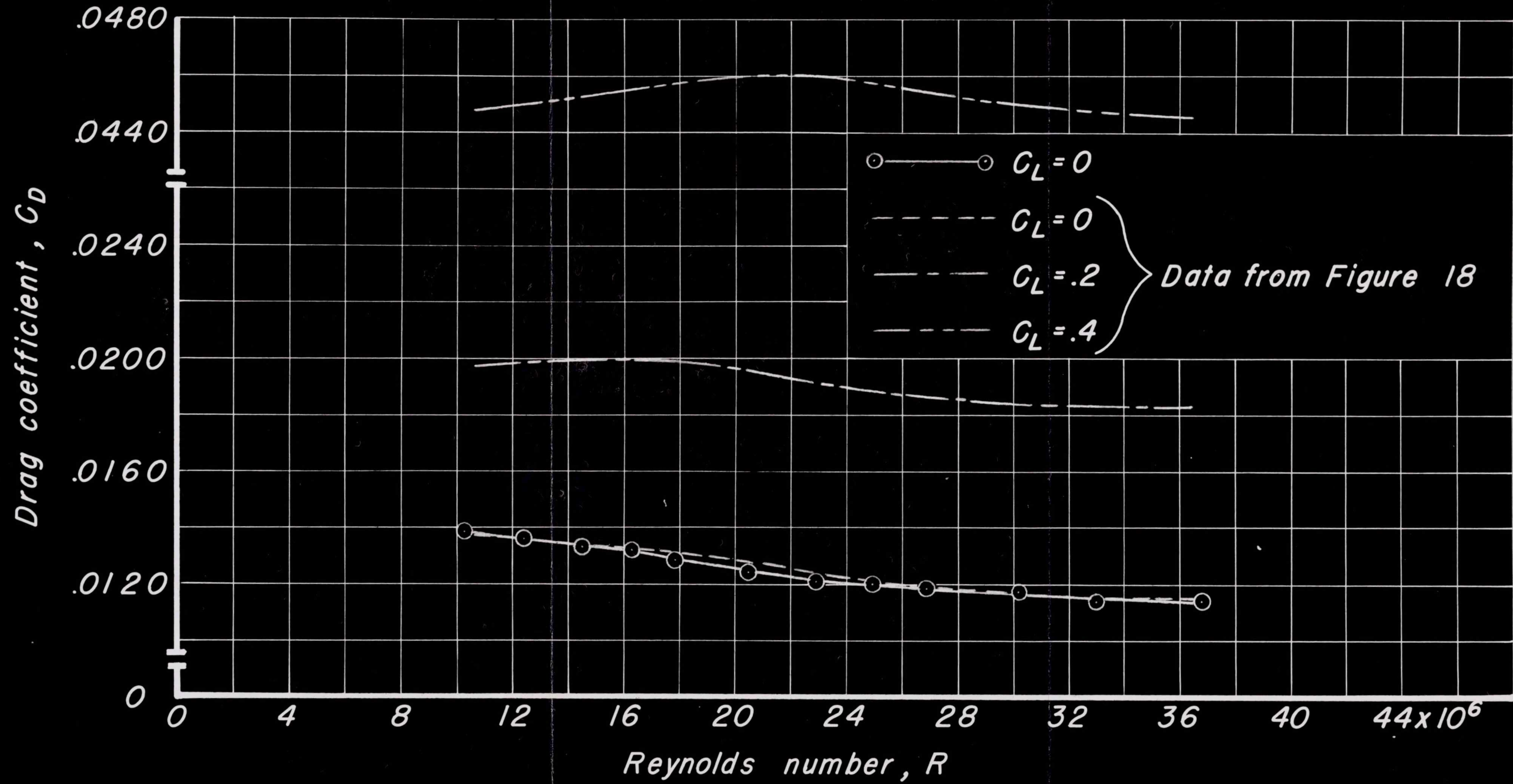

Figure 24.– Effect of Reynolds number on drag coefficient at constant lift coefficient.

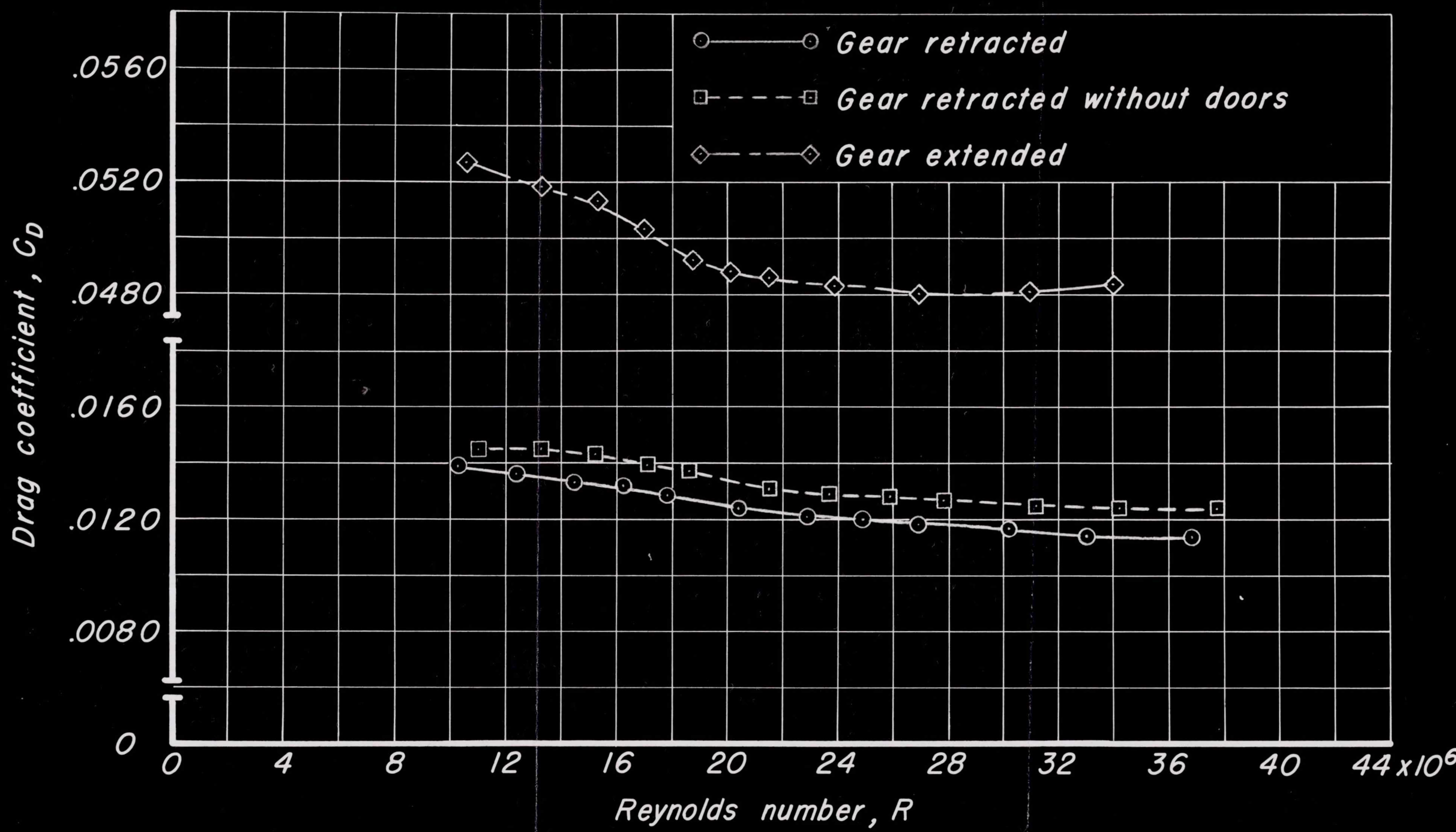

Figure 25.– Effect of various landing gear configurations on the variation of drag coefficient with Reynolds number, $C_L = 0$.

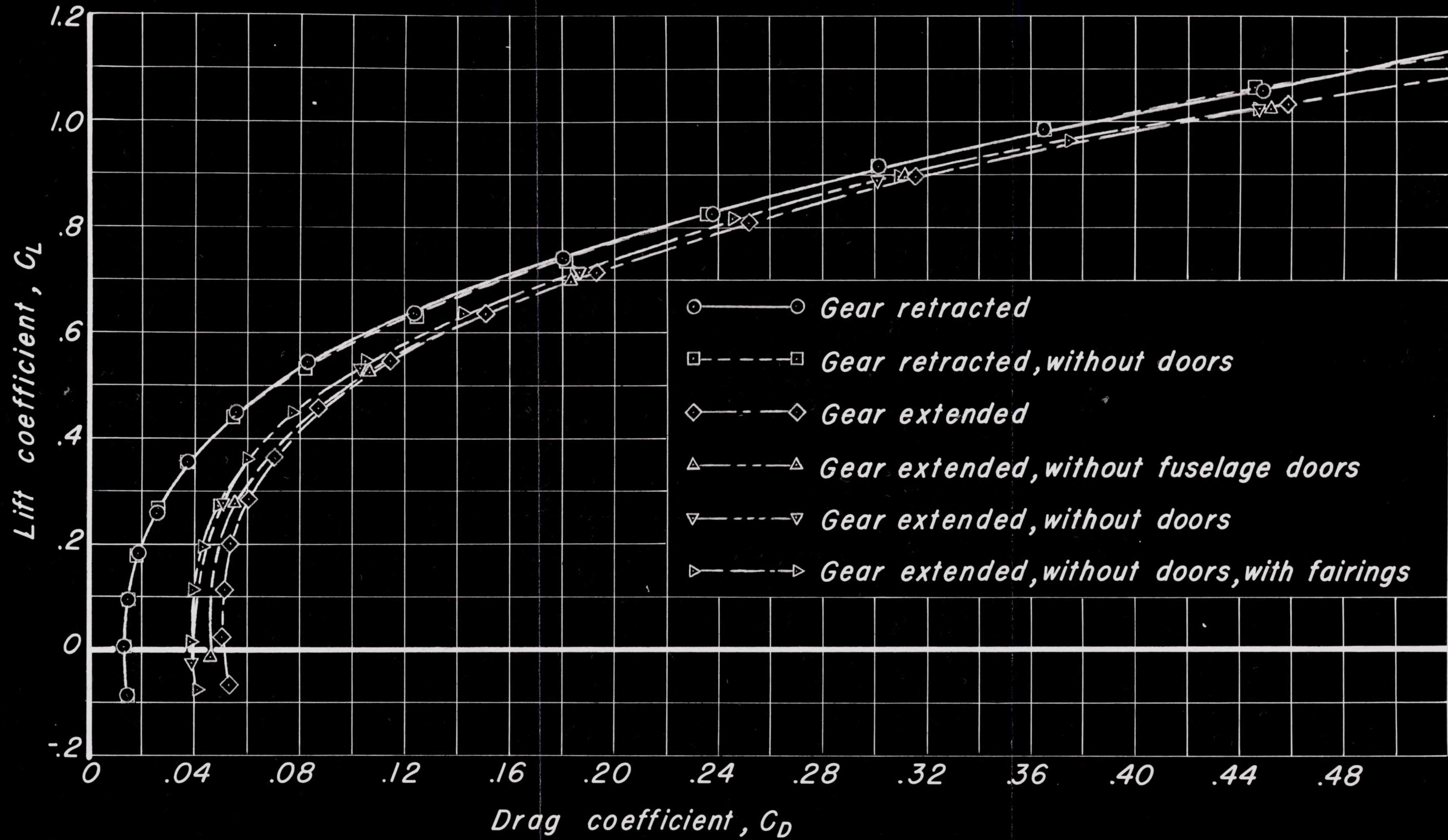

Figure 26.– Effect of various landing gear configurations on drag coefficient variation with lift coefficient.

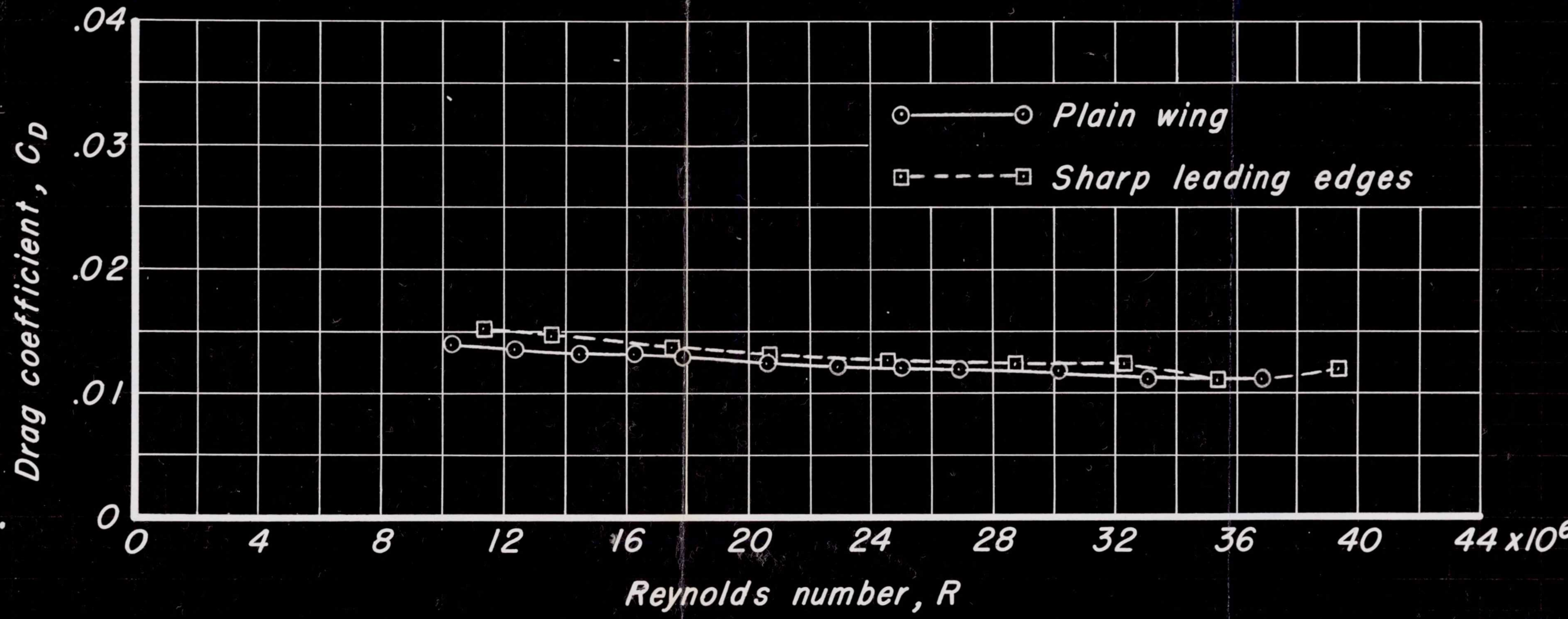

Figure 27.- Effect of sharp leading edges on the variation of drag coefficient with Reynolds number, $C_L = 0$.

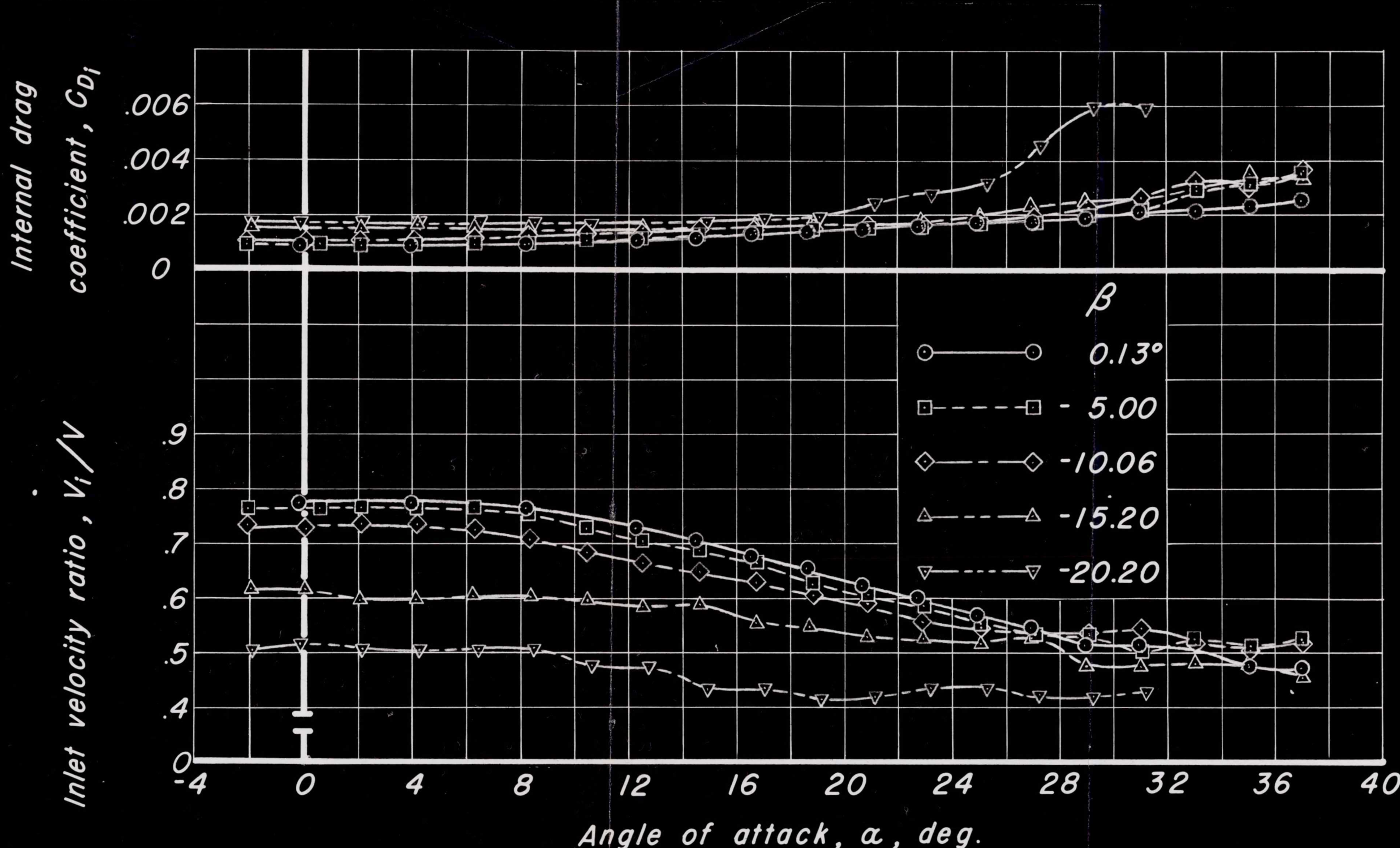

Figure 28.– Internal drag coefficient and inlet velocity ratio of the ducted fuselage at various angles of sideslip.

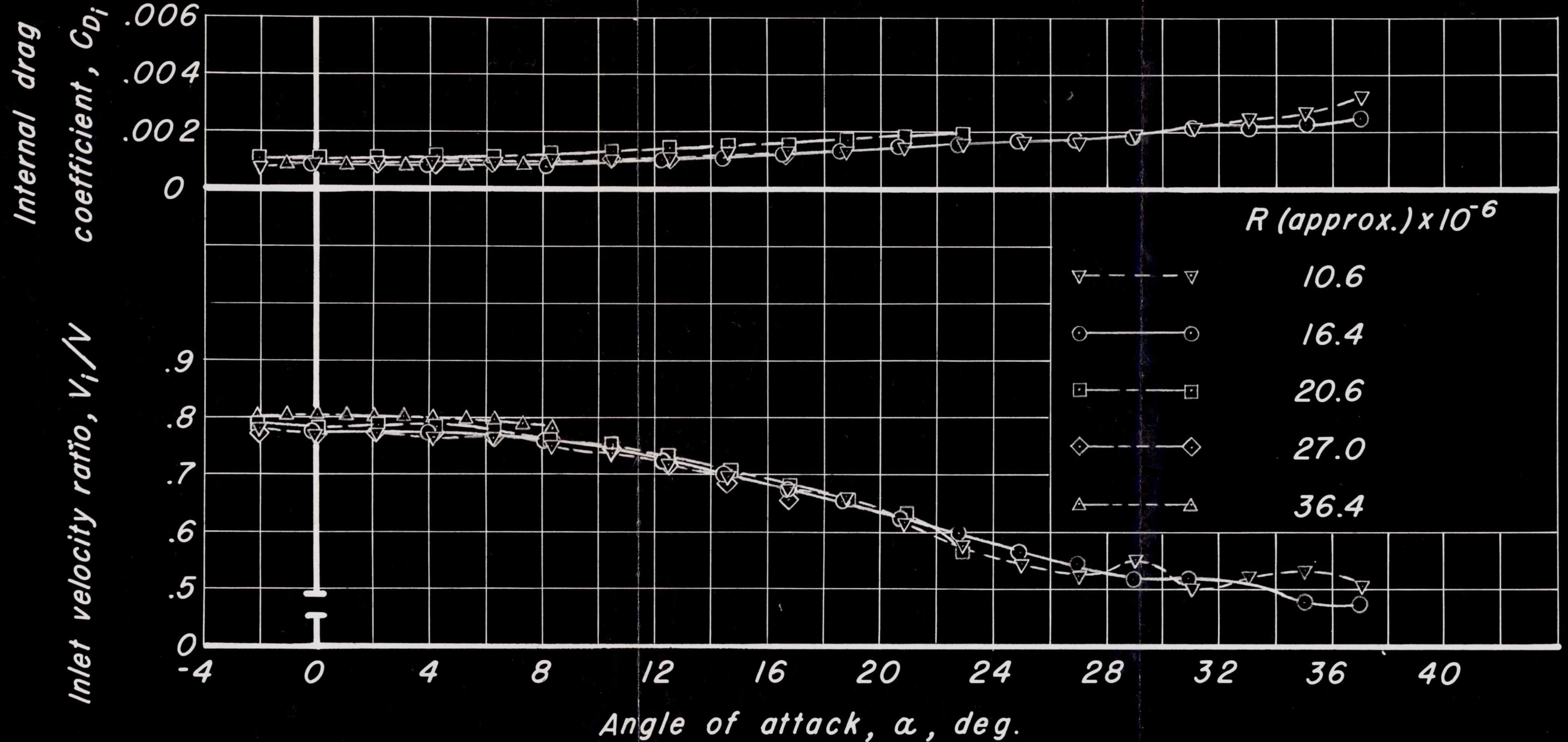

Figure 29.– Internal drag coefficient and inlet velocity ratio of the ducted fuselage at various Reynolds numbers, β=0.13°.